Exploring the potential energy landscape of glass-forming systems: from inherent structures via metabasins to macroscopic transport

2008 J. Phys.: Condens. Matter 20 373101

(http://iopscience.iop.org/0953-8984/20/37/373101)

IOP PUBLISHING JOURNAL OF PHYSICS: CONDENSED MATTER

J. Phys.: Condens. Matter **20** (2008) 373101 (56pp) doi:10.1088/0953-8984/20/37/373101

TOPICAL REVIEW

Exploring the potential energy landscape of glass-forming systems: from inherent structures via metabasins to macroscopic transport

Andreas Heuer

Institut für Physikalische Chemie, Westfälische Wilhelms-Universität Münster, D-48149 Münster, Corrensstraße 30, Germany

Received 7 November 2007, in final form 30 April 2008
Published 26 August 2008
Online at stacks.iop.org/JPhysCM/20/373101

Abstract

In this review a systematic analysis of the potential energy landscape (PEL) of glass-forming systems is presented. Starting from the thermodynamics, the route towards the dynamics is elucidated. A key step in this endeavor is the concept of metabasins. The relevant energy scales of the PEL can be characterized. Based on the simulation results for some glass-forming systems one can formulate a relevant model system (ideal Gaussian glass-former) which can be treated analytically. The macroscopic transport can be related to the microscopic hopping processes, using either the strong relation between energy (thermodynamics) and waiting times (dynamics) or, alternatively, the concepts of the continuous-time random walk. The relation to the geometric properties of the PEL is stressed. The emergence of length scales within the PEL approach as well as the nature of finite-size effects is discussed. Furthermore, the PEL view is compared to other approaches describing the glass transition.

(Some figures in this article are in colour only in the electronic version)

Contents

1. Introduction

Understanding the properties of glass-forming systems has been a major scientific issue for quite some time. Due to the complex multi-particle behavior progress has been slow. This paper aims to discuss the phenomenology of glass-forming systems in terms of the potential energy landscape (PEL). This is a multi-dimensional surface describing the dependence of the potential energy on the coordinates of the atoms or molecules [1]. Several important review articles and books have been recently written about properties of supercooled liquids [1–15] and some specifically concentrating on the properties of the PEL [1, 2, 10, 11]. Before presenting the specific scope of the present article a summary of relevant experimental and numerical observations as well as a brief introduction into the concept of the PEL will be given.

1.1. Characterizing the glass transition

Once crystallization has been avoided during cooling down a melt, e.g. by using a high cooling rate, the system is denoted supercooled. Thermodynamically it is in a metastable state. Its structure is still liquid-like and the dynamics becomes more and more sluggish upon further cooling down. Finally, when the viscosity has reached $\eta = 10^{13}$ P, the system behaves solid-like on typical experimental timescales of seconds. Often this temperature is denoted the glass transition temperature T_g.

1.1.1. Structural relaxation and non-exponentiality. A central quantity above T_g is the structural or α-relaxation time τ_α. It is related to η via the Maxwell relation $\tau_\alpha = \eta/G_\infty$ where G_∞ is the instantaneous shear modulus. Since G_∞ is only weakly temperature dependent, the temperature dependence of η and τ_α is very similar. The structural relaxation, as determined, e.g., by the incoherent scattering function

$$S(q,t) \equiv \langle \cos[\vec{q}(\vec{r}(t) - \vec{r}(0))] \rangle, \tag{1}$$

is strongly non-exponential and often fitted by a KWW function $\exp(-(t/\tau_{\mathrm{KWW}})^{\beta_{\mathrm{KWW}}})$. The non-exponentiality is typically related to dynamic heterogeneities, i.e. the presence of fast and slow molecules [16–18]. In the low-temperature regime β_{KWW} often decreases with decreasing temperature [19]. Tentatively, one may identify the structural relaxation time τ_α via the condition

$$S(q_{\max}, \tau_\alpha) = 1/e \tag{2}$$

where $q_{\max}$ corresponds to the maximum of the structure factor. Thus, on the timescale of τ_α a typical particle moves a distance of about the nearest-neighbor distance, leading to a local reorganization of the structure.

1.1.2. Fragility and Stokes–Einstein relation. The viscosity of systems such as silica displays an Arrhenius behavior in the experimentally accessible temperature range. This is characteristic of a *strong* system. Most systems, however, only show an Arrhenius behavior at very high temperatures, whereas in the supercooled regime they display an increase of the apparent activation energy $E_{\mathrm{app}}(T) \equiv \mathrm{d}\ln\eta/\mathrm{d}(1/T)$ [20], which is the apparent slope in the Arrhenius representation of η versus $1/T$. From this one can define the kinetic fragility index

$$m_{\mathrm{kin}} = \frac{E_{\mathrm{app}}(T_g)}{T_g}. \tag{3}$$

This is the apparent slope in figure 1 at the right end. The larger the increase of $E_{\mathrm{app}}(T)$ with temperature the larger the fragility index and, thus, the more *fragile* the system.

Interestingly, systems with different fragilities also show different temperature dependences of the entropy [20]. Thus, fragility is considered to be an important characteristic of a glass-forming system.

Similarly, one can also study the temperature dependence of the diffusivity $D(T)$. Whereas it shows the same general behavior as $\tau_\alpha(T)$ (or $\eta(T)$), a closer analysis reveals that $D(T)\tau_\alpha(T)/T$ is not constant, thereby violating the Stokes–Einstein relation [21]. Typically one can write

$$D(T)\tau_\alpha(T) \propto (\tau_\alpha(T))^\alpha \tag{4}$$

with the dynamic exponent α around 0.25 [21]. Simulations of a Lennard-Jones system yield $\alpha \approx 0.35$ [22], although currently a smaller value of 0.17 is discussed, based on a different value of z (see section 1.1.4) [23].

Finally, it is noted that often the temperature dependence of τ_α is fitted by the Vogel–Fulcher–Tamman (VFT) relation [24]

$$\tau_\alpha(T) \propto \exp(B_{\mathrm{VFT}}T_0/(T - T_0)). \tag{5}$$

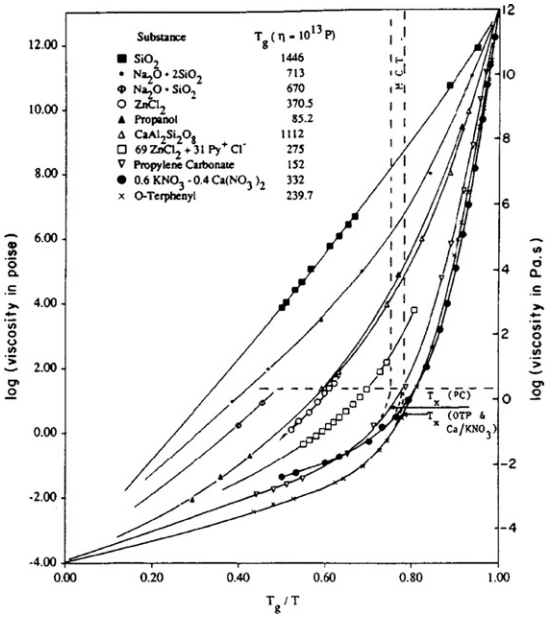

Figure 1. Angell plot for different glass-forming systems, displaying the difference between strong and fragile systems. Reprinted with permission from [7]. Copyright 2000, American Institute of Physics.

1.1.3. Fragility versus non-exponentiality. A crucial question is whether fragility and non-exponentiality are correlated. As shown in figure 2, polymers show a significant correlation between both quantities. More fragile systems (m large) are more non-exponential (β_{KWW} small) [5, 25]. Furthermore, considering all systems together also a strong correlation is observed. Subgroups, however, display a much weaker correlation. This holds, e.g., for network-forming systems which are on the strong side and display nearly exponential relaxation as well as molecular glass-formers. Their values of β_{KWW} and m_{kin} are scattered significantly but only show a very weak correlation; see figure 2. The presence of a significant correlation between non-exponentiality and fragility has recently been questioned by Dyre [26].

1.1.4. Dynamic heterogeneities and length scales. It has been shown that the non-exponentiality of the relaxation is mainly due to a superposition of fast and slow relaxing entities, i.e. the presence of *dynamic heterogeneities*. This spread in mobility is observed in computer simulations, e.g. [27–33] (and many, many more), and also from different experimental techniques [16, 34–36]. Furthermore, the occurrence of fast and slow molecules is spatially correlated. Roughly speaking, three different length scales have to be distinguished.

First, a rearrangement process between inherent structures (see below for the definition), characterized by a participation ratio z_1 (see section 7.1), corresponds to an elementary excitation. The collective process requires the motion of $\mathrm{O}(10^1)$ particles, a number which is only weakly dependent on temperature in the numerically accessible temperature range [37].

Second, at a given time the mobility of nearby molecules is correlated. Thus, one can define a correlation length ξ_{coll} of dynamic heterogeneities. It is a collective correlation effect. Of course, many different specific definitions are possible, e.g. monitoring the size of slow or fast regions. A direct measurement of the length scale of dynamic heterogeneities ξ_{coll} is possible via multi-dimensional NMR experiments. Measuring the size of slow regions along its shortest direction (in the case of non-spherical shapes) yields values around 2 ± 1 nm for different glass-forming systems close to the glass transition [38–40]. These length scales can be also determined from computer simulations via so-called four-point susceptibilities $\chi_4(t)$ or related observables [12, 41–44], correlating the dynamics at two different positions. In all cases $\chi_4(t)$ displays a maximum for times around τ_α [43, 45]. In principle, the spatial structure of the dynamic heterogeneities has to be known in order to extract a well defined length scale [46]. ξ_{coll} is related to the relaxation time, τ_α, by a power law $\tau_\alpha \propto \xi_{\mathrm{coll}}^z$, where $z \approx 8.5$ for a Lennard-Jones system (taking the recent data from [47]). Other data yield a somewhat smaller value $z \approx 5$ [48]. Recently, a general way to extract length scales from dynamical susceptibilities has been suggested which can be easily applied to experimentally accessible observables [49]. Interestingly, no significant correlation of ξ_{coll} at T_{g} with fragility is observed.

Third, there is a length scale from which point on the single-particle dynamics is non-Fickian, i.e. displays a

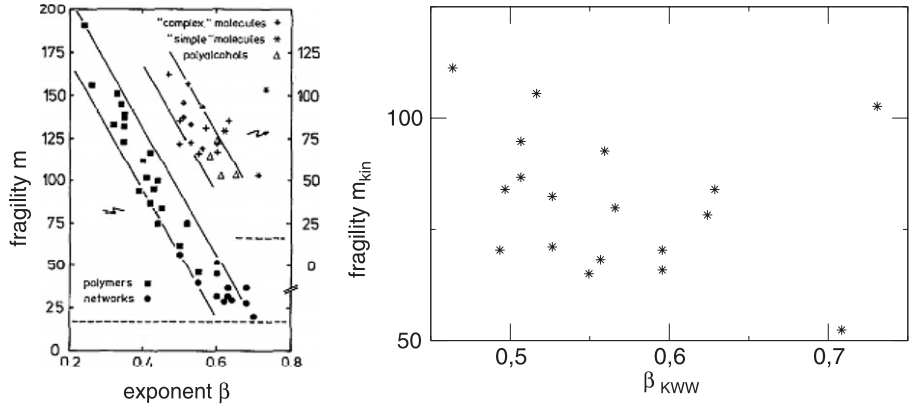

Figure 2. Left: non-exponentiality parameter β_{KWW} versus fragility index m for simple and complex molecular glass-formers, network systems, polymers and polyalcohols, as presented in [25]. Right: subset of simple and complex molecular glass-formers. The correlation coefficient between both quantities is around -0.28.

wavevector-dependent (apparent) diffusion constant. This length scale is denoted ξ_{single}. Recent experiments from the Ediger group have shown for an organic glass-forming system that close to T_g the value of ξ_{single} can be significantly larger than 5 nm [50]. From the numerical data in [22] it seems that the temperature dependence of ξ_{single} is similar to that of ξ_{coll}. This temperature dependence can under special model assumptions be directly related to the violation of the Stokes–Einstein relation [51].

Computer simulations can characterize the properties of dynamic heterogeneities on a more microscopic level. Different entities have been identified. Elementary cooperative motions have the structure of strings [29]. On longer timescales, the region of mobile particles appear to be more compact and these are denoted clusters [30, 52]. Is there a structural origin for some region of the supercooled liquid to be particularly slow or fast? The key idea to approach this question is to perform repeated simulations from the same configuration with different initial velocities (*isoconfigurational* ensemble). For a *small* system it has been shown in this way that configurations exist for which the mobility of the whole system during the next time interval was always higher than the average mobility (starting from an average configuration) [53]. Thus, there exists indeed a structural reason for the system to be fast or slow. In a recent series of interesting papers [54, 55] a similar approach has been chosen for a *large* system where in the same system there are fast and slow regions. Again, specific regions appeared for different initial velocities and thus structure dominates the dynamic heterogeneities. Here it is important not to consider the single-particle mobility because of the strong residual fluctuations from run to run but rather consider a coarse-grained observable [47]. The actual structural origin, determining the local mobility, is still under debate. For $Ni_{0.5}Zr_{0.5}$ around the glass transition temperature the residual mobility of the small atom (Ni) is clearly related to the local cage volume around the Ni atoms [56]. For systems in equilibrium a correlation of mobility and local volume seems to be absent [57].

1.2. Characterizing the potential energy landscape via inherent structures

1.2.1. General. *. . . when all is said and done, the existence of potential energy barriers large compared to thermal energy are intrinsic to the occurrence of the glassy state, and dominate flow, at least at low temperatures* [58]. In that paper by Goldstein from 1969 the stage is set for describing the properties of a supercooled liquid via its potential energy landscape (PEL). Formally, the PEL of an N-particle system is just given by the representation of the potential energy function $V(\vec{r}_1, \ldots, \vec{r}_N)$ in the $3(N-1)$-dimensional configuration space. At fixed volume this representation is *temperature independent*. The statement by Goldstein suggests that at low temperatures the system is close to local minima (also called *inherent structures* (ISs)) of the PEL, separated by large barriers relative to $k_B T$ (in the following we will always set $k_B = 1$). This statement is somewhat trivial in the limit of zero temperature. Goldstein, however, estimated that already for temperatures for which the relaxation processes occur in the microsecond regime, the PEL approach may be useful, i.e. far above the calorimetric glass transition temperature T_g. In this temperature regime the physics of the system is mainly determined by the ISs and their local (and thus harmonic) surroundings, as well as the transition paths between them. As compared to the full potential energy function $V(\vec{r}_1, \ldots, \vec{r}_N)$ this is a dramatic simplification because mainly the locations of the minima and barriers, i.e. a subset of measure zero of the total space, enter the description of the vitrification process. This is sketched in figure 3.

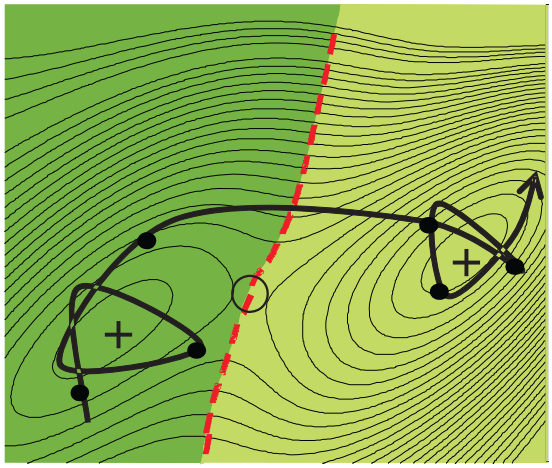

Figure 3. Sketch of a 2D landscape together with the IS (crosses), transition state (open circle) and basin border (dashed line). The solid line indicates a possible molecular dynamics trajectory at low temperatures. The solid circles denote the positions of the system from which the minimization procedure may have started, respectively. For that case both minima would be found exactly three times as the result of a minimization via steepest descent.

Formally, nearly all configurations can be uniquely mapped on an IS by minimizing its potential energy along the steepest descent path (except for configurations exactly on a saddle, which, however, is a set of measure zero). Then the potential energy of a system can be viewed as a superposition of the energy of the related IS and some additional vibrational energy. More than a decade after the Goldstein work Stillinger and Weber have used this idea to determine properties of the IS from molecular dynamics simulations [59–61]. For this purpose they have regularly quenched the actual configuration to determine the related IS. Its energy will be denoted e. In this way they have observed how the system explores the PEL in terms of the related IS. This is sketched in figure 3. A real space sketch of the actual trajectory can be found in figure 4. Most numerical examples, which will be shown in this section, have been obtained for the binary mixture Lennard-Jones (BMLJ) system; see section 1.4 for a closer description. As usual, all temperatures will be given in units of the interaction parameter between the majority particles.

Naturally, dynamic observables may look somewhat different when comparing the original and the IS trajectory. Qualitatively, the IS trajectory corresponds to discrete hopping processes rather than to a continuous process as for the

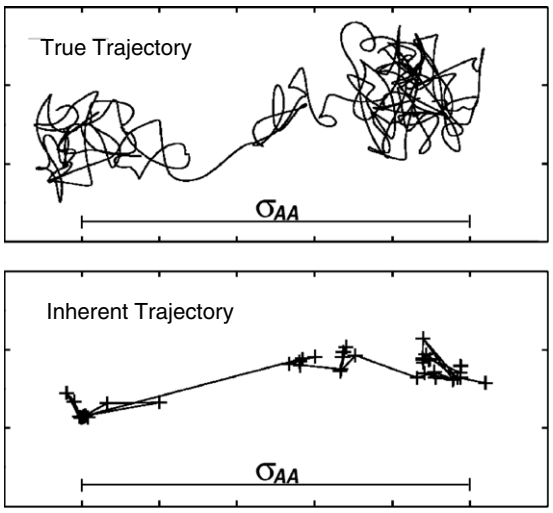

Figure 4. Comparison of the actual trajectory and the trajectory of inherent structures. σ_{AA} reflects the equilibrium distance between adjacent particles. Reprinted with permission from [62]. Copyright 2000, American Institute of Physics.

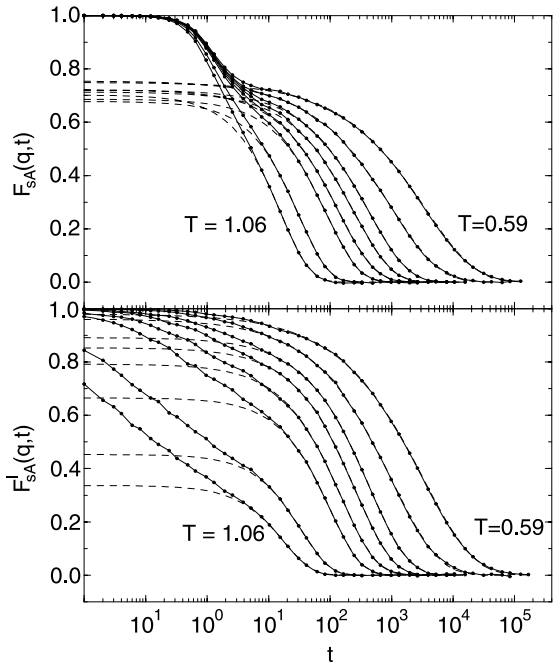

Figure 5. Comparison of the incoherent scattering function of the actual trajectory (upper figure) as compared to that of the inherent structure trajectory (lower figure) for a binary Lennard-Jones system. The temperature scale for that system is slightly higher than that for the often-used Kob–Andersen model. The later part of the incoherent scattering function, corresponding to the α-relaxation, has been fitted by a KWW function. It turns out that except for the highest temperature the timescale as well as the non-exponentiality parameter β_{KWW} are the same within statistical uncertainty. The initial part in the upper figure corresponds to the local vibrations and the fast β-process. Due to the very nature of the inherent structure trajectory the effect of local vibrations is not present in its trajectory. Reprinted with permission from [62]. Copyright 2000, American Institute of Physics.

original trajectory. This is exemplified in figure 5 for the incoherent scattering function $S(q,t)$. The decay characteristics of the α-relaxation is basically identical. The main difference can be found in the short-time regime of local vibrations and the fast β-process, related to the gradual escape from the local cage. Because in the IS trajectory the fluctuations around the respective IS have been taken out, the incoherent scattering function is mainly sensitive to the α-process. More quantitatively, one can approximate $S(q,t) = f(q,t)S_{\mathrm{IS}}(q,t)$, where the function $f(q,t)$, possessing some finite long-time plateau, describes the initial decay of the incoherent scattering function. The second factor mainly reflects the structural relaxation and is just the incoherent scattering function, extracted from the IS trajectory. This analysis implies that the standard definition of τ_α, namely $S(q_{\max}, t = \tau_\alpha) = 1/e$ does not fully reflect the timescale of the structural relaxation because of the additional influence of $f(q,t)$.

1.2.2. From energy to mobility. As a next scientific cornerstone a relation between the IS properties and the dynamics has been established in the paper by Sastry, Debendetti and Stillinger [63]. They asked whether the different dynamical temperature regimes, observed for the model glass-former BMLJ, can be related to properties of the PEL. Basically three temperature regimes can be identified. Starting from high temperatures a first transition around $T \approx 1$ can be best studied from analyzing the temperature and time dependence of the incoherent scattering function $S(q,t)$, which is the spatial Fourier transform of the self-part of the van Hove self-correlation function $G_{\mathrm{s}}(r,t)$. For $T > 1$, $S(q,t)$ can be described by a simple exponential, and its decay time, i.e. the α-relaxation time, shows an Arrhenius temperature dependence. When cooling down below $T = 1$, $S(q,t)$ becomes non-exponential and furthermore displays a non-Arrhenius temperature dependence as known for fragile glass-forming systems. A second transition seems to occur below $T \approx 0.45$ because $G_{\mathrm{s}}(r,t)$ displays a nearest-neighbor peak, which may tentatively be interpreted as a signature of activated hopping dynamics.

Interestingly, these three temperature regimes are reflected by the average IS energy as shown in figure 6, obtained from the Stillinger–Weber procedure [63]. For $T > 1$ the energy does not depend on temperature, i.e. the temperature dependence of the dynamics is not reflected by the properties of the visited IS. This is the regime of free diffusion. The potential energy is so high that the dynamics of the system is hardly influenced by the little barriers between the minima (more formally this can be described in terms of anharmonic contributions; see section 3). For $0.45 < T < 1$ the average IS energy strongly decreases with decreasing temperature. This means the system is exploring lower and lower IS on the PEL. For even lower temperatures the energy becomes a constant. A closer analysis shows that the system is basically stuck in some region of the PEL. Since the temperature of the second transition in figure 6 strongly depends on the cooling rate it is suggested that here the glass transition sets in. Stated differently, for a much smaller cooling rate (not possible for computer simulations) the transition to the constant energy

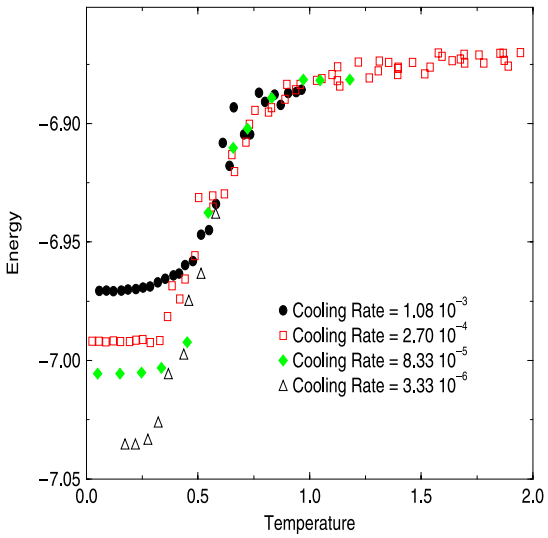

Figure 6. Average IS energy versus temperature for different cooling rates for a binary mixture Lennard-Jones system. Reprinted by permission from Macmillan Publishers Ltd: *Nature* [63] copyright 1998.

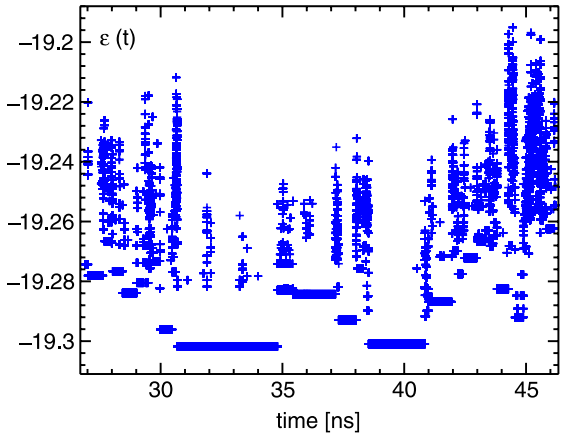

Figure 7. The time series of IS energies for a model of silica at 3000 K, obtained via frequent minimization of the molecular dynamics trajectory.

regime would be at significantly lower temperatures. More than one decade earlier, Jonsson and Andersen already reported similar results and also interpreted them in terms of the PEL approach [64].

A direct relation between energy and dynamics is shown in figure 7 for simulations of a small silica model. Several important features can be observed: (i) the residence in low-energy ISs is very long as compared to the residence in high-energy ISs. (ii) Subsequent energies are correlated. (i) and (ii) naturally give rise to the fountain-type appearance of this plot. (iii) There exist correlated forward–backward dynamics (e.g. during the long residence in a low-energy IS between 30.5 and 35 ns the system attempts a few times to leave this IS but then returns to the same configuration). Also for large systems some correlation between particle mobility and a locally defined potential energy is observed [30]. One goal of this review is to elucidate the different pieces of information from this energy-resolved IS trajectory.

1.2.3. Going beyond supercooled liquids. In recent years a lot of work has also been devoted to the study of the PEL of clusters and biopolymers. A detailed account of this work can be found in the book by Wales [10]. For these systems one is typically interested in one or a few low-energy ISs, corresponding, e.g., to the native state of the biopolymer. For the case of Lennard-Jones clusters this low-energy IS is directly connected to a large number of other ISs [65]. As a consequence, it serves as a kind of hub in the network topology and properties of small-world and scale-free networks can be identified [65]. In contrast, for glass-forming systems one expects that there exists a large variety of different amorphous low-energy states. This very different behavior implies that the theoretical description for the transport and relaxation will be quite different for supercooled liquids as opposed to clusters or biopolymers. However, for the characterization of the local dynamics similar concepts can be used.

1.3. Alternative characterization of the PEL

Beyond the interpretation of the dynamics in terms of transitions between ISs, different characteristics of the PEL have also been used to relate the PEL to the dynamics.

1.3.1. Using barrier information via instantaneous normal modes. In the INM approach one calculates the Hessian for equilibrium configurations. Close to a minimum all eigenvalues are positive. However, at ambient temperatures the Hessian also displays negative eigenvalues which correspond to a negative curvature of the energy along the direction of the corresponding eigenvector. The goal is to take the negative curvature as an indicator for the modes close to a saddle, along which the system may therefore easily move in configuration space [66–68]. A closer analysis reveals that some of these modes are not related to saddles (or, equivalently, to the presence of double-well potentials) but rather to different types of anharmonicities (*shoulder modes*) [67]. After subtracting these modes one ends up with the so-called *double-well modes*. The fraction is denoted f_{dw}. Strictly speaking, a further distinction has to be made to exclude double-well modes which belong to intra-IS dynamics [69].

It turns out for a model of water [67] that over the whole temperature regime accessible by computer simulations the number of double-well modes [67] is related to the diffusion constant via $D \propto (f_{\mathrm{dw}} - f_0)^2$ with a fitting parameter f_0; see figure 8. For a model of silica one finds $D/T \propto f_{\mathrm{dw}}^{1.3}$ [68]. These results suggest that in the weakly supercooled region the slowing down of the dynamics is related to the decreasing number of free directions. In this interpretation barriers do not play a significant role. This picture is supposed to break down in the limit of very low temperatures for which the transport requires an activated process over a barrier [67]. As will be discussed in section 6.5 a strong relation of D and f_{dw} can also be rationalized in the opposite scenario for which the crossing of barriers is indeed an essential ingredient for the understanding of the dynamics.

Interestingly, the spatial analysis of the unstable modes has revealed a correlation between clusters of particles having

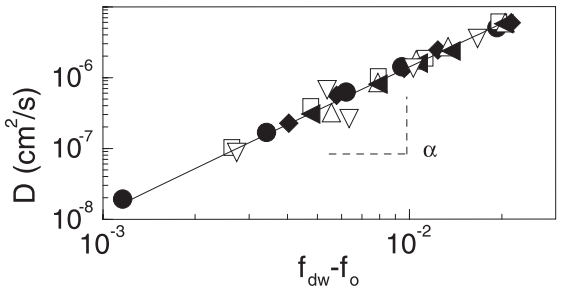

Figure 8. The number of diffusive directions versus the diffusion constant for the case of water, using different densities and temperatures. Reprinted with permission from [67]. Copyright 2001 by the American Physical Society.

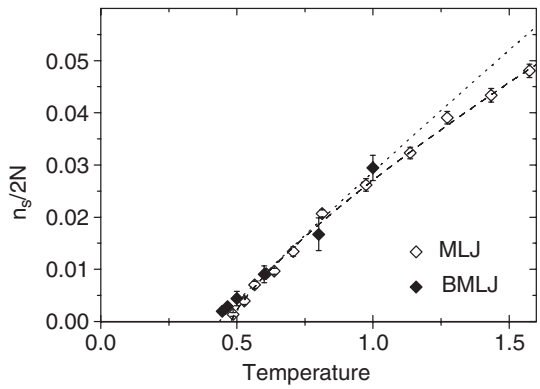

Figure 9. Temperature dependence of the fraction of the negative eigenvalues of the Hessian calculated at the inherent saddle configurations for two different Lennard-Jones models. Adapted with permission from [72]. Copyright 2000 by the American Physical Society.

large displacements in the unstable modes and dynamical heterogeneities [70].

1.3.2. Using barrier information via saddle indices. Whenever the gradient of the potential energy function $V(\vec{r}_1, \ldots, \vec{r}_N)$ vanishes, one either has a minimum (IS) or a saddle point. A saddle point configuration can be classified according to its number of negative eigenvalues of the Hessian matrix n_s and the potential energy e_s of this configuration. By definition, ISs simply correspond to saddle points with $n_s = 0$. A convenient way to identify saddle point configurations is via an auxiliary function W, using the gradient of V,

$$W = (1/2)|\vec{\nabla} V|^2. \tag{6}$$

By definition, W is strictly non-negative. For configurations which correspond to a saddle point in V, one naturally gets $W = 0$. Thus, saddle points in V correspond to local minima in W and thus can be identified by a minimization procedure. Of course, there may be minima of W which are not saddles of V [71]. On a qualitative level, however, these additional minima do not change the relevant results [71]. In what follows a distinction between saddle points of V and minima of W is not made.

As for the potential energy V, the total configuration space can be partitioned into different basins of attraction of the minima of W. A configuration can thus be characterized, on the one hand, by n_s and e_s, obtained from minimization of W, and by e, obtained from minimization of V. By performing a Stillinger–Weber-type analysis of W at a given temperature T one can determine $\langle e_s(T)\rangle$ and $\langle n_s(T)\rangle$ as the average values of e_s and n_s of the different minima of W. Analogously, one can define $\langle e(T)\rangle$ as the average IS energy, obtained from analysis of V. Angelani *et al* calculated the temperature dependence of these three observables [72]. They obtained the following results. (1) For different Lennard-Jones systems $\langle n_s(T)\rangle$ seems to disappear after extrapolation on a linear scale close to some temperature T_c which turns out to be close to the mode-coupling temperature T_{MCT}; see section 2.2 for a short description of the mode-coupling theory. These results are shown in figure 9. The authors conclude that the mechanism of the dynamics is changing around T_c. Whereas for $T > T_c$ the system explores basins of W related to saddle points, below T_c the system spends most of its time close to IS. Thus, the presence of IS only becomes important for temperatures around T_c. In particular this seems to imply (in agreement with the INM analysis) that the diffusion process is entropy driven, i.e. not governed by barrier crossing events. (2) $\langle e_s(T)\rangle - \langle e(T)\rangle$ scales linearly with $\langle n_s(T)\rangle$. This implies that there is a fixed energy difference Δe between pairs of minima of W for which the saddle index differs by one. Comparing different systems one finds $\Delta e \propto T_c$ [73]. These findings suggest that the properties of the PEL around an IS are highly regular and do not depend on the energy of the IS.

A related but somewhat different analysis has been performed by Grigera *et al* [74]. In that work e_s is correlated with n_s (using the above notation). They observe that the average saddle point index n_s for a given energy e_s is roughly linearly correlated with e_s. Again, after linear extrapolation to low e_s one can define a threshold energy e_{th} below which (in the sense of that extrapolation) one has $n_s = 0$, i.e. all low-energy saddle points are minima. The critical temperature T_c related to this energy in equilibrium is again close to T_{MCT}. The authors conclude that the change in behavior when going below T_c, and thus T_{MCT}, is geometric in nature. Basically, this interpretation agrees with the analysis of Angelani *et al*, described above. Similar results have also been reported in [75].

Another aspect of this work is the determination of barrier heights. Starting from a saddle point with unit index they determine the minima on both sides of that saddle. From this the authors obtain the barrier height, defined as the energy difference between saddle point and minimum energy. The results are shown in figure 10. First, the barriers which are related to minima around e_{th} are of the order of $10T_c$, which agrees with a corresponding estimate in [73]. Second, they find that ISs with lower energies have higher barriers. If plotted against the total IS energy, the slope in the linear low-energy regime is around -0.5. These results will be taken up again in section 5.3.

This type of analysis yields relevant information about the nature of the PEL. However, one important problem has been mentioned in the literature [53, 76]: the disappearance of

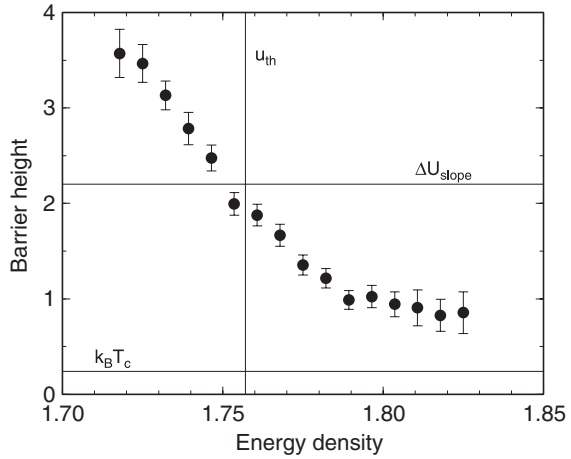

Figure 10. The typical barrier height for an IS, obtained from finding the two minima, related to a saddle point configuration and calculating the difference in energy. The simulations have been performed for a soft-sphere system with $N = 70$ particles. Note that the x-axis displays the energy per particle. The variable u_{th} is denoted e_{th} in the text. Reprinted with permission from [74]. Copyright 2002 by the American Physical Society.

$\langle n_s(T)\rangle$ at T_c is only apparent. A closer analysis shows that it just displays an Arrhenius behavior, i.e. there is no change in mechanism around T_c; see section 3.6. Actually, in the IS approach, discussed in the later part of this review, the energy scale e_{cross} rather than e_{th} turns out to be relevant. This is the energy from which point on the barrier height starts to increase for decreasing energies (see figure 10). Central quantities such as the fragility can be explicitly expressed in terms of e_{cross}.

1.4. Scope of the article

The main topic of this review is the description of the equilibrium properties of supercooled liquids in terms of properties of the PEL (neglecting, of course, the crystalline contributions which would be present in true equilibrium). Unfortunately, to stay focused many important properties of supercooled liquids cannot be explicitly discussed (e.g. aging, rotational dynamics of non-spherical elementary units, shear effects, ...). In many of these problems, the concepts discussed in this work can be very fruitfully applied (e.g. describing aging in terms of the PEL [77]). Special emphasis is given to the description of the underlying concepts. Furthermore, the relation of the PEL approach to other theories and models of the glass transition is explicitly discussed.

1.4.1. Hierarchy of questions. For a simple one-dimensional model PEL with seven ISs (denoted IS_1, ..., IS_7), shown in figure 11, a set of questions and problems is formulated which have to be answered in the process of understanding the dynamics in this PEL. These questions will correspond to the different sections in this review. Of course, the configuration space of a real supercooled liquid is highly multi-dimensional rather than one-dimensional.

(1) *Thermodynamics* (section 3). Characterizing the location of the particle at a randomly chosen time at sufficiently low temperatures (qualitatively, $T \ll$ barrier heights) requires knowledge about the nature of the different ISs, i.e. their energy distribution and the curvature at the minima. In contrast, in the limit of high temperatures the full basin of attraction, i.e. the region from the minima up to the respective saddles, matters for the thermodynamics. Both scenarios can be distinguished by analysis of the equilibrium population of the barriers. Only in the latter case will a significant population of the high-energy regions be observed.

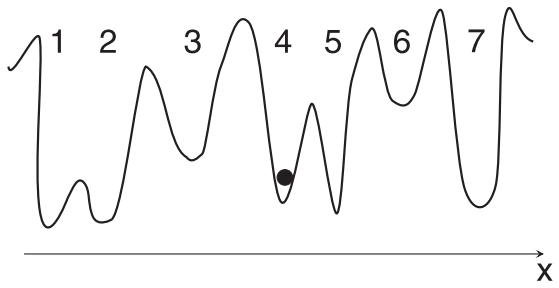

Figure 11. A one-dimensional model PEL for the general discussion.

(2) *Leaving an IS* (section 4). First, there is the obvious question about the elementary transition between two adjacent ISs. For a given pair of ISs the transition rate mainly depends on the barrier height. Thus, even for low temperatures, transitions between IS_1 and IS_2 may still occur on relevant timescales. This is important for the so-called low-temperature anomalies [78–80]. Analyzing the escape from IS_3 a second question emerges. Because a transition to IS_2 is faster than a transition to IS_4, very likely the particle will first jump back to IS_2 before much later the rest of the configuration space can be explored. For a disordered PEL the presence of correlated forward–backward jumps between ISs turns out to be a central property. Having this in mind one may be interested in the rate with which a particle *effectively* leaves an IS, i.e. just returns with a small statistical probability. For the model PEL the effective escape from IS_3 would be complete after the barrier to IS_4 is crossed. Thus, two different waiting times can be defined: (1) the time to leave an IS; (2) the time to effectively leave an IS. In general, the latter can be much longer and is finally relevant for the relaxation properties.

(3) *Relation between energy and effective waiting time* (section 5). The timescale for a effective escape from IS_3 is similar to that of IS_1 (or IS_2) because it is most likely that the particle at IS_3 first jumps to IS_2 before entering IS_4. Thus, no clear relation between IS energy and effective waiting time can be formulated. This problem disappears if one considers a coarse-grained PEL where IS_1–IS_3 and IS_4–IS_5 are regarded as single elementary states with an allocated energy of IS_1 and IS_5, respectively. In contrast, IS_6 and IS_7 are not modified. These states will be denoted metabasins (MBs). Thus, for our model PEL four MBs (IS_1–IS_3, IS_4–IS_5, IS_6, IS_7) exist. On the level of MBs a significant relation between energy and waiting

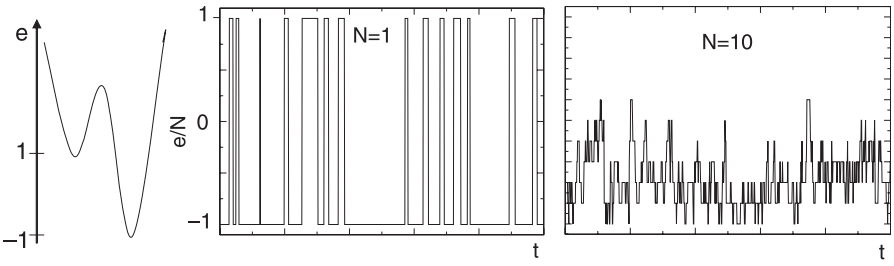

Figure 12. Time dependence of the energy of one (left) or ten (right) particles in independent asymmetric DWPs.

time is expected. For example, the third MB, originally denoted IS_6, possesses the highest energy and the shortest waiting time. Furthermore, with this choice the effective escape from IS_3 is governed by the effective escape from IS_1 and thus determined by the energy of IS_1. On the level of MBs we no longer have to distinguish between waiting time and effective waiting time. Furthermore, a dramatic reduction of correlated forward–backward jumps is expected. Of course, the present description of MBs is just qualitative. It becomes more quantitative in section 5.

(4) *Averaged local dynamics* (section 6). Knowing the energy distribution of MBs and the relation between energy and waiting time it is, of course, possible to calculate the average waiting time. This quantity turns out to be very important because it is directly related to the diffusivity. Furthermore, the temperature dependence of the average waiting time is directly related to the question of fragility. This will allow us to suggest which PEL parameters influence the fragility.

For the model PEL it would be sufficient to know the waiting times of the different (and countable) MBs to predict quantities such as the diffusivity. For glass-forming systems there is no possibility to obtain a systematic enumeration of the PEL because of the exponentially large number of ISs (and MBs). Rather, one has to rely on a finite sample, obtained, e.g., from a finite-time MD simulation. Since both ingredients, mentioned above, can be obtained from a finite set of ISs (or MBs) a statistical approach is easy to implement. Of course, the results of the statistical analysis can be compared with phenomenological approaches which try to capture the essential properties of the PEL.

(5) *Exploration of the whole configuration space and the relation to the real space properties* (section 7). In the last step one has obtained information about the waiting time of an MB. In the model PEL the global dynamics can be basically described as a random walk between the four MBs. *A priori* it is not clear whether this also holds for the high-dimensional PEL of a glass-forming system. Furthermore, to describe the transport and thus to calculate observables such as the diffusion constant or the incoherent scattering function one needs to know the real space realization of the transitions between MBs.

(6) *Dependence on system size* (section 8). Going beyond the simple model PEL one always has to take into account that a PEL depends on the choice of the system size. For example, one has to tackle the important question about the optimum system size to extract the relevant processes for the slowing down of the dynamics. For most types of simulations it is best (apart from possible computer time or memory problems) to use systems as large as possible [12]. This does not hold if one wants to analyze the PEL. To illustrate the problem we analyze the dynamics of a particle in an asymmetric DWP with energies at -1 and $+1$ and with a population difference of 4:1. In figure 12 we show the time-dependent energy, obtained from a simple Monte Carlo simulation. These data allow one to reconstruct the underlying physical situation. The resulting energy histogram is bimodal with the correct population ratio of 4:1 (apart from noise). Additionally, we consider the case where one has ten particles which independently jump in their respective DWPs. The temporal evolution of the average energy is also shown in figure 12. Basically, these data look like white noise and in particular do not reflect the underlying physics of a DWP. Thus, the energy histogram would not reveal the underlying bimodality of the individual DWP because of a trivial superposition effect.

This is exactly what happens when performing the PEL analysis for very large systems. The waiting time distribution becomes very narrow and specific properties of the energy histogram trivially disappear, leading to a reduction of the information content. Therefore, it is advantageous to choose system sizes which are, on the one hand, as small as possible but which, on the other hand, do not show relevant finite-size effects. To a first approximation the large system can then be regarded as a superposition of independent subsystems.

(7) *Length scales* (section 9). If these subsystems are fully independent the maximum length scale of cooperative dynamics would be given by the size of these subsystems. Naturally, due to its spatial proximity adjacent subsystems (in real space) will have some kind of interaction if a macroscopic system is considered. It will be explored whether this interaction may give rise to a length scale extending the size of the individual subsystems. This aspect is crucial for the question of whether the PEL approach may contain the possibility of temperature-dependent length scales.

This closes the logical string of problems which has to be solved for a broader understanding of the properties of supercooled liquids in terms of the underlying PEL.

1.4.2. Computer simulations. A lot of insight in this field naturally stems from computer simulations. However, the simultaneous development and analysis of concepts to describe the PEL are essential for an appropriate interpretation of simulation results. Most simulation results will be reported for constant volume. Conceptually, the analysis at constant volume is easier to perform than at constant pressure. As discussed, e.g., in [81, 82] the density changes at constant pressure have only little influence on the nature of the glass transition and the degree of fragility remains constant when changing the pressure [83]. In a few cases, the PEL at constant pressure has also been analyzed in the literature [84, 85] and a consistent analysis in terms of PEL properties has been presented [86]. Furthermore, characterization of the PEL has been performed also as a function of volume [87].

In recent years many systems have been studied via computer simulations [88]. In this review we particularly refer to the BKS model of silica (BKS-SiO_2) [89] and the binary mixture Lennard-Jones system (BMLJ), which is one of the prototype computer glass-forming systems. This was first introduced by Stillinger [90] and then improved and first systematically analyzed by Kob and Andersen [91, 92]. In its standard version it contains 80% large and 20% small particles. Other important potentials, used in the study of the PEL properties, are that of orthoterphenyl [93] and the Dzugatov potential [94]. Water has also been studied extensively; see, e.g., [95, 96]. Due to the fast hydrogen dynamics it seems that one has strong fluctuations even in the IS energy time series. This somewhat hampers a clear-cut analysis of the dynamics in terms of energies. To study small systems it is, of course, necessary to use periodic boundary conditions in order to recover properties of supercooled liquids rather than those of clusters. Whether the PEL is explored via molecular dynamics or Monte Carlo routines is, for most questions that are raised in this work, of minor relevance (exceptions are, e.g., the determination of dynamic susceptibilities such as $\chi_4(t)$ [97–99]).

2. Theoretical approaches for glass-forming systems

In this section alternative theoretical approaches are briefly summarized. We will start with the mode-coupling theory which results from the description of the liquid [100]. Activated processes do not explicitly appear in this approach. In particular there is no direct reference to the PEL. Many other approaches directly start from a phenomenological characterization of the nature of activated processes. It is generally accepted that somewhat above the glass transition temperature the particle rearrangements correspond to localized collective dynamical processes. Thus, these approaches have to tackle the following questions in order to characterize the relaxation of a glass-forming system.

- What is the elementary subvolume for which the relaxation processes are described?
- What is the free energy barrier for the activated transition?
- How do fluctuations enter?
- How do adjacent elementary subvolumes interact with each other?

2.1. Mode-coupling theory

A very well established theoretical framework is the mode-coupling theory, promoted in particular by Götze and co-workers [100, 101]. The key approximation is based on the assumption that the relevant slow variables are the pair-density modes. Starting from the static structure factor, predictions are then made for different dynamic observables. Since the structure itself can be obtained from the microscopic Hamiltonian of the system, the mode-coupling theory can be regarded as a first-principle approach. In its standard version it predicts a divergence of transport quantities around some temperature $T_{\rm MCT}$ which is far above the calorimetric glass transition temperature $T_{\rm g}$. This divergence is not seen experimentally. In practice, the value of $T_{\rm MCT}$ can be extracted from quantities like the diffusion constant by fitting $D(T)$ with a power law $(T - T_{\rm MCT})^{-\gamma}$ for a temperature range above $T_{\rm MCT}$. This artificial divergence is typically related to the factorization approximations, inherent in the mode-coupling approach. It has been speculated that this approximation corresponds to a neglect of activated processes [100, 102, 103], which can be included by additional consideration of current modes. This would imply a change of the dynamic mechanism around $T_{\rm MCT}$. Recently, however, it has been suggested that these modes are not relevant to avoid the MCT singularity [98, 104, 105].

However, many non-trivial predictions of the mode-coupling theory for temperature above $T_{\rm MCT}$ have been successfully compared with experimental and simulated data. In particular, the scaling properties of the fast β-relaxation regime are often in very good agreement with experiments or simulations [101]. It turns out, however, that the predictions for the absolute values of quantities like the non-Gaussian parameters are far too small [106]. Recently, a generalized version of the mode-coupling theory has been suggested in which a non-perturbative limit has been implemented [107]. This approach avoids the divergence at a finite temperature. Thus, one may speculate that in this version of the mode-coupling theory activated processes are somehow included. Furthermore, by adding external static inhomogeneous potentials dynamic length scales can be extracted within the MCT formalism, which diverge at $T_{\rm MCT}$ [108, 109]. It turns out that $\xi_{\rm coll} \propto (T - T_{\rm MCT})^{-\nu}$ with $\nu = 1/4$. This yields $D(T) \propto \xi_{\rm coll}^{z}$ with $z = 8$, in good agreement with recent numerical data for BMLJ [47]; see section 1. Interestingly, already in old work by Götze and Sjögren [110] it has been stated that the mode-coupling results are consistent with a picture of particle motion in an energy landscape where its dynamics is characterized by an algebraic waiting time distribution (see also section 7).

Schweizer *et al* [111–113] use nonlinear Langevin equations of barrier hopping with a distribution of local barriers, depending on the respective local structure. In this way they combine the MCT approach with concepts from statistical dynamical theories. This approach corresponds to a dynamically defined landscape. In this way observations such as violation of the Stokes–Einstein relation can be naturally described; see below and section 6.4.

2.2. Characterization of activated processes via thermodynamic approaches

2.2.1. General. To characterize the rearrangement of particles in a volume $(\xi^\star)^3$, comprising $N^\star$ particles, two major effects have to be taken into account for estimating the relaxation rate. First, the rate $\Gamma(T, \xi^\star)$ is proportional to the number of accessible states. This number can be estimated as $\exp(N^\star s_c(T))$, where $s_c(T)$ is the configurational entropy per particle; see section 3. This somewhat phenomenological approach implies that the number of relevant escape paths from a typical initial state is directly related to the equilibrium number of accessible final states. Second, the activation energy $V(T, \xi^\star)$ determines the energy cost to cross the barrier between both states. In total one obtains ($\beta = 1/T$)

$$\Gamma(T, \xi^\star) \propto \exp(N^\star s_c(T)) \exp(-\beta V(T, \xi^\star)). \qquad (7)$$

Note that the total relaxation processes can be very complex in nature and may contain many individual steps. The general approach explicitly relates thermodynamic and dynamic properties. Different models differ by the choice of the activation energy and of the elementary subvolume.

2.2.2. Adam–Gibbs approach. Adam and Gibbs [114] call an elementary subvolume a *cooperatively rearranging region* (CRR). They claim that the system chooses a CRR by the condition that the configurational entropy $s_{c,CRR}(T) = N^\star s_c(T)$ has a temperature-independent small value B (e.g. $\ln 2$), i.e. some fixed number of new configurations is thermodynamically accessible. Since $s_c(T)$ decreases with decreasing temperature, the size of the CRR increases with decreasing temperature. The energy barrier is chosen to be proportional to the volume of the CRR, i.e. proportional to $N^\star$. This assumption is quite ad hoc. As a consequence, one has $V \propto N^\star = B/s_c(T)$. On this basis the relaxation rate can be written as ($B_{AG} \propto B$)

$$\Gamma(T) = \Gamma_0 \exp(-B_{AG}/T s_c(T)). \qquad (8)$$

If the configurational entropy s_c vanishes at a specific temperature, thereby defining the Kauzmann temperature T_K, the dynamics would become infinitely slow. The CRRs are considered to be independent of each other.

To check the quality of the Adam–Gibbs (AG) relation equation (8), one may compare $s_c(T)$ with $D(T)$ (which may be assumed to be proportional to the local relaxation rate (see section 7)). For simulations a reasonable agreement with the AG relation can be found for OTP [115], BMLJ [84] (see figure 13), and for water [116, 117]. However, for BKS-SiO_2 [118] and the Dzugutov liquid [119] $D(T)/T$ rather than $D(T)$ fulfills the AG scaling. Experimental data are also reported to be fitted quite well by equation (8) for sufficiently low temperatures [120].

One of the central assumptions of the AG relation has been explicitly checked in [117]. For this purpose the average cluster size z of the relaxation process has been compared with $1/s_c(T)$, yielding $z - 1 \propto 1/s_c(T)$ over a limited range of temperatures. In later work the Glotzer group has checked

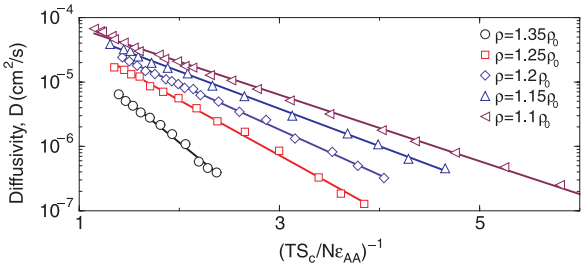

Figure 13. Adam–Gibbs scaling for BMLJ. The AG relation is fulfilled for different densities. Reprinted by permission from Macmillan Publishers Ltd: *Nature* [84] copyright 2001.

that not only cluster sizes but also string sizes fulfill a similar relation [119]. They claim that strings are better candidates than clusters because they are smaller in size.

The theoretical foundation of the AG approach has been critically discussed [14, 121]. Points of criticism are the purely phenomenological character of the model, the small size of CRRs at T_g, of the order of a few molecules [122], and the problem of identifying the configurational entropy $s_c(T)$ with the total excess entropy (glass minus crystal) for the experimental validation. Furthermore, as argued in [123], it is possible to construct different model potentials with the same configuration entropy $s_c(T)$ but with different kinetics. This somewhat limits the possible generality of equation (8), unless there exist some subtle relations between the energy scales of the PEL in real systems (see section 6.3.2).

2.2.3. Kirkpatrick–Thirumalai–Wolynes approach. Kirkpatrick, Thirumalai and Wolynes have presented somewhat similar ideas but on a much stronger theoretical basis [124, 125]. Their approach is partly guided by the physics of mean-field spin-glasses where below a critical temperature (the analog of T_{MCT}) ergodicity is broken and the system is trapped close to one of the exponentially large number of metastable states. For non-mean-field systems like supercooled liquids one may postulate that a similar freezing effect happens, albeit with restoration of ergodicity on large timescales via activated processes.

They denote the separation into elementary subvolumes the *mosaic structure*. To estimate $V(T, \xi^\star)$ they consider the elementary volume as a droplet, immersed in the surrounding medium. In contrast to Adam and Gibbs they do not fix the configurational entropy of the elementary volume but rather request that $\Gamma(T, \xi^\star)$ is a maximum with respect to $\xi^\star$ ($(\xi^\star)^3 \propto N^\star$). The energetic penalty for rearrangement is assumed to be mainly due to the surface energy $V(T, \xi^\star) = 4\pi(\xi^\star)^2\sigma(\xi^\star)$ with the surface tension $\sigma(\xi^\star) \propto (\xi^\star)^{-1/2}$ [125]. The latter ingredient is based on the random first-order transition (RFOT) theory. The RFOT theory takes into account the random contributions to the surface tension which allows the system to reduce the surface tension for large droplets. This is analogous to the interface of spin-up and spin-down regions in the random field Ising model [15, 124]. With this contribution one finally obtains $V(T, \xi^\star) \propto (N^\star)^{2/3}(N^\star)^{-1/6} \propto (N^\star)^{1/2}$. Together with the entropic term, equation (7), one has to minimize the

free energy barrier $\Delta F(N^\star) = \gamma(N^\star)^{1/2} - N^\star T s_c(T)$ with respect to $N^\star$. Most likely, transitions will occur on this length scale. Naturally, at lower temperatures the energetic mismatch becomes more relevant, which increases the resulting length scale. With the same argument as above $\xi^\star$ will diverge for $T \to T_K$. However, whereas in the Adam–Gibbs scenario the entropy per elementary unit is constant, in the mosaic picture the entropy per elementary volume increases with decreasing temperature and also diverges at T_K [121]. One obtains for the minimum free energy barrier

$$\Delta F^\star = \frac{\gamma^2}{4 s_c(T) T}. \tag{9}$$

Formally, this is identical to the AG relation in equation (8). The value of γ can be estimated from general arguments [125].

In equilibrium the fluctuations of the entropy density are related to the specific heat [34, 126] via $\langle \delta s_c^2 \rangle \propto c_p$. Here c_p corresponds to the specific heat, related to the configurational degrees of freedom. Via equation (9), fluctuations in entropy directly translate into fluctuations of the free energy barrier, yielding a distribution $p(\Delta F)$. Thus, within this approach the different parts of the mosaic are described by a distribution of free energy barriers. Using Gaussian fluctuation theory and choosing some reasonable assumption for the temperature dependence of the entropy, it is finally possible to characterize a glass-forming system by the single parameter $c_p(T_g)$.

As a consequence, many relevant observables such as the fragility as well as the non-exponentiality (based on the distribution of free energy barriers) can be expressed in terms of Δc_p [125]; see also section 6.4. It turns out that non-exponentiality and fragility are strongly correlated. Unfortunately, the degree of non-exponentiality is far too strong. This can be cured by a modification of the distribution of free energy barriers ΔF. When claiming that all free energy barriers with $\Delta F > \Delta F^\star$ are shifted to $\Delta F^\star$, a very good agreement with experimental data is found. The authors rationalize this modification by possible deviations from spherical droplet sizes [125] and later on by the presence of dynamic coupling effects with surrounding regions [15]. This is exactly the mechanism that will be discussed in section 9.

Another important implication is the relation of the fragility to thermodynamic properties via the empirically observed relation [127]

$$m_{\rm kin} \propto \frac{T_g \Delta c_p(T_g)}{\Delta H_m}, \tag{10}$$

where Δc_p corresponds to the specific heat difference of liquid and glass and ΔH_m describes the melting enthalpy. Subsequently, this expression could be derived within the RFOT approach with a similar prefactor [128].

In the context of the RFOT approach the overlap distribution of many low-energy states was analyzed for a Lennard-Jones system at low temperatures [129]. The overlap of two distributions measures the fraction of particles in the second structure which is close (defined via some cutoff) to a particle in the first structure. It turns out that the overlap distribution is unstructured and similar to the distribution of liquid states. In contrast, in spin-glass theory one expects for this quantity a bimodal distribution in the range of one-step replica symmetry breaking [130]. This is one indication that the understanding of the glass transition of structural glasses may be distinct from understanding mean-field spin-glass behavior. Very recently this question has also been analyzed in [131]. These authors study the dynamics within a sphere of variable radius r with fixed boundary conditions. From the absence of any dramatic dependence on r they conclude that a critical length scale $\xi^\star$ cannot be identified from computer simulations.

2.2.4. Further approaches. Another model, based on thermodynamic considerations, has been formulated by Kivelson, Tarjus and others [132]. It is argued that the immobilization at low temperatures is related to an avoided second-order phase transition (frustration-limited domain approach).

From general considerations of the properties of complex systems as well as the assumption of time–temperature superposition, Ngai has formulated the coupling model, which relates the relaxation in the α-relaxation regime to a faster timescale [133]. In his general scheme he has introduced three central timescales to characterize cooperative relaxation. Whereas t_c denotes the time from which point on collective dynamics becomes important, t_0 describes the timescale of microscopic exponential relaxation. Finally, the relaxation is described by a stretched exponential with timescale $\tau_{\rm KWW}$ and non-exponentiality parameter $n = 1 - \beta_{\rm KWW}$. From the continuity requirements he obtains the relation $\tau_{\rm KWW} = [(1-n) t_c^{-n} t_0]^{1/(1-n)}$ [133]. This can be used, e.g., to correlate properties in the β- and α-regime by identifying t_0 with the Johari–Goldstein β-relaxation timescale [133, 134].

A very different class of models relates the energy barrier of a relaxation process to the elastic properties of the system; see [14] for an overview. The key idea is that the IS force constant, determining the local vibrations as well as properties such as the shear modulus, is proportional to the barrier height to leave this IS. In this way one can derive a proportionality between the temperature dependence of the shear modulus G_∞ and that of the activation energy. Within a field-theoretical approach long-wavelength relaxation modes turn out to be dominant for relaxation [135].

Finally, some workers have also promoted the analysis of the *free* energy landscape (FEL) to characterize the glass transition; see, e.g., [136–140]. For example, one can start with the Ramakrishnan–Yussouff free energy functional [138]

$$F(\alpha) = -F_{\text{ideal gas}} - (T/2) \int \mathrm{d}\vec{r} \int \mathrm{d}\vec{r}'[n(\vec{r}) - n] \times C(|\vec{r} - \vec{r}'|)[n(\vec{r}') - n] \tag{11}$$

with

$$n(\vec{r}) \propto \sum_i \exp[-\alpha(\vec{r} - \vec{r}_i)^2] \tag{12}$$

where the $\vec{r}_i$ are the positions of the N particles of the system. Furthermore, $C(r)$ is the direct correlation function of the liquid [138] and n the average density. Application of this

functional to the hard-sphere system at different densities shows that in the limit of high densities the minimum of the free energy with respect to α is lower than the free energy of the uniform state. Interestingly, the crossover density $\tilde{n}$ corresponds to the density which is obtained by fitting the relaxation time to a power law $\tau \propto (n - \tilde{n})^{-\gamma}$ [138]. This suggests a relation between the energetics via the free energy and the resulting dynamics.

2.3. Models about defect motion and facilitated spins

Already in old work by Glarum the idea has been expressed that the dynamics of defects is a key element for the dynamics in supercooled liquids [141]. It has been assumed that the arrival of the defect triggers a local relaxation process. Unfortunately, for a three-dimensional system a diffusing defect cannot induce non-exponential behavior [142]. Only if the defect dynamics can be described by a broad distribution of waiting times with infinite first moment, stretched exponential relaxation is obtained [143, 144].

Somewhat similar ideas have been expressed via dynamic facilitation models, also denoted kinetically constrained models (KCMs) [145–148]. A real molecular liquid is coarse grained over a short time period and a small volume. Then the coarse-grained volume is in one of two possible states (jammed and unjammed regions—equivalently spin up and spin down). To account for a temperature dependence of the fraction of unjammed states one formally attributes a energy difference to both states so that their ratio is governed by a Boltzmann distribution. In the limit of zero temperature all states are jammed. The crucial assumption is that a state can only switch between both states if at least one neighbor is unjammed. At low temperatures, where unjammed states are rare, this basically leads to the picture of moving defects in the same spirit as the Glarum picture. This defines a length scale ξ_{defect} as the typical distance between these defects. In contrast to the previous models, the timescale of relaxation displays a power law rather than an exponential dependence on ξ_{defect}. If this class of models indeed describes the physics of supercooled liquids, the AG relation would be physically irrelevant because entropy does not play any role here and thus cannot determine the dynamics. Non-Arrhenius temperature dependence, and thus fragile systems, are often related to the East model [146], which is a non-isotropic KCM.

In the spirit of the general questions posed above, the KCM has a trivial local dynamics if the mobility is non-zero. The complexity stems from the interaction of adjacent spins corresponding to adjacent regions of the system, which gives rise to a dynamic length scale. Thus, ξ_{defect} can be qualitatively related to the collective length scale ξ_{coll}. It has been checked in simulations that mobile regions of a glass-forming systems are indeed spatially correlated [149, 150].

In order to study translational diffusion for the facilitated spin model a probe molecule was added [148]. Whenever the site of the probe molecule is mobile it can randomly jump to an adjacent site. Detailed balance is guaranteed by the condition that the new site has to be mobile as well. In this way it is possible to define a probe diffusion constant.

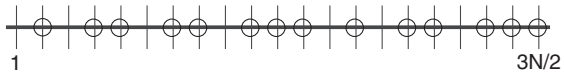

Figure 14. Sketch of an IS of the toy model discussed in the text.

Some basic questions emerge when trying to describe a molecular supercooled liquid in terms of a dynamic facilitation model. Are mobile regions indeed *strictly* correlated, i.e., fulfill the facilitation principle? If yes, a mobile region is only mobile because it was triggered by an adjacent region to become mobile. Do strong and fragile systems belong to different topologies of the phase space? Is there a molecular basis for the directional persistence of the East model? Does the bimodality of the local relaxation motion (fast or immobile, depending on the neighborhood) capture the general physical features of the local variability of possible transition processes?

In section 9 a model is suggested which combines the PEL and the facilitation approach and which is derived from observations for molecular glass-forming systems.

3. Individual inherent structures and thermodynamics

3.1. Number of inherent structures

Here it is discussed how the absolute number of ISs G_N^∞ and the number of adjacent ISs depend on the system size N.

3.1.1. Simple toy models for the PEL. A simple model to visualize the positions of ISs in the high-dimensional configuration space is the corners of a hypercube. Each corner is characterized by series $(i_1, \ldots, i_N)$ with $i_n \in 0, 1$ [151] which is equivalent to spins in a one-dimensional Ising model. Accepting this mapping one trivially has $G_N^\infty = 2^N = \exp(\alpha N)$ ISs with $\alpha = \ln 2$. The number of ISs with just one different spin orientation may be interpreted as the number of adjacent ISs. This is consistent with the locality of transitions between ISs: its number is exactly N, corresponding to the N possible spin flips in the related Ising model.

This model suffers from the fact that no particle motion is involved. Due to the importance of these scaling relations with the system size N, another simple toy model is briefly discussed, explicitly based on particles. One considers a one-dimensional lattice of length $3N/2$ (with periodic boundary conditions) on which N particles are distributed (for reasons of simplicity one may take N to be even). An IS is defined by the condition that two adjacent particles are on lattice sites j and $j + 1$ or j and $j + 2$; see figure 14. This condition reflects the fact that low-energy states typically display a homogeneous particle density, i.e. do not possess large voids. Of particular interest is the absolute number of ISs G_N^∞ as well as the number of adjacent ISs. For this model an adjacent IS is defined as an IS which is accessible by the move of only one particle. The latter condition again reflects the fact that transitions between ISs occur on a localized spatial scale.

In appendix A it is shown that $\alpha = \ln 2 - \ln N/(2N)$ and that the number of adjacent ISs is given by $f(N)N$ with $f(N) = 0.5/(1 - 1/N)$. Thus, for large N this model has

the same scaling relations for the total number of ISs and the number of nearest neighbors as the hypercube model.

One might be tempted to regard the ISs as homogeneously distributed over the N-dimensional phase space. If this is true, the N scaling of the number of adjacent ISs should be identical to the N scaling of the N-dimensional unit sphere, which is $V_N \propto \pi^{N/2}/\Gamma(N/2+1)$. This is very different to a simple N scaling. The reason is that for a homogeneous IS distribution the locality of this IS transition is neglected.

Recently, a model of aligned 2D hard discs has been studied, which can also be mapped on a series of 0 and 1 [152]. A more complex but still analytically solvable 1D model has been analyzed in [153].

3.1.2. General statements. The scaling relations can also be obtained from more general arguments. The key assumption is the *factorization hypothesis*. It states that for system sizes larger than some critical system size N^* the system can be divided into N/N^**independent* subsystems [59, 125, 154–156]. Stated differently, in a macroscopically huge sample of a glass-forming system the dynamics of a group of molecules does not influence the dynamics of another group of molecules, which is 1 m away. Of course, N^* can still be a very large number. For short-range potentials, which are present for molecular glass-formers, this hypothesis is generally believed to be true. In [156] it has been strictly demonstrated that even a small interaction among adjacent subsystems does not change the nature of the results, obtained from the assumption of independent subsystems. This hypothesis, e.g., rationalizes why the number of low-energy excitations such as the tunneling systems (see section 4), is proportional to the system size. As an immediate consequence of the factorization hypothesis the number of adjacent ISs has to be proportional to the system size. Furthermore, for $N > 2N^*$ one can write

$$G_N^\infty = [G_{N/2}^\infty]^2. \tag{13}$$

This functional relation is exactly fulfilled for $G_N^\infty = \exp(\alpha N)$. These arguments have also been generalized to the number of saddle points for which the N scaling has been derived analytically [156, 157]. They are identical to the analogous question of why the entropy is an extensive observable.

Finally, we introduce $G(e)$ as the number density of ISs with energy e. For very small systems $G(e)$ can be obtained from counting. For example, for an LJ system with $N = 32$ particles the relevant low-energy ISs have been identified [158]. For larger systems no systematic counting is possible and one has to resort to statistical methods (see below). Nevertheless, via extensive simulations specific information about the low-energy regions can also be obtained here [159].

3.2. The partition function

3.2.1. Different contributions to the partition function. First we consider the configurational part of the partition function

$$\begin{aligned} Z(T) &\equiv \int \mathrm{d}\vec{r}_1 \ldots \mathrm{d}\vec{r}_N \exp(-\beta V(\vec{r}_1, \ldots, \vec{r}_N)) \\ &\equiv \exp(-\beta A_{\mathrm{total}}(T)). \end{aligned} \tag{14}$$

A_{total} denotes the free energy and $\beta = 1/T$. The key idea is to rewrite $Z(T)$ in terms of contributions from the individual ISs as well as their corresponding basins of attraction. Ω_i is defined as the set of points in configuration space which, upon minimization, end up in inherent structure i with energy e_i. Since the mapping of configurations on inherent structures via energy minimization is unique (except for a set of configurations with measure zero, corresponding to the saddle points of the PEL), the total configuration space can be decomposed into disjoint partitions Ω_i. A similar reasoning in the context of broken ergodicity can be found in [160]. Thus one can write $Z(T) = \sum Z_i(T)$, where the $Z_i(T)$ describe the configurational part of the partition function, restricted to the basin of attraction of the ith IS, i.e. Ω_i. Z_i can be conveniently rewritten as

$$Z_i = \exp(-\beta e_i) \exp(-\beta A_{\mathrm{vib},i}) \tag{15}$$

stressing the separation of the contributions from the minimum of basin i itself and the vibrational degrees of freedom. At low temperatures $A_{\mathrm{vib},i}$ is dominated by the harmonic fluctuations around the minimum. One may therefore introduce $A_{\mathrm{harm},i}$ as the harmonic contribution to the total free energy, i.e.

$$\beta A_{\mathrm{harm},i}(T) = \sum_{j=1}^{3N} \ln(\beta\hbar\omega_{j,i}) \tag{16}$$

where $\omega_{j,i}$ denotes the jth eigenmode frequency of basin i. Here we have used the classical partition function of an harmonic oscillator. Finally, one may write

$$Z_i = \exp(-\beta e_i) \exp(-\beta A_{\mathrm{harm},i}(T)) \exp(-\beta A_{\mathrm{anh},i}(T)) \tag{17}$$

where the remaining contribution to $A_{\mathrm{vib},i}$ is denoted $A_{\mathrm{anh},i}$, i.e. the anharmonic parts of the total free energy. It describes the deviations from purely harmonic behavior, e.g. by the influence of the finite size of any basin.

Anticipating that the energy e_i is the key parameter which characterizes the basin i, one may combine all contributions of inherent structures with the same energy e. It turns out that to an excellent approximation

$$\exp\left(\left\langle \sum_{j=1}^{3N} \ln(\beta\hbar\omega_j) \right\rangle'\right) \approx \left\langle \exp \sum_{j=1}^{3N} \ln(\beta\hbar\omega_j) \right\rangle' \tag{18}$$

where the average is over all states with energy e (indicated by the prime) [161]. Thus one can write for the total partition function $Z(T)$

$$Z(T) = \int \mathrm{d}e\, G(e) \exp(-\beta(e + A_{\mathrm{harm}}(e,T) + A_{\mathrm{anh}}(e,T))) \tag{19}$$

with $A_{\mathrm{harm}}(e,T) = \langle A_{\mathrm{harm},i}(T)\rangle'$ and $G(e)$ defined in section 3.1. Again, the term $A_{\mathrm{anh}}(e,T)$ accounts for possible anharmonic effects.

Via

$$\beta A_{\mathrm{harm}}(e,T) = \left\langle \sum_{j=1}^{3N} \ln(\hbar\omega_j/\hbar\omega_0) \right\rangle' + \left\langle \sum_{j=1}^{3N} \ln(\beta\hbar\omega_0) \right\rangle' \tag{20}$$

$$\equiv F_{\mathrm{harm}}(e) + G_{\mathrm{harm}}(T) \tag{21}$$

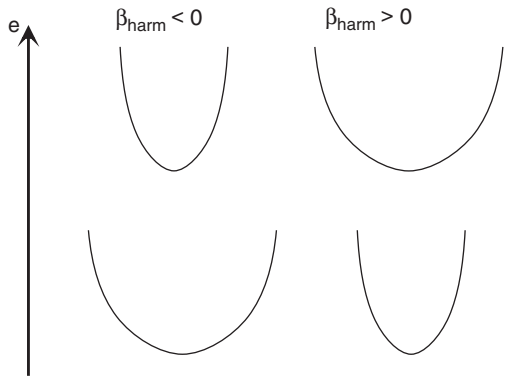

Figure 15. A sketch of the cases $\beta_{\rm harm} < 0$ and $\beta_{\rm harm} > 0$. Shown are typical curvatures around representative ISs at different energies.

$\beta A_{\rm harm}(e, T)$ can be decomposed into an energy-dependent and a temperature-dependent part. ω_0 is some arbitrarily chosen frequency. This decomposition will be important for the later analysis. We note in passing that recently the partition function has been extended to take into account contributions from regions around saddles [162].

$F_{\rm harm}(e)$ is easily accessible by first calculating and then diagonalizing the Hessian matrix in different ISs. For different systems it has been shown in this way that to a very good approximation one has a linear energy dependence for $F_{\rm harm}(e)$ [84, 115, 163–167], i.e.

$$F_{\rm harm}(e) = \text{const} - \beta_{\rm harm} e. \tag{22}$$

The constant $\beta_{\rm harm}$ is a material constant. The meaning of the sign of $\beta_{\rm harm}$ is visualized in figure 15. Then in the harmonic approximation the vibrational entropy can be written as

$$S_{\rm harm}(e) = N[\text{const} + 3\ln(\beta)] + \beta_{\rm harm} e. \tag{23}$$

Via the standard procedure of thermodynamic integration $A_{\rm tot}(T)$ or, equivalently, $Z(T)$ can also be numerically determined starting from the ideal gas limit [163, 168–170] or from the harmonic low-temperature limit [170]. Furthermore, advanced simulation algorithms have been employed to calculate the density of states at rather low energies [171, 172].

3.3. Thermodynamic properties

3.3.1. Boltzmann probability. The normalized integrand

$$p_{\rm eq}(e, T) = G(e)\exp(-\beta(e + A_{\rm harm}(e, T) + A_{\rm anh}(e, T)))/Z(T) \tag{24}$$

denotes the temperature-dependent probability that an equilibrium configuration at temperature T is related to an IS with energy e. In what follows the temperature argument in $p_{\rm eq}(e, T)$ will be simply omitted, i.e. $p_{\rm eq}(e, T) \to p_{\rm eq}(e)$.

According to the Weber–Stillinger procedure the probability $p_{\rm eq}(e)$ can be obtained if during a MD simulation the configurations are quenched in regular time intervals and the distribution of the corresponding IS energies e is recorded. In what follows we indicate the procedures which are necessary to finally obtain $G(e)$.

To relate the IS distribution $G(e)$ and $p_{\rm eq}(e)$ one has, strictly speaking, to take into account the anharmonic effects [11]. At low temperatures they become less relevant. Formally one has $\beta A_{\rm anh}(e, T \to 0) = 0$ because only the harmonic part matters. In contrast, if regions of the basins of attraction beyond the harmonic part start to be populated significantly (e.g. regions close to barriers), anharmonic effects may become visible. Exactly, if $A_{\rm anh}(e, T)$ either disappears or only depends on temperature one has

$$p_{\rm eq}(e) \propto G(e)\exp(-\beta e)\exp(-F_{\rm harm}(e)) \tag{25}$$

or, equivalently,

$$G_{\rm eff}(e) \equiv G(e)\exp(-F_{\rm harm}(e)) \propto p_{\rm eq}(e)\exp(\beta e), \tag{26}$$

with a temperature-dependent proportionality constant. This allows one to obtain the energy dependence of $G_{\rm eff}(e)$ (and thus via knowledge of $F_{\rm harm}(e)$ that of $G(e)$) with a straightforward reweighting method; see, e.g. [173] for application of this method in Monte Carlo simulations. For every temperature, $p_{\rm eq}(e)$ is multiplied by the inverse Boltzmann factor. After relative scaling, the energy dependence of $G(e)$ can be constructed successively. It is crucial to perform this analysis for a large number of different temperatures in order to have sufficient overlap between the energy range of different temperatures.

Note that the above argument can be reversed. If the rescaling procedure of $p_{\rm eq}(e)$ yields a well defined curve $G(e)$ the energy dependence of $A_{\rm anh}(e, T)$ can be neglected. This question is of crucial importance because anharmonicities have to be small (or even better to vanish) so that the physics is indeed governed by the properties of the IS. In general, the *harmonic approximation* means that anharmonic effects are neglected.

Finally, equation (22) allows one to rewrite equation (26) as

$$p_{\rm eq}(e) \propto G_{\rm eff}(e)\exp(-\beta e) \propto G(e)\exp(-(\beta - \beta_{\rm harm})e). \tag{27}$$

3.3.2. Configurational entropy. $S_{\rm c}(e) = \ln G(e)$ is the energy-dependent configurational entropy. To calculate the entropy in the canonical ensemble one can start with the general expression $S_{\rm c}(T) = -\sum_i p_i \ln p_i$, summing over all states. For a continuous energy distribution this translates into

$$S_{\rm c}(T) = \int \mathrm{d}e\, p_{\rm eq}(e)\ln(G(e)/p_{\rm eq}(e)) = \int \mathrm{d}e\, p_{\rm eq}(e) S_{\rm c}(e) - \int \mathrm{d}e\, p_{\rm eq}(e)\ln p_{\rm eq}(e). \tag{28}$$

The last term is often neglected. Additional, very small terms emerge if the variations of the harmonic contributions for states with the same IS energy e are taken into account, i.e. going beyond the approximation equation (18).

Furthermore, one can define the average energy $\langle e(T)\rangle$ via

$$\langle e(T)\rangle = \int \mathrm{d}e\, e\, p(e, T). \tag{29}$$

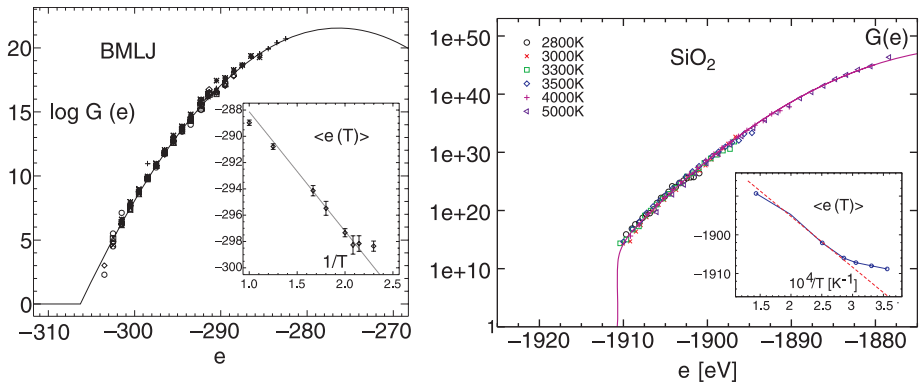

Figure 16. The distribution $G(e)$ of inherent structures in BMLJ [53] and BKS-SiO_2 [175], obtained from reweighting at different temperatures. The inset show the temperature dependence of the average IS energy. The straight lines correspond to the prediction for a Gaussian $G(e)$.

In the thermodynamic limit $S_c(T)$ is exclusively related to the first term in equation (28). Furthermore, fluctuations can be neglected so that one can approximate $p_{eq}(e) = \delta(e - \langle e(T)\rangle)$. This yields

$$S_c(T) \equiv S_c(\langle e(T)\rangle). \tag{30}$$

In the equilibrium situation the free energy $-T[S_c(e) - \beta e + \beta_{harm} e] + \text{const}(T)$ is a minimum with respect to energy. This yields (in the harmonic approximation)

$$\frac{\partial S_c(e)}{\partial e} = \beta - \beta_{harm}. \tag{31}$$

Expressing the configurational entropy in terms of temperature rather than energy directly yields

$$\mathrm{d}S_c(T)/\mathrm{d}T = (\beta - \beta_{harm})\, \mathrm{d}\langle e(T)\rangle/\mathrm{d}T. \tag{32}$$

This shows a direct relation between the temperature dependence of the configurational entropy and that of the average energy. Note that in the Adam–Gibbs theory the T-dependent configurational entropy $S_c(T)$ is of major importance.

Finally, it is interesting to note that the thermodynamics of glasses can also be calculated via analytical means [169, 174].

3.4. Simulation results

Starting from $p_{eq}(e)$ as determined for different temperatures one can use equation (26) to determine both $G_{eff}(e)$ and $G(e)$. The results for BMLJ and BKS-SiO_2 are shown in figure 16.

It turns out that the reweighting yields a well defined function $G(e)$. This means that for temperatures smaller than $2T_{MCT}$ for BMLJ and 5000 K for BKS-SiO_2 the anharmonic contributions do not hamper the reweighting analysis. Of course, in the high-temperature limit the system has to leave the harmonic regime due to the finite size of the IS in configuration space. Formally, in the limit of infinite temperatures one approaches the ideal gas limit, implying that the potential is equivalent to a box potential and the negative anharmonic contributions to the specific heat exactly cancel the harmonic contribution [164]. Actually, for BMLJ and BKS-SiO_2 the effect of anharmonic contributions is indeed seen for even higher temperatures.

This does not mean that anharmonic contributions are not present at lower temperatures. For the case of BKS-SiO_2 this is explicitly shown in figure 17, where the different contributions to the total entropy $S(T)$ are shown. Beyond the configurational entropy $S_c(T)$ the harmonic contributions $S_{harm}(T)$ have been determined. The remaining difference $S_{anh}(T) = S(T) - S_c(T) - S_{harm}(T)$ is due to anharmonic effects. One can clearly see that even at the lowest temperatures, accessible via computer simulations, the anharmonic contributions are still present. However, they do not hamper the determination of $G_{eff}(e)$ and $G(e)$ via the reweighting method. According to above this implies that the energy-dependence of $A_{anh}(e, T)$ must be weak.

Most importantly, $G_{eff}(e)$ turns out to be Gaussian, i.e.

$$G_{eff}(e) \propto \exp(-(e - e_{0,eff})^2/2\sigma^2). \tag{33}$$

Together with equation (27) this implies

$$G(e) = \exp(\alpha N)\frac{1}{\sqrt{2\pi\sigma^2}} \exp(-(e - e_0)^2/2\sigma^2) \tag{34}$$

with $e_{0,eff} = e_0 + \beta_{harm}\sigma^2$. Note that $G_{eff}(e)$ rather than $G(e)$ determines the Boltzmann distribution.

In the harmonic approximation $\langle e(T)\rangle$ is given by

$$\langle e(T)\rangle = e_{0,eff} - \beta\sigma^2 \tag{35}$$

which yields a straight line in the $\langle e(T)\rangle$ versus $1/T$ representation. The numerical data are indeed consistent with this relation for BMLJ; see figure 16. This is just a different representation of the data shown in figure 6. On first sight the constant value for $\langle e(T)\rangle$ for $T > 1$ might indicate that the top of the PEL has been reached. However, the presence of a Gaussian distribution nearly up to the maximum implies that this interpretation is not correct. Rather, it reflects the dominance of anharmonic contributions as seen, e.g., from deviations when performing the reweighting analysis for $T > 1$ [164].

Of particular interest is the resulting configurational entropy for the Gaussian distribution. Using equation (28) one obtains

$$S_c(T) = N\alpha - (1/2)\sigma^2\,(\beta - \beta_{harm})^2\,. \tag{36}$$

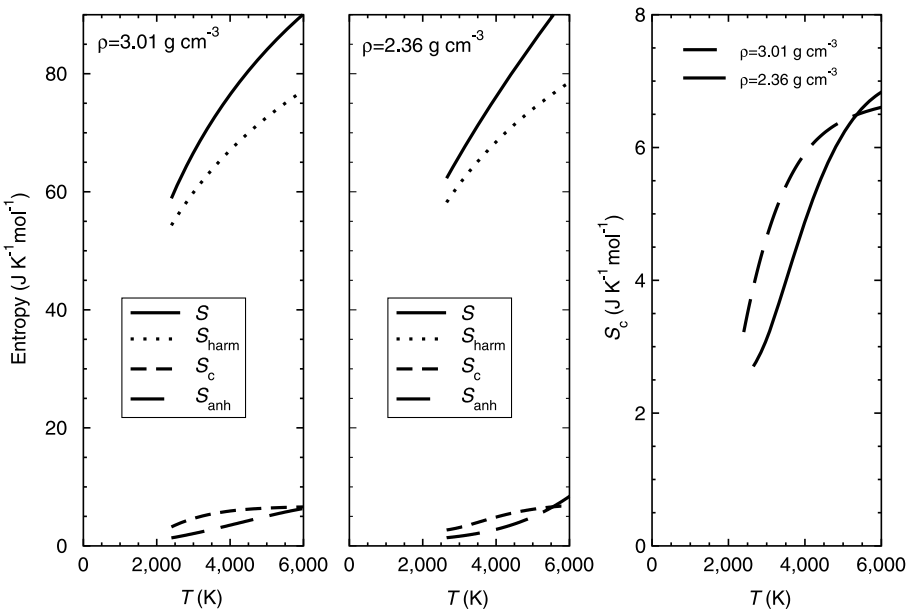

Figure 17. The different contributions to the entropy for BKS-SiO_2 at different densities. Reprinted by permission from Macmillan Publishers Ltd: *Nature* [116] copyright 2001.

For large N one expects that $\sigma^2 \propto N$ due to the central limit theorem. Then $S_c(T)$ becomes extensive as expected.

Formally, one can define the Kauzmann temperature T_K from the condition $S_c(T_K) = 0$, yielding [24, 176]

$$1/T_K = \sqrt{2\alpha N}/\sigma + \beta_{harm}. \quad (37)$$

At this temperature one has

$$\langle e(T_K)\rangle = e_0 - \sqrt{2\alpha N}\sigma. \quad (38)$$

With the definition of T_K, equation (36) can be equivalently expressed as

$$T S_c(T) = [(N\alpha) + \sigma^2\beta\beta_K/2 - \sigma^2\beta_{harm}^2/2](T - T_K). \quad (39)$$

Neglecting the temperature dependence of the second term this is equivalent to the VFT-relation equation (5) when identifying T_0 with T_K and starting with the Adam–Gibbs relation (8) [84]. Using a similar way of rewriting the configurational entropy, this type of argument can be already found in [84]. In any event, for the further analysis we use expression (36) rather than (39) due to its simplicity.

The IS distribution of BKS-SiO_2 was first extensively analyzed in [68, 116, 118]. In that work deviations of $\langle e(T)\rangle$ from the $1/T$ behavior have been observed in the low-temperature limit, implying non-Gaussian contributions. To clarify the underlying reason for these observations, simulations for a small system ($N = 99$) have been performed [175]. It turned out from the reweighting analysis that $G(e)$ is Gaussian with a relatively sharp cutoff; see figure 16. The resulting thermodynamics of this small system agrees with that of larger systems (e.g. in terms of $\langle e(T)\rangle$). Around the cutoff the entropy is still finite, implying a high degeneracy of these states. Interestingly, configurations in this energy range are void of defects, distorting the local tetrahedral structure, whereas with increasing energy the average number of defects also increases. Thus, the mechanism of energy reduction by decreasing local defects has to stop when the perfect tetrahedral network structure is reached. This rationalizes the presence of a low-energy cutoff and shows that this cutoff is very likely a direct consequence of the network structure [175]. Similar reasoning was put forward by Angell a long time ago [177]. High-density BKS-SiO_2 does not possess a well defined network. Correspondingly, the indication of a low-energy cutoff also vanishes [118]. As discussed further below, this cutoff is directly responsible for the non-Arrhenius to Arrhenius crossover around $T = 3500$ K and thus to the strong behavior of SiO_2. It was already suggested in [165] that the non-Arrhenius to Arrhenius crossover has its origin in structural reasons based on the network properties.

In the temperature range of water simulations (SPC/E) one observes $S_c(T)$ which is compatible with a Gaussian picture [165]. It is speculated, however, that deviations might occur for lower temperatures to rationalize a possible non-Arrhenius to Arrhenius transition [178]. Also for the molecular glass-former OTP a Gaussian energy distribution has been observed [179]. In contrast, for another model system with translational and rotational degrees of freedom one has found two different regimes where $\langle e(T)\rangle$ scales with $1/T$. Interestingly, close to the crossover temperature the coupling between rotational and translational dynamics breaks down [180].

The characteristic values for the PEL parameters of BMLJ and BKS-SiO_2 are given in section 5. Here we just note that typical values of α are close to unity. For the very fragile system OTP, α has been experimentally estimated to be 13 [181]. Thus, one may speculate that α is larger for more fragile systems. Interestingly, α approaches zero when compressing a glass-forming system [87]. Whereas for BKS-SiO_2 the energy dependence of $a_{harm}(e)$ can be

neglected, i.e. $\beta_{\text{harm}} = 0$, there is a dependence for BMLJ. Interestingly, here the sign of β_{harm} changes when going from constant-volume ($\beta_{\text{harm}} < 0$) to constant-pressure ($\beta_{\text{harm}} > 0$) conditions [85]. A possible explanation is as follows: high-energy states possess several unfavorable repulsive interactions. As a consequence, it is particularly favorable for the system to expand. In turn, the force constants will on average become smaller for the high-energy states at constant pressure, i.e. variable volume.

In general, all properties such as the free energies can be determined for different densities of the system. In particular they can be parametrized in terms of PEL properties [182]. In this way one can, e.g., express the equation of state in terms of PEL properties.

3.5. Properties of energy distributions

As mentioned above, many systems are compatible with a Gaussian distribution $G(e)$. Qualitatively, the total energy can be regarded as a sum of many different contributions x_i. If one assumes that the different contributions are described by a probability function $r(x_i)$ (which, for reasons of simplicity, is taken as identical for all x_i), the resulting distribution for the total energy $G(e)$ can be expressed in terms of the different moments of $r(x_i)$. In general, $r(x_i)$ will be non-Gaussian. In the most extreme case it would be described as a bimodal distribution, reflecting, e.g., the presence of local excitations. The dominant contributions to $G(e)$ stem from the second moment (assuming that $r(x_i)$ is symmetric) of $r(x_i)$ and the non-Gaussian parameter α_2, reflecting the fourth moment. It turns out for BMLJ that the degree of Gaussianity of $G(e)$ is so prominent that α_2 must be very small [183]. Thus, already on the local level the distribution $r(x_i)$ needs to be close to a Gaussian.

For the calculation of $S_c(T)$ in equation (36) it has been assumed that $G(e)$ is Gaussian up to $e = -\infty$. This is, of course, unphysical because finally the lowest energy state with energy e_{cut} (excluding the crystalline states) must have been reached. This energy is, to first approximation, given by $\langle e(T_K)\rangle$ with T_K defined by equation (37).

The behavior of $S_c(e)$ for e close to e_{cut} can, in principle, have different energy dependences. There is, however, a generic limit for the case where $r(x_i)$ contains a ground state and a first exited state, differing by an energy Δe. If one assumes for simplicity that the system under consideration is composed of a superposition of $M \gg 1$ independent subsystems (each having a ground state of energy e_{cut}/M) [184] then the contributions to $e_{\text{cut}} + K\Delta e$ result from excitations in K subsystems. Thus,

$$S_c(e_{\text{cut}} + K\Delta e) = S_c(e_{\text{cut}}) + \ln\binom{M}{K} \approx S_c(e_{\text{cut}}) - K\ln(K/M) + K \tag{40}$$

yielding

$$S_c(e) = S_c(e_{\text{cut}}) - \frac{e - e_{\text{cut}}}{\Delta e}\ln\left(\frac{e - e_{\text{cut}}}{M\Delta e}\right) + \frac{e - e_{\text{cut}}}{\Delta e}. \tag{41}$$

Additional harmonic contributions just modify the prefactor of the last term. The corresponding equation for $S_c(T)$ in this limit can be easily obtained. For low temperatures ($\beta\Delta e \gg 1$) a straightforward calculation gives

$$S_c(T) = N\beta\Delta e\exp(-\beta\Delta e). \tag{42}$$

A bimodal energy distribution has also been discussed in [185]. More generally, both levels have been broadened and the excitation energy has been rendered temperature dependent (two-Gaussian excitation model). Whereas this cannot describe a system at constant volume (because $G(e)$ is temperature independent), this may be an appropriate model description to account for possible volume and thus energy variations at constant pressure ensemble when the excited level is populated at higher temperatures.

An explicit example for this scenario is given in [186, 187], where a hard-sphere model with additional constraints is introduced. These constraints limit the maximum number of bonds and are supposed to reflect the properties of strong liquids. For this model Δe is equal to half of the binding energy of adjacent hard spheres, which itself is identical to the activation energy of diffusion. Naturally, diffusion occurs by simple and independent bond breaking processes. The authors suggest that the PEL of that model reflects the properties of SiO_2. One may ask whether the entropy, presented in figure 16, can be indeed described in this way. Unfortunately, due to the large number of fitting parameters as well as numerical uncertainties close to e_{cut} it is not possible to distinguish equation (41) from different mathematical forms. Going back to the physical interpretation the validity of equation (41) implies that (i) the energy range for which deviations from a Gaussian distribution are expected is at least of the order of Δe and (ii) for $e \geqslant e_{\text{cut}} + \Delta e$ most if not all configurations should contain at least one defect. Choosing $e_{\text{cut}} = -1910.5$ eV and $\Delta e = 2.4$ eV (half of the macroscopic activation energy), one finds for the simulated IS that for $e = -1908.1$ eV only one out of eight configurations (on average) contains one defect, i.e. a silicon atom bound to three or five oxygen atoms. Stated differently, for the BKS-SiO_2 system the energy distribution of defect-free configurations is broader than Δe. Thus, the shape of $G(e)$ and $S_c(e)$ close to e_{cut} is not dominated by the presence of defect states but rather by the additional disorder, reflected, e.g., by the ring statistics [188].

If (i) a macroscopic system can be described as a superposition of independent subsystems of finite size for all temperatures and (ii) finite-size systems contain a finite number of ISs, then from the very definition of the configurational entropy one has $S_c(T) > 0$ for $T > 0$. Explicit calculations for the properties of finite systems at very low temperatures can be found, e.g., in [176]. Then, a finite Kauzmann temperature does not exist. A similar argument has been presented by Stillinger [189]. The basic assumption is that for an amorphous ground state there exist many independent excitations; see section 4, where the tunneling model is discussed, which implies the presence of these excitations. In spirit, this is similar to the decomposition property used above. Then one ends up (in the thermodynamic limit) with an entropy of the form of equation (41). In particular, one has $\lim_{e\to e_{\text{cut}}} \mathrm{d}S_c(e)/\mathrm{d}e = \infty$. This implies (see (31)) that the temperature for which $\langle e\rangle = e_{\text{cut}}$ and thus $S_c(T) = 0$ is $T = 0$.

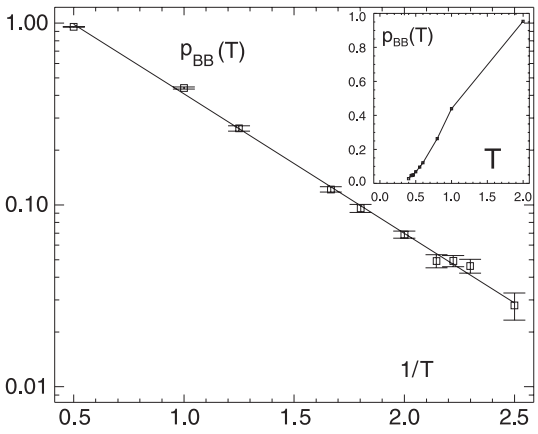

Figure 18. Probability $p_{BB}(T)$ that the IS, related to an equilibrium configuration at temperature T, changes if the configuration is randomly shifted by a small amount. Reprinted with permission from [53]. Copyright 2003 by the American Physical Society.

Some subtle effects, arising from the harmonic contributions, are discussed in [190].

In agreement with these results, it has been shown in [184] that the assumption of a Gaussian up to its low-energy end is not consistent with the notion that the number of excitations, starting from the lowest-energy state, have the scale with the system size. Furthermore, the strict simultaneous validity of the Adam–Gibbs and the VFT relation requires a hyperbolic density [24]

$$G(e) \propto \exp[1 - \exp(-2(e - e_{\text{cut}})/e_0)]. \tag{43}$$

3.6. Population of barriers

So far, the properties of the IS distribution $G(e)$ and the related Boltzmann probability $p_{\text{eq}}(e)$ and (in section 2.3) the possible relevance of the population of saddles for intermediate temperatures ($T > T_{\text{MCT}}$) have been discussed. One way to quantify the population of barriers has been reported in [53, 76] for BMLJ. It has been checked whether an equilibrium configuration ends up in the same IS after quenching if some of its particles are randomly shifted by a small amount; see figure 18. From repeated simulations with different initial configurations and initial translations one can determine the probability p_{BB} that the pair of ISs is not identical. On a qualitative level, p_{BB} is a measure for the probability that the system resides close to a saddle. Interestingly, p_{BB} does not disappear for T_{MCT} but rather shows a simple Arrhenius law [53, 76]. This suggests that nothing special happens around T_{MCT}. Note that p_{BB} is also a measure for the average index number; see section 2.3. Furthermore, if plotting p_{BB} versus temperature in a linear representation one may be erroneously tempted to conclude that p_{BB} vanishes close to $T \approx T_{\text{MCT}}$ [53].

4. Local dynamics on the PEL

4.1. Pairs of inherent structures—low-temperature anomalies

4.1.1. Physics of tunneling states. For temperatures in the Kelvin regime glasses display anomalous properties as compared to their crystalline counterparts. For example the specific heat has a linear rather than a cubic temperature dependence as one would expect from the Debye theory of solids. This implies that additional contributions to the specific heat must be present in glasses.

In the tunneling model [78–80], as well as in its generalization, the soft-potential model [191–194], it is postulated that via local rearrangements of a few atoms or molecules a transition between two adjacent ISs is possible. Conveniently, this pair of ISs is denoted a double-well potential (DWP). In disordered systems for temperatures significantly below T_{g} local relaxation processes are due to the presence of these DWPs. For temperatures in the Kelvin regime the system can no longer classically cross the saddle and dynamical processes are related to tunneling rather than to activated dynamics. Of course, only for DWPs with a sufficiently small relaxation time (e.g. less than seconds) and a small asymmetry (e.g. less than 2 K) can the system tunnel between both states on typical experimental timescales. These specific DWPs are denoted tunneling systems.

This model is purely phenomenological and very successful to explain the different low-temperature anomalies in a consistent manner [80, 195]. Naturally, many important questions emerge about the microscopic nature of the tunneling systems as well as their role as part of the PEL. This has been clarified via computer simulations. A review on this topic can be found in [196].

4.1.2. Simulation results. To test the tunneling model for real glass-forming systems via computer simulations, one first has to *systematically* identify pairs of adjacent ISs which may act as tunneling systems. In practice it is very difficult to directly identify pairs of ISs with an asymmetry less than 1 K. The typical energy ranges for systems like silica are of the order of 1 eV so that only one tunneling system per one million SiO_2 tetrahedra is present [197].

It is possible, however, to extract the relevant properties of the tunneling systems from the pairs of minima with a larger asymmetry of, e.g., 1500 K for SiO_2 [197–199]. For this purpose the potential energy around one minimum of a DWP is written as

$$V_{\text{DWP}}(x) = \sum_{i=2}^{4} w_i x^i \tag{44}$$

where the w_i are determined by the condition that the asymmetry, the barrier height and the distance between both minima of the DWP is recovered. x is the coordinate, parametrizing the reaction path between both minima. Characterization of local potentials by quartic potentials has been inspired by the soft-potential model [191]. In agreement with the assumptions of the soft-potential model it turns out that the w_i are statistically independent [196]. Thus the set of DWPs allows one, in the first step, to extract the distributions $p_i(w_i)$ and, in the second step, to generate the distribution of tunneling systems with the correct statistics. In figure 19 the distribution of barrier heights for the DWPs and for the tunneling systems is shown. The specific parameters such as barrier heights display a broad distribution. The typical energy

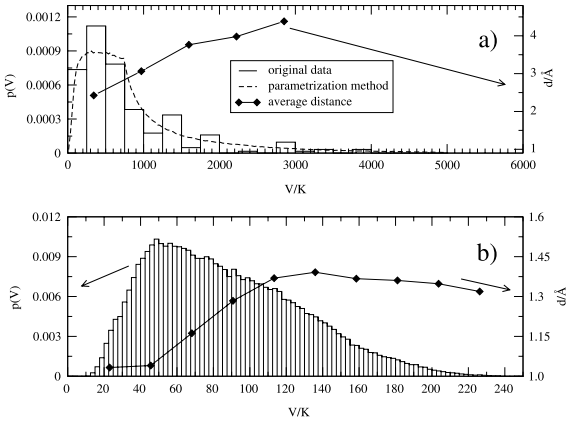

Figure 19. In the upper panel the distribution of barrier heights is shown for the DWPs, found during a systematic search procedure for BKS-SiO_2. The curve is peaked for barriers around 500 K. Furthermore, it is shown how the distance between both minima of the DWPs is correlated with the potential height. It turns out that all three parameters of the DWPs, i.e. asymmetry, potential height and distance, are positively correlated. It is possible via the parametrization method to extract the distribution of tunneling systems (DWPs with asymmetry < 2 K and relaxation time < 1 s) from this set of DWPs. The resulting distribution of barrier heights is shown in the lower panel. The typical barrier heights and distances of the tunneling systems are significantly smaller as compared to the DWPs. Adapted with permission from [197]. Copyright 2005 by the American Physical Society.

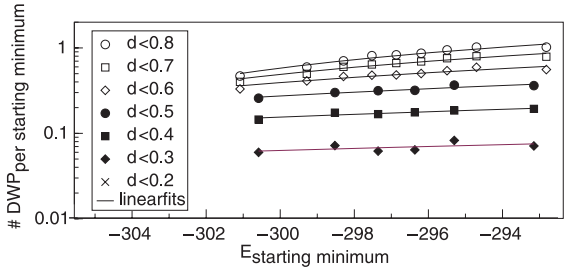

Figure 20. The dependence of the number of DWPs per starting minimum on its energy for different constraints on the distance for the BMLJ system with system size $N = 65$. LJ units are used. The asymmetry was constrained to a value smaller than 0.8. Adapted with permission from [198]. Copyright 2004 by the American Physical Society.

scales of the potential heights of tunneling systems (around 50 K) is significantly smaller than 1 eV, i.e. the typical energy scale on the PEL. Thus these tunneling systems correspond to little wiggles on the PEL.

In previous work on silica the trajectories, generated either by molecular dynamics [200] or by activation–relaxation techniques [201], have been analyzed with respect to transitions between adjacent configurations. Although an interesting insight into the nature of relaxation processes in silica is available from these simulations it is not possible to derive, e.g., the *absolute* number of DWPs, relevant for the low-temperature anomalies. Such an algorithm has been suggested in [196, 197, 202, 203]. For silica the experimentally determined number of tunneling systems is roughly three times larger than the value found from simulations of defect-free silica (i.e. taking into account only those ISs with a perfect local tetrahedral structure). This discrepancy can be easily explained by the fact that in experiments one has additional contributions from impurities and local defects like non-bridging oxygens. Furthermore, the dipole moment has been determined for the tunneling systems in pure SiO_2 and for the additional presence of impurities. In both cases an excellent agreement with experimental data has been obtained [199].

In the more general context of this review, one may ask the question of whether the properties of pairs of adjacent minima depend on the energies of the ISs which are involved. This question is important for two different reasons. First, generation of glassy configurations via computer simulations involves very large cooling rates [204]. As a consequence, the energies of the ISs obtained via simulations are always higher in energy than those one would get with experimentally relevant cooling rates. Thus any dependence of the DWP properties on energy would translate into systematic differences between the tunneling systems, obtained via simulations, and those observed experimentally. Second, as discussed in the last section the density of ISs, i.e. $G(e)$, exponentially increases with increasing energy. Thus one might speculate that the number of pairs of ISs with energies e_0 and e_1 (where $|e_1 - e_0|$ is small relative to the width of the IS energy distribution) strongly increases with increasing energy.

From detailed simulations of the BMLJ system it turns out that the properties of the DWP are basically independent of the IS energy [198]. Thus, it is indeed possible to obtain a realistic picture of tunneling systems via computer simulations. As shown in figure 20 the absolute number of DWPs is also independent of energy as long as the DWPs are restricted to pairs of ISs with very small (Euclidean) distances in configuration space. For a weaker distance criterion of 0.8 (in Lennard-Jones units) one observes a slight increase of the number of DWPs with energy. The typical distance of tunneling systems in the BMLJ system is 0.1 [203], so that the number of tunneling systems is independent of the energy of the PEL.

Since for sufficiently large systems the number of adjacent ISs scales with the system size N, the number of adjacent ISs can be much larger than one. Actually, this is already the case for the system size of 65 particles, analyzed in [198]. For a few instances a lower bound for the number of neighbors has been obtained by performing repeated simulations for the same starting IS and checking the nature of the first IS visited after escaping the starting IS. For a few low-energy ISs it turned out that the number was of the order of 10 (again for $N = 65$ particles).

DWPs have also been numerically identified for clusters in [205]. Interestingly, it turns out that for clusters the most mobile particles are typically at the surface. Thus, it has to be expected that DWPs in clusters have somewhat different properties from those in bulk systems.

Middleton and Wales have performed an extensive analysis of IS transitions for glass-forming systems [159]. To characterize the different transitions they analyzed the translation of the particle which moves most. If this distance

is less than half the average distance between particles they denote the translation as a *non-diffusive* rearrangement, otherwise as *diffusive*. Furthermore they observed a broad distribution of barriers, similar to figure 19. Transitions with low barriers typically correspond to non-diffusive rearrangements and vice versa. Furthermore, low-barrier transitions are more cooperative [206]. This result is fully consistent with the insight from [197, 202].

4.2. Escape from an IS: concepts

4.2.1. General. In section 1 evidence has been presented that the dynamics is strongly related to the energy. In particular, as illustrated in figure 7, the system is stuck for a long time in low-energy states. As will be shown below, the macroscopic transport properties are to a large extent related to the residences in these stable configurations. Therefore it is of utmost importance to understand the escape from an IS. Two aspects have to be taken into account. First, a typical IS will have several adjacent ISs. Therefore, many escape paths are possible. They all have to be taken into account to predict the escape dynamics. Second, after escaping to the first adjacent IS there is a finite backjump probability to return to the initial IS. This backjump probability will be particularly pronounced if the initial IS is very low in energy and the adjacent ISs have a higher energy. Thus, in particular at low temperatures one can expect that the system is returning to the initial IS quite often. For the long-range transport it is important that the system leaves an IS irreversibly. Therefore, it is convenient to define the waiting time in the initial IS as the time difference between the starting time and the time when the system leaves this IS for the last time. Due to the exponentially large number of ISs a much later return to the same IS can be safely excluded, so that the waiting time is a well defined observable. Is it possible to relate the local properties of the PEL to the waiting time?

In the physical chemistry literature the formulation of rate equations for a PEL with many ISs has been an important topic; see, e.g., [207] and the references in [10]. Only if the system resides long enough close to the individual IS may the system be regarded as Markovian. This implies that the future dynamics does not depend on how the system entered the present IS. Then straightforward rate equations can be formulated. This limit will be considered in the subsequent analysis. For reasons of simplicity the transition rate from state i to state j is just taken as $k_0 \exp(-V_{ij})$ with a common prefactor k_0 and the barrier height V_{ij} the system has to cross on the way from i to j.

4.2.2. Analysis of model PEL. *A priori* it seems to be a very complex problem to calculate the escape rate from some groups of minima because a very large set of rate equations has to be solved. Indeed, often only numerical solutions are available [208]. However, despite the complexity of the PEL of glass-forming systems some quantitative predictions can be formulated for the typical situation encountered in glass-forming systems. Specifically, we analyze the waiting time of a low-energy IS (*central* IS) which is surrounded by ISs with higher energies. In general, it will be impossible to elucidate the local properties of the PEL in such detail that observables like the waiting time of the central IS can be predicted quantitatively. First, the number of ISs which may contribute is simply too large. Whereas it may be possible to identify all nearest-neighbor ISs as done for the systematic search of tunneling systems, it will not be possible to extend this search to all ISs which are, e.g., fourth-nearest neighbors. Second, even if one had this information one would have to solve a very high-dimensional system of rate equations.

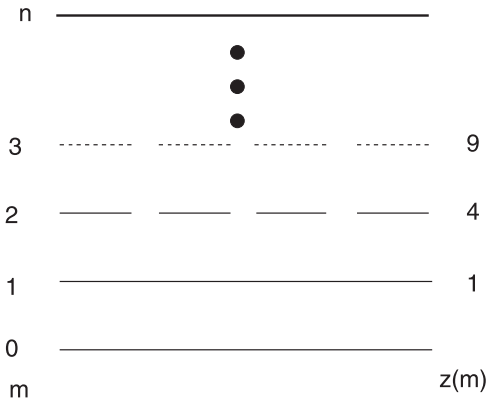

Figure 21. Sketch of a simple model PEL. The constant energy distance between neighboring ISs is denoted Δe. On the mth level the degeneracy is $z(m)$, which here is chosen as $z(m) = m^2$. The different energy levels are denoted $0, \ldots, n$. The transition rate for an upward transition from an IS at level m to any IS at level $m+1$ is $\Gamma_0 z_{m+1} \exp(-\beta \Delta e)$. The downward rate is Γ_0. The waiting time is defined as the average time which is needed for the system to escape from the central IS at level 0 to one IS at level n.

Despite these general problems, it is nevertheless possible to make quantitative statements. Some key concepts can be discussed for the model landscape in figure 21. It is similar to the landscape studied in [209]. For very large n one may expect that the probability to go back to the bottom of the PEL is very small once some level $1 \ll m < n$ has been reached. Qualitatively, this may be attributed to the fact that the probability to proceed to ISs with higher energies is sufficiently large that it is more likely to end up at level n rather than at the central IS, i.e. at level 0. In some sense this argument reflects the counter-effects of energy and entropy. Whereas for energetic reasons the system would like to climb down in energy, the large degeneracy of the ISs at the next higher energy and thus the large number of options to go up may reduce the energetic driving force.

On a more quantitative basis, this effect is captured by the backward-jump probability $p_{\mathrm{back}}(m)$. It is defined as the probability that the system, starting at level m, will reach the bottom, i.e. level 0, before escaping, i.e. reaching level n. We define that exactly for levels m with $p_{\mathrm{back}}(m) > 0.5$ the system is still in the attraction basin of the central IS. m_{c} defines the level for which for the first time $p_{\mathrm{back}} < 0.5$. Due to the relevance of energetic aspects at low temperatures, one may expect that m_{c} increases with decreasing temperature. This concept has also been used in the field of protein dynamics to identify the range of transition states before folding [210]. Furthermore, it is similar to the dynamic bottlenecks introduced by Chandler and co-workers [211].

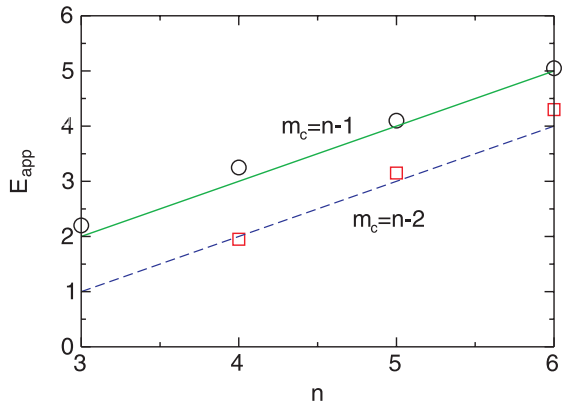

Figure 22. The apparent activation energy $E_{\rm app}$ for the cases $m_{\rm c} = n - 1$ and $m_{\rm c} = n - 2$ for the model shown in figure 21 for different values of n. The lines correspond to $E_{\rm app} = m_{\rm c}\Delta e$.

To characterize the temperature dependence of the waiting time $\langle\tau\rangle$ in the central IS, we define the apparent activation energy

$$E_{\rm app} = \frac{{\rm d}\ln\langle\tau\rangle}{{\rm d}\beta}. \tag{45}$$

In general, $E_{\rm app}$ depends on temperature. Intuitively, one may expect that the value of $E_{\rm app}$ is related to the height of the levels from which point on the system starts to leave the attraction basin of the central IS. In analogy to the results in [209], this hypothesis can be quantified for the model potential in figure 21. In a first step the temperature dependence of the average waiting time is calculated by performing repeated MC simulations, starting from the central IS and recording the time until level n is reached. Then $E_{\rm app}(\beta)$ can be directly estimated via equation (45). Alternatively, for fixed temperature one can calculate $p_{\rm back}(m)$ by repeated MC simulations, starting from level m and recording the probability to end up at the central IS before reaching level n. $E_{\rm app}$ can be estimated as $\Delta e m_{\rm c}$, where $m_{\rm c}$ is the level for which $p_{\rm back}(m_{\rm c}) \approx 0.5$. In figure 22, data are shown for two temperatures, implicitly defined via $m_{\rm c} = n - 1$ and $m_{\rm c} = n - 2$. Furthermore, different values of n are considered. Indeed, both estimates of $E_{\rm app}$ agree very well. For all model landscapes analyzed so far, we get similar results. This strongly suggests that the quantity $p_{\rm back}$ contains important information about the local escape rates from a central IS.

It is also possible to obtain analytical results in the limit where $z(m)$ very strongly increases with m [53, 209], which will be needed for the elucidation of PEL properties via computer simulations. To obtain a somewhat more general expression we introduce the barrier $V_{m,m+1}$ which the system has to cross when jumping from level m to $m+1$. Naturally one has $V_{m,m+1} - V_{m+1,m} = \Delta e$. To proceed further we define the probability $p_{\rm ret}(m)$ to jump back from level m to level $m - 1$. It is given by

$$p_{\rm ret}(m) = \frac{\exp(-\beta V_{m,m-1})}{\exp(-\beta V_{m,m-1}) + z_{m+1}\exp(-\beta V_{m,m+1})}. \tag{46}$$

In the limit that $z(m)$ very strongly increases with m the return probability is close to unity for $m < m_{\rm c}$, and very small for $m \geqslant m_{\rm c}$. Then an escape process from level 0 to $m_{\rm c}$ corresponds to a fortunate sequence of unlikely upward jumps, each occurring with probability $1 - p_{\rm ret}(m)$. The statistical weight of sequences which contain correlated forward–backward jump processes (not involving level 0) can then be neglected. This is similar to the observation that a particle when crossing a saddle after leaving a deep minimum displays a very fast uphill motion. Of course, for jump processes from level $m_{\rm c}$ up to the final level n the return probability is very small so that the forward motion will continue. Furthermore, for the waiting time $\langle\tau\rangle$ the contribution to the residences in excited levels can be neglected. This comes from the observation that for an escape from the central IS one only has uphill processes whereas for all excited levels a downhill process is also possible. Putting these arguments together one can thus estimate the inverse average waiting time as the rate $\tau_{\rm micro}^{-1} z_1 \exp(-\beta V_{0,1})$ to leave level 0 multiplied by the probability that the system performs successive uphill processes $1 \to 2, \ldots, (m_{\rm c} - 1) \to m_{\rm c}$

$$\langle\tau\rangle^{-1} = \tau_{\rm micro}^{-1} z_1 \exp(-\beta V_{0,1}) \times (1 - p_{\rm ret}(1)) \cdot \ldots \cdot (1 - p_{\rm ret}(m_{\rm c} - 1)). \tag{47}$$

Note that for $1 - p_{\rm ret}(m) \ll 1$ one has $1 - p_{\rm ret}(m) \approx z_{m+1}\exp(-\beta(V_{m,m+1} - V_{m,m-1}))$. Then one obtains after a straightforward calculation

$$\langle\tau\rangle^{-1} = \tau_{\rm micro}^{-1} \prod_{m=1}^{m_{\rm c}} z_{\rm m} \exp(-\beta[(m_{\rm c}-1)\Delta e + V_{m_{\rm c}-1,m_{\rm c}}]). \tag{48}$$

In particular, this result means that the apparent activation energy will vary from $(n - 1)\Delta e + V_{n-1,n}$ at very low temperatures (where $m_{\rm c} = n$) to $V_{0,1}$ (where $m_{\rm c} = 1$) at very high temperatures. Also note that there is an increase of the apparent attempt frequency by a factor $z_1 \cdot \ldots \cdot z_{m_{\rm c}}$. We mention in passing that equation (47) can be reformulated as

$${\rm d}\ln\langle\tau\rangle/{\rm d}\beta = V_{0,1} + \sum_{m<m_{\rm c}} p_{\rm ret}(m)(V_{m,m+1} - V_{m,m-1}). \tag{49}$$

Equation (48) allows one to formulate a simple recipe to identify $E_{\rm app}$ from properties of the PEL. For this purpose, one monitors the final escape process from a central IS and records the energies of the sequence of ISs and the saddle energies between them. Furthermore, one determines $p_{\rm back}$ from repeated runs starting from these ISs. Then one may first determine $m_{\rm c}$ from the $p_{\rm back}$-criterion and finally estimate $E_{\rm app}$ as the energy difference between the energy of the saddle between levels $m_{\rm c} - 1$ and $m_{\rm c}$ and the energy of the central IS.

These arguments can be extended to the PEL where the states at the different levels are no longer degenerate so that the probabilities to climb up the different paths may vary. The number of paths is equivalent to the number of ISs on level n. The different ISs on this level may be distinguished by the index a. Then the total rate to leave the central IS $\Gamma \equiv 1/\langle\tau\rangle$ can be written as $\sum_a \Gamma_a$, where Γ_a is the rate at which the system escapes the central IS via this specific IS with index a. One can write

$$\frac{{\rm d}\ln\langle\tau\rangle}{{\rm d}\beta} = -\frac{{\rm d}\ln\Gamma}{{\rm d}\beta} = -\sum_a \frac{\Gamma_a}{\Gamma}\frac{{\rm d}\ln\Gamma_a}{{\rm d}\beta} = \sum_a p_a E_{0.5,a}. \tag{50}$$

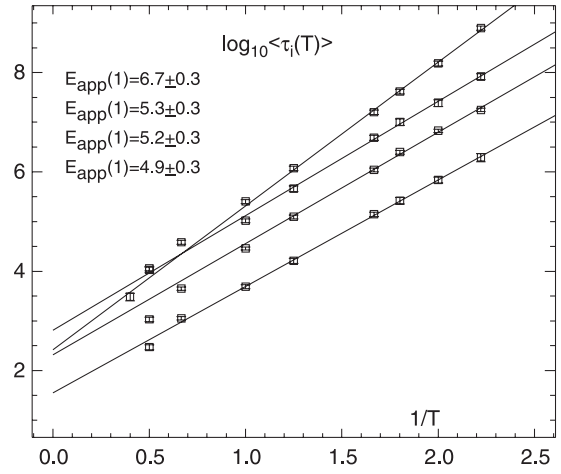

Figure 23. Mean waiting times of four low-lying, randomly selected ISs, computed from repeated runs for the BMLJ system. The activation energies, obtained from the Arrhenius fit, are indicated. Curves have been shifted by 0.5(4-i) orders of magnitude for better visualization. Reproduced with permission from [53]. Copyright 2003 by the American Physical Society.

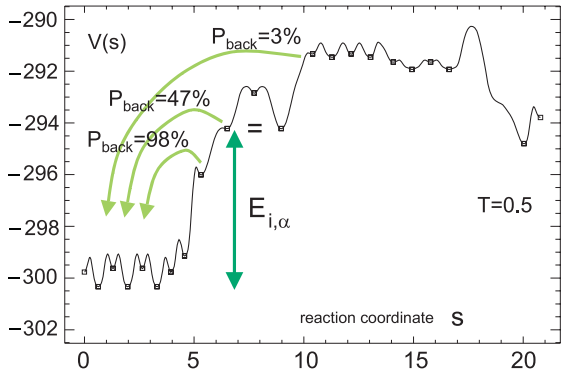

Figure 24. Potential energy along a typical escape path from a low-lying IS of the BMLJ system. p_{back} denotes the probability of returning to the bottom of the MB. Reproduced with permission from [53]. Copyright 2003 by the American Physical Society.

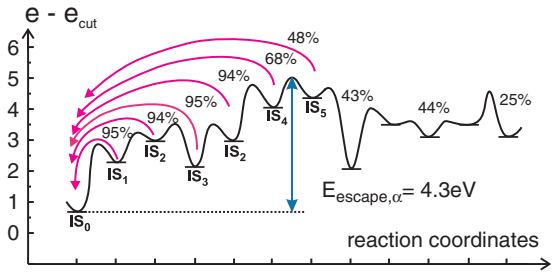

Figure 25. The same as in figure 24, determined for BKS-SiO_2.

Here we have introduced p_a as the probability to escape via path a and $E_{0.5,a}$ as the value of the effective barrier for path a according to the p_{back}-criterion. They can be estimated in full analogy to equation (48). For a finite sample of escape paths one just has to take the average value of $E_{0.5,a}$, because the weighting factors p_a are reflected in the relative probabilities for the different observed escape paths.

Somewhat related approaches can be found in [208], where different archetypical energy landscapes, characterized by specific motifs (palm, willow tree, banyan tree), have been studied. In that work the analysis has been generalized to take into account non-Markovian effects.

4.3. Escape from an IS: simulations

In [53] the concepts, discussed above, have been explicitly applied to the BMLJ system. In the first step repeated simulations have been started from four randomly selected low-energy ISs and it has been recorded when this region in configuration space is left. An exponential waiting time distribution has been observed [212], which is consistent with a similar analysis shown in [213]. The temperature dependence of the waiting time as well as the estimation of the apparent activation energies are shown in figure 23. The escape is indeed activated since the resulting activation energy is much higher than the temperature.

The general scenario of local relaxation in a complex PEL can indeed be retrieved from the numerical analysis. To leave a low-lying IS the system typically jumps back several times until finally the system escapes. This final part of the trajectory is shown in figures 24 and 25 for BMLJ and BKS-SiO_2, respectively. In agreement with the theoretical expectation during the final escape process the system does not perform any correlated forward–backward motion. Via additional repeated simulations from the different ISs the respective values of p_{back} have been determined. Via the p_{back}-criterion the effective barrier for this escape can then be obtained. A histogram of all effective barriers, obtained from repeated runs, is shown in figure 26 for all four low-energy ISs. Indeed, the estimation of the effective barrier agrees very well with the observed respective activation energy in figure 23. This strongly suggests that the local dynamics can be quantitatively related to the local topology of the PEL. A similar analysis has been performed for BKS-silica with a similar agreement. Also below the glass transition temperature both the reversible forward–backward jumps, returning to the same configuration, and the irreversible jumps, leading to an escape process, can be observed [214]. In agreement with expectation the irreversible jumps show larger displacements and larger energy variations.

Some interesting additional observations can be made: (1) the barrier $V_{0,1}$ of the first transition is significantly smaller than the effective barrier. This shows that it is a multi-step relaxation sequence which is required to leave the attraction region of a low-energy IS. (2) For the example in figure 24 it is clear that the main contribution to the effective barrier stems from the energy difference between the initial and the final IS and not from the additional barrier between the last and the second but last IS. This holds in general. For BKS-SiO_2 the additional barrier contribution between two ISs is approximately 20% of the total effective barrier. Thus, the apparent barrier reflects the local topology in terms of ISs rather than saddles [215]. (3) In the case of BKS-SiO_2 (using again $N = 99$ particles) it has been

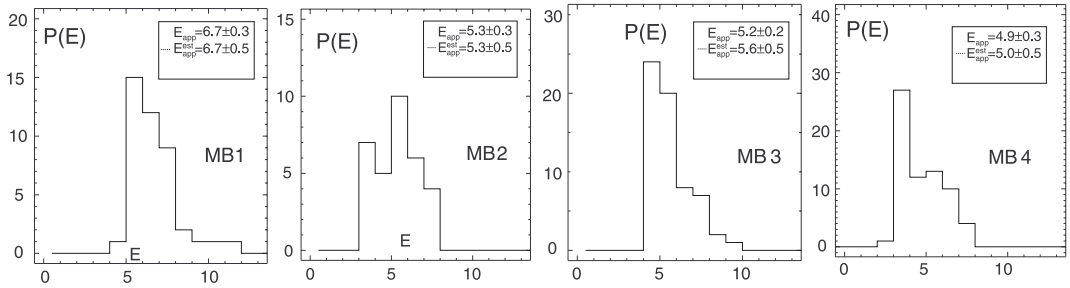

Figure 26. Histograms of barriers overcome when escaping the four low-energy ISs in figure 23. Apparent activation energies and mean barriers are given in the figure. Reproduced with permission from [53]. Copyright 2003 by the American Physical Society.

explicitly checked that the sequence of IS transitions can be interpreted as an sequential process rather than a sequence of independent transitions [215]. (4) In the case of silica most IS transitions are connected to bond breaking and/or formation processes. Thus an elementary relaxation process has to be visualized as a complex sequence of bond breaking and formation events. After completion of one relaxation process the system has, on average, changed five bonds. (5) For the elementary barriers between ISs a strong correlation with the total displacement has been observed: high barriers correspond to large-displacement dynamics [216] in agreement with results, reported in 4.1.2. The large displacement is mainly related to the high degree of cooperativity, involved in high-barrier dynamics.

The presence of multi-minimum paths for escape implies that the effective barrier $E_{\rm app}$ is a non-local property of the PEL, since it involves the complex topology of the IS. Thus, it remains to be shown whether the elastic models, postulating a direct relation between the local force constants and the barriers, can also be rationalized for a more complex PEL.

5. Impact of energy on the local mobility

After having discussed the escape properties from a central IS in section 4, the relation of quantities such as $E_{\rm app}$ to the energy of the central IS are studied. As reflected by the data in figure 7, one expects a strong correlation between energy and mobility. For a quantitative analysis the concept of metabasins will turn out to be essential.

5.1. Activated transitions on the PEL: models

There is a long history of models which describe the dynamics in configuration space on a phenomenological level [217–222]. Qualitatively, one considers a region of the viscous fluid which can cooperatively rearrange via a transition state. For the time being the initial and final states may be characterized by the energy of the respective IS. For sufficiently low temperatures ($T < T_{\rm MCT}$) the elementary rearrangement process is considered to be activated: the system leaves a state with energy e, crosses a high-energy transition state with rate $\Gamma(e)$ and ends up in a new state which is uncorrelated to the initial one. Different names can be found for essentially identical models (e.g. trap model, free energy model) following this scenario. A thoughtful discussion of the physical background

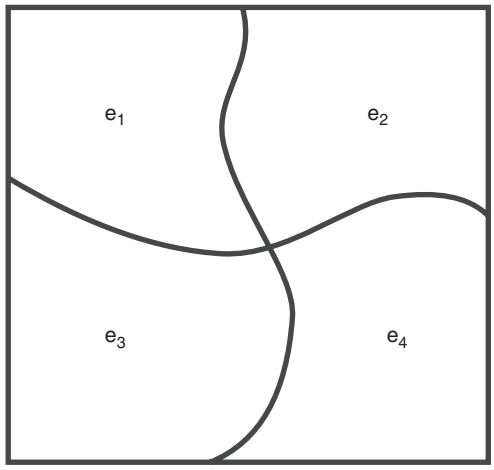

Figure 27. Sketch of four subsystems.

can be found, e.g., in [223]. Later on this scenario will be extended to larger regions, which to a first approximation may be regarded as a superposition of independent elementary systems. To be able to predict the macroscopic behavior it is further assumed that the total macroscopic system can be regarded as a superposition of independent systems; see figure 27. As outlined in section 9 the exact meaning of the term *independent* turns out to be a somewhat subtle issue. Finally, a density of states $G(e)$ has to be specified to complete the model definition.

First, the hopping rate $\Gamma(e)$ is discussed. In section 4 it has been argued that the escape from a state of energy e is a multi-step process; see figure 28. Two energies can be defined. $e_{\rm cross}$ denotes the energy of the IS just after the final barrier, which has a height V_0. According to the model assumptions $e_{\rm cross}$ and V_0 are independent of the initial energy e. Actually, even in more complex systems like the random energy model one can argue via percolation arguments that $e_{\rm cross}$ is independent of e [223]. For reasons of simplicity one may choose a fixed value of $e_{\rm cross}$. This yields

$$\Gamma(e) = \Gamma_0(e)\exp(-\beta E_{\rm app}(e)) \tag{51}$$

with

$$E_{\rm app}(e) = e_{\rm cross} + V_0 - e \tag{52}$$

for $e \leqslant e_{\rm cross}$ and $E_{\rm app}(e) = V_0$ for $e \geqslant e_{\rm cross}$. Stated differently, the escape for energies lower than $e_{\rm cross}$ is solid-

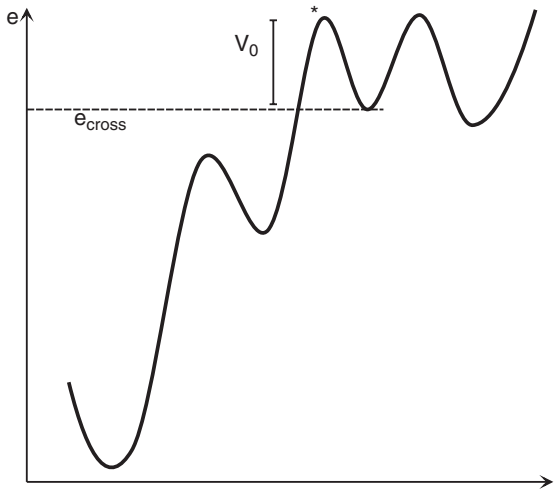

Figure 28. Sketch of the multi-step escape process, including the definition of V_0. The barrier with the star is supposed to be the critical barrier beyond which $p_{\rm back} < 0.5$. Reproduced with permission from [226]. Copyright 2008 by the American Physical Society.

like (activated) whereas otherwise it is liquid-like [224]. The factor $\Gamma_0(e)$ displays possible entropic effects (see below).

Now we briefly review the properties of $e_{\rm cross}$, V_0 and $\Gamma_0(e)$ as discussed in the literature.

(1) The choice of $e_{\rm cross}$ relative to the distribution $G(e)$ is hardly discussed in literature. In the case of a Gaussian $G(e)$ with a maximum at energy e_0 the standard choice is $e_{\rm cross} = e_0$ [219, 220, 222], although also $e_{\rm cross} \neq e_0$ has also been studied numerically [223]. Since for $e_{\rm cross} = e_0$ the model predicts non-Arrhenius behavior (see section 6), this is taken as a generic choice for fragile systems [219]. It has been speculated that for strong systems one has to take into account the additional effect of the barrier height V_0 [219]. For sufficiently large barrier height this additional factor $\exp(-\beta V_0)$ dominates the temperature dependence of the dynamical process, giving rise to strong behavior. The actual simulations for BKS-SiO_2 and BMLJ are not compatible with this interpretation of strong systems (see section 5.3).

(2) In general, the prefactor $\Gamma_0(e)$ contains an energy-dependent factor $M_{\rm entro}$ which denotes the number of escape paths to reach a high-energy state with energy $e_{\rm cross}$. Most of the authors have neglected this effect by choosing $\Gamma_0(e) = \Gamma_0$. This would be justified in the case of 1D reaction paths or low-dimensional percolation paths. A simple expression for $M_{\rm entro}$ can be formulated if every state with energy $e_{\rm cross}$ can be reached from exactly one state with energy $e(< e_{\rm cross})$. It is given by $M_{\rm entro} = G(e_{\rm cross})/G(e)$. More generally, if every state with energy $e_{\rm cross}$ can be reached from $f(e, e_{\rm cross})$ states with energy e one obtains $M_{\rm entro} = f(e, e_{\rm cross})G(e_{\rm cross})/G(e)$.

A simple model PEL has been suggested by Brawer, for which $f(e, e_{\rm cross})$ can be estimated [217, 225]. It is close to the hypercube model discussed in section 3. He starts from a defect picture of the supercooled liquid. Every atom can either possess a low (no defect) or a high coordination number (defect). Increasing the energy just means that the number of defects is increased, each giving a contribution of Δe. A state is thus fully characterized by the number n of defects. In the simplest version of this model one has $f(e = n\Delta e, e_{\rm cross} = N_{\rm cross}\Delta e) = N_{\rm cross}!/[n!(N_{\rm cross} - n)!]$. This binomial coefficient expresses in how many ways $N_{\rm cross} - n$ atoms can be selected out of $N_{\rm cross}$ atoms to reduce the energy from $N_{\rm cross}\Delta e$ to $n\Delta e$ in a monotonic way. Correlation effects may reduce the number of possible transitions $f(e, e_{\rm cross})$ [217, 225]. Unfortunately, this model is not consistent with the requirement that the system has to climb up to a state with energy $e_{\rm cross}$. If $f(e, \tilde{e}) > 1$ for $e < \tilde{e} < e_{\rm cross}$, it is possible for the system to switch between different states of energy e without having to climb up to an energy $e_{\rm cross}$ but at most up to the energy $\tilde{e}$. As a consequence, $f(e, e_{\rm cross})$ must be identical to $f(e_{\rm cross} - \Delta e, e_{\rm cross})$ and is thus independent of e. Therefore one can write

$$\Gamma_0(e) = \Gamma_0 G(e_{\rm cross})/G(e). \tag{53}$$

For $e_{\rm cross} - e \ll e_0 - e_{\rm cross}$ this can be approximated as

$$\Gamma_0(e) \approx \Gamma_0 \exp((e_0 - e_{\rm cross})(e_{\rm cross} - e)/\sigma^2). \tag{54}$$

For later purposes this is rewritten as

$$\Gamma_0(e) = \Gamma_0 \exp(\kappa k_{\rm entro}(e_{\rm cross} - e)) \tag{55}$$

with

$$k_{\rm entro} = (e_{0,\rm eff} - e_{\rm cross})/\sigma^2 \tag{56}$$

and

$$\kappa = \frac{e_0 - e_{\rm cross}}{e_{0,\rm eff} - e_{\rm cross}}. \tag{57}$$

This somewhat complicated way to rewrite equation (54) is motivated in two ways. First, because $p_{\rm eq}(e)$ is directly related to $G_{\rm eff}(e)$ and thus to $e_{0,\rm eff}$, see equation (27), it is more convenient to use $e_{0,\rm eff}$ rather than e_0 for the definition of $k_{\rm entro}$. Second, in practice the factor κ has to be treated as an empirical parameter because the increase of the entropic term $\Gamma_0(e)$ with decreasing energy can somewhat deviate from the ideal scenario, described above.

A natural choice for $e > e_{\rm cross}$ is $\Gamma(e) = \Gamma_0$. However, if not mentioned otherwise, we always consider the relevant case $e < e_{\rm cross}$.

In figure 29 a sketch of the relevant energies used in the present context, is shown.

It is convenient to introduce the shifted inverse temperatures

$$\tilde{\beta} = \beta - \kappa k_{\rm entro}. \tag{58}$$

In principle all calculations shown in this work can be performed for $\kappa \neq 1$. However, since the influence of the entropic prefactor is not as important as the energetic term, the additional complexity of the expressions is not worth the additional information for $\kappa \neq 1$. In what follows we therefore always choose $\kappa = 1$ if not mentioned otherwise.

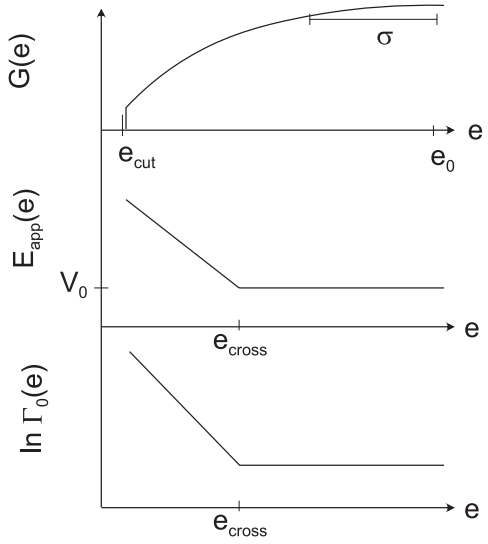

Figure 29. Sketch of the energies introduced in the text. A possible difference between $G(e)$ and $G_{\rm eff}(e)$ is neglected. Reproduced with permission from [226]. Copyright 2008 by the American Physical Society.

Now one can rewrite equation (51) as

$$\Gamma(e) = \Gamma_0 \exp(-\tilde{\beta}(e_{\rm cross} - e)) \exp(-\beta V_0). \qquad (59)$$

Furthermore, for a Gaussian density of states one can express $p_{\rm eq}(e)$ as

$$p_{\rm eq}(e) \propto G_{\rm eff}(e) \exp(-\beta e) \propto \exp[-(e - e_{\rm cross} + \sigma^2\tilde{\beta})^2/2\sigma^2]. \qquad (60)$$

When comparing equation (59) with simulations one has to take into account that the simulated system may contain more than one elementary system; see figure 27. Each subsystem is characterized by an energy e_i and $e = \sum e_i$. For a superposition of M independent subsystems the total hopping rate $\Gamma_M(e)$ is just the sum of the individual hopping rates $\Gamma(e_i)$. To a first approximation one may assume that the energy e is equally distributed among the M subsystems, yielding $\Gamma_M(e) = M\Gamma(e/M)$. The quantitative analysis in section 8 shows that the exact expression for $\Gamma_M(e)$ contains another energy-independent factor. The estimation for $\Gamma_M(e)$ suggests generalizing equation (59) to

$$\Gamma(e) = \Gamma_0 \exp(-\lambda\tilde{\beta}(e_{\rm cross} - e)) \exp(-\beta V_0). \qquad (61)$$

Here $1/\lambda$ is a measure for the number of elementary subsystems present in the specific system.

In what follows we call a system an *ideal Gaussian glass-former* if $G_{\rm eff}(e)$ is Gaussian and $\Gamma(e)$ is given by equation (61). In section 6 several analytical results will be presented for the ideal Gaussian glass-former to estimate, e.g., the temperature dependence of the diffusion constant [226]. For later purposes we introduce the dimensionless quantity

$$\mu \equiv \tilde{\beta}\sigma. \qquad (62)$$

It will turn out that μ is the central property which determines the properties of the ideal Gaussian glass-former.

Another simple picture of the PEL has been discussed in [227] which starts from the low-temperature picture of an ensemble of independent DWP. With increasing temperature the asymmetries of the DWP start to fluctuate due to their mutual interaction, mediated via the viscoelastic medium. Among others this influences the shear response.

5.2. Metabasins

5.2.1. Motivation. One major goal of the PEL approach is to relate the dynamics to properties of the PEL. In particular, one would like to analyze whether the escape process from a configuration is correlated with its energy. In section 4.2 we have analyzed the escape from an IS which is surrounded by IS with higher energies. There we have seen that at low temperatures the apparent activation energy $E_{\rm app}$ to leave the central IS ($m = 0$) is related to the energy difference of the initial energy and the barrier before reaching the IS ($m = m_{\rm c}$) with $p_{\rm back} < 0.5$. Basically the same activation energy has to be used to describe the escape from an excited IS ($m < m_{\rm c}$), because most likely the system will first go to the central IS. In general, for the model in section 4.2 the rate to escape from an IS with energy e at level m is approximately given by the escape rate of the central IS $\Gamma(e_{\rm central})$ with $e_{\rm central} = e - m\Delta e$. Thus, the energy e alone is not sufficient to predict the escape rate from an arbitrary IS. How to arrive at a function $\Gamma(e)$? A straightforward way is to identify all ISs with $m < m_{\rm c}$ as one effective state with an energy e, given by the energy of the central IS. This kind of coarse-graining is therefore mandatory if one wants to formulate a relation between energy and mobility.

The concept of grouping together adjacent ISs goes back to Stillinger [61]. Starting from the experimental observation of the Johari–Goldstein β process, typically observed in fragile systems, one may relate the β process to local transitions between a finite number of ISs whereas the α process corresponds to a concerted sequence of these transitions, transferring the system between two *metabasins* (MBs). However, in this scenario it is still not clear how the large activation energy of the Johari–Goldstein β-process ($\approx 24T_{\rm g}$) [228] can be understood. Furthermore, these correlated forward–backward motions are often related to the presence of low-barrier transitions, at the extreme of the tunneling systems [159, 197, 202, 229].

5.2.2. Definition. For the simple model system in figure 21 the definition of an MB is straightforward. But how to construct MBs if the only available information is the trajectory of ISs as obtained from Stillinger–Weber-type simulations (figure 7)? If one had performed a corresponding simulation for the model potential in figure 21 one would have likely seen a long sequence of forward–backward jumps between ISs with $m < m_{\rm c}$. This may be taken as the motivation to define a general coarse-graining procedure [229, 230]. Whenever the system is performing forward–backward jumps between a finite number of ISs, these ISs are grouped together as one MB. It is characterized by two observables. First, one naturally has the waiting time τ between the entry and the exit time of the

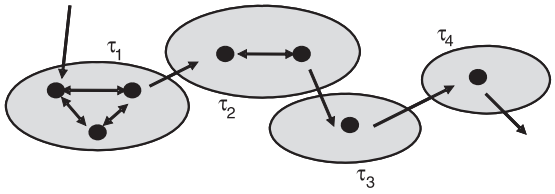

Figure 30. Visualization of the definition of MBs as sets of ISs. The key criterion is the presence of forth- and backjumps within an MB.

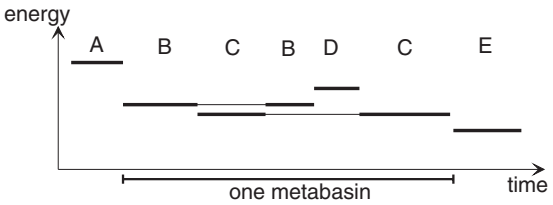

Figure 31. Identification of a metabasin by identifying the largest overlapping region, formed by the visited inherent structures.

MB. Second, the energy is chosen as the lowest energy of the ISs visited during this time. This idea is sketched in figure 30. For a typical time series of ISs one expects that MBs with low energies will contain a larger number of ISs. In contrast, high-energy ISs are often only visited once so this IS alone will be considered an MB.

A strict definition of MBs based on the inherent dynamics trajectory $\xi(t)$ is possible with the following algorithm [231]. (a) Determine the regions $[t_i^*, t_i^\dagger]$ where t_i^* is the time of the first and $t_i^\dagger$ the time of the last occurrence of minimum $\xi(t_i)$. (b) Any two regions overlapping by less than $\tau_{\rm mol}$ are cut so that $[t_i^*, t_i^\dagger] \cap [t_j^*, t_j^\dagger] = \emptyset$, where $\tau_{\rm mol}$ is a small molecular timescale. (c) Any two regions overlapping by more than $\tau_{\rm mol}$ are combined to $[t_i^*, t_i^\dagger] \cup [t_j^*, t_j^\dagger]$. Step (b) is motivated by the observation that very fast recrossings of a basin border during a transition are very probable. Finally, the whole trajectory can be regarded as a succession of different MBs. A more pictorial view of the definition of a metabasin is shown in figure 31.

Strictly speaking, due to the stochastic elements of the actual trajectory the formation of MBs is not unique but depends on the specific trajectory. However, in a statistical sense it is well defined and, as shown below, yields unprecedented information about the relation between the PEL and the dynamics.

In principle one would have to minimize the potential energy after every MD step in order to obtain a maximum accuracy of the MB transitions. In practice this can simplified. First, one minimizes after regular time intervals. If two subsequent ISs are identical there cannot be an MB transition in this time interval. In the other case one uses interval bisectioning techniques to identify the elementary transitions.

5.2.3. Applicability. The introduction of MB was motivated by the goal to relate energy and mobility. There is, however, a second major advantage. Naturally, the mean square displacement for long times does not change if one takes the real trajectory, the IS trajectory or the MB trajectory. Thus one may also extract the diffusion constant from $\xi_{\rm MB}(t)$. Of particular importance will be the average waiting times in an IS or an MB. On the MB level the diffusion constant turns out to be directly related to the average MB waiting time. In contrast, on the IS level the long-range transport is also strongly influenced by the temperature-dependent fraction of forward–backward jumps. Then knowledge of the average IS waiting time does not allow one to predict the long-range transport.

Conceptually, a different definition of MBs would also have been conceivable. As already discussed in [231] and reflected in figure 7, the system is immobile for some time then shows a time of high mobility until it becomes immobile again. One might identify the immobile periods as residences in MBs and the time in between as transitions between MBs. Probably, this is the picture which Stillinger had in mind. This was exactly the definition of so-called valleys, introduced in [231] and revisited in [52]. From a practical point in this way the waiting for a MB could be to a good approximation obtained from the analysis of the real space dynamics without the need of minimization [52]; see also section 7. However, this alternative definition of MBs has some drawbacks: First, due to the broad distribution of waiting times (see below) the distinction between immobile and mobile (and thus between MBs and transition between MBs) depends on an arbitrarily chosen timescale. Actually, as shown below, there exists at least one relatively well defined timescale $\tau^\star$, which might be appropriate for this purpose. Second, due to the unknown effect of the transition periods on the long-range transport it is impossible to relate the typical MB waiting time to quantities like the diffusion constant. A related definition of MBs has been presented in [87, 232]. Starting from rates between ISs subsets are identified in which equilibration can be achieved within a pre-fixed time. As compared to the previous definitions this allows one in some limit (no unbalanced transition rates [232]) to perform a unique partition of the configuration space in MBs, independent of a specific trajectory. However, in practice many details of the PEL have to be discarded for the application of this approach.

On a qualitative level the presence of MBs, reflecting the substructure of the PEL, has also been invoked to rationalize that more highly annealed glasses remain in their initial region of configuration space up to larger strains [233]. Interestingly, the MB dynamics can be studied experimentally by analysis of the lifetime fluctuations in single molecule spectroscopy experiments [234]. Actually, with similar coarse-graining procedures transitions in crystalline compounds have been analyzed [235].

5.2.4. Energy distribution of MB. For BMLJ and BKS-SiO_2 it has been shown that the Boltzmann distribution of ISs and MBs is basically identical in the harmonic regime; see figure 32 where data for BMLJ are shown. Only at higher temperatures do differences emerge. The similar distribution of ISs and MBs can be easily rationalized. Since the energy of an MB is defined as that of its lowest energy minimum, the mapping from IS to MB transfers the weights of the elevated IS of an MB to its lowest one. Thus, the distribution of MBs will be shifted

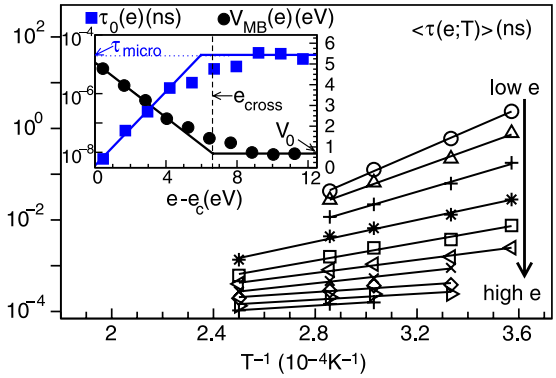

Figure 33. Arrhenius plot of the average MB waiting time $\langle\tau(e, T)\rangle$ and the resulting effective activation energy $V_{\mathrm{MB}}(e)$ and the prefactor $\tau_0(e)$ for BKS-SiO_2. Note that e_c corresponds to e_{cut} in the present terminology. Reprinted with permission from [215]. Copyright 2006 by the American Physical Society.

to lower energies. However, at low temperatures typically the lowest minimum of an MB is populated. Thus, the shift is very small. In contrast, for high temperatures the system will spend a significant time in the elevated minima of an MB such that this shift becomes relevant.

5.3. Insight from simulations

As discussed above, low-energy MBs on average have longer waiting times than high-energy MBs. This effect can be easily quantified by averaging the waiting time for MBs of similar energies, obtained from long simulations at different temperatures. This analysis has been performed for BKS-SiO_2 (figure 33) and BMLJ (figure 34). For BKS-SiO_2 $N = 99$ particles have been used, for BMLJ $N = 65$ particles. A discussion of this specific choice of the system size as well as a discussion of other system sizes can be found in sections 8 and 9.

The escape from an MB can be characterized by an Arrhenius behavior, quantified by an activation energy $V_{\mathrm{MB}}(e)$ and a prefactor $\Gamma_0(e)$, i.e.

$$\Gamma(e, T) = \Gamma_0(e) \exp(-\beta V_{\mathrm{MB}}(e)). \tag{63}$$

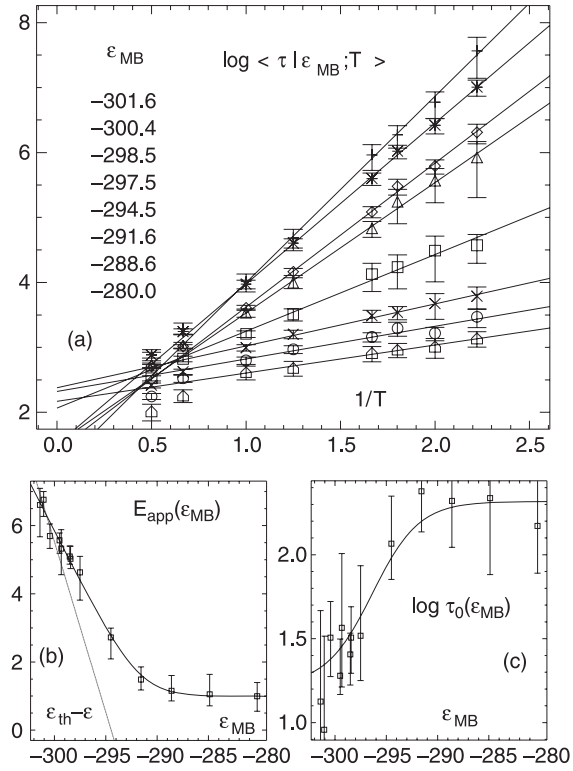

Figure 34. Arrhenius plot of (a) the average MB waiting time $\langle\tau(e, T)\rangle$, (b) the resulting effective activation energy $V_{\mathrm{MB}}(e)$ (denoted $E_{\mathrm{app}}(e)$ in the figure) and (c) the prefactor $\tau_0(e)$ for BMLJ. Reproduced with permission from [53]. Copyright 2003 by the American Physical Society.

Some interesting conclusions can be drawn about $V_{\mathrm{MB}}(e)$ and $\Gamma_0(e)$ which hold both for BMLJ and BKS-SiO_2.

(1) $V_{\mathrm{MB}}(e)$. There exists a crossover energy scale e_{cross} such that in the high-energy limit $e > e_{\mathrm{cross}}$ the energy dependence of $V_{\mathrm{MB}}(e)$ approaches a constant V_0, whereas in the opposite limit $V_{\mathrm{MB}}(e)$ increases linearly with decreasing energy, i.e.

$$V_{\mathrm{MB}}(e) = \lambda(e_{\mathrm{cross}} - e) + V_0. \tag{64}$$

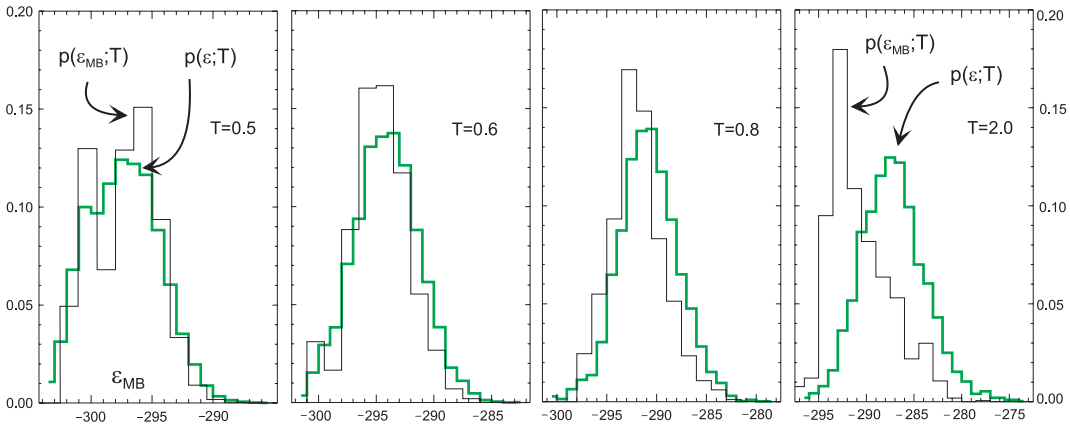

Figure 32. MB versus IS energy distribution $p_{\mathrm{eq}}(e)$ for the BMLJ system.

Table 1. The thermodynamic and dynamic PEL parameters, obtained from simulation of BKS-SiO_2 and BMLJ. The energy values are given relative to $e_{0,\mathrm{eff}}$.

		Thermodynamic				Dynamic				
	N	σ	$-e_{\mathrm{cut}}$	β_{harm}	α	$-e_{\mathrm{cross}}$	λ	κ	V_0	Γ_0
BKS-SiO_2	99	3.5 eV	43.4 eV	≈ 0	1.14	37.5 eV	0.66	0.62	0.8 eV	1/(20 fs)
BMLJ	65	3.0	—	-0.3	0.73	12.9	0.55	0.3	1.0	1/150

Table 2. Relevant temperatures as derived from the data in table 1.

	T_{cross}	T_{cut}	T_{K}	$T_{\mathrm{cross}}/\sqrt{\lambda\sigma^2}$	$T_{\mathrm{cut}}/\sqrt{\lambda\sigma^2}$	$T_{\mathrm{K}}/\sqrt{\lambda\sigma^2}$
BKS-SiO_2	3800 K	3275 K	2700 K	0.115	0.099	0.08
BMLJ	0.70	—	0.34	0.31	—	0.15

For a few single low-energy ISs the apparent activation energy has been quantitatively related to the local topology of the PEL; see section 4. Generalizing this procedure one can also relate the value of $V_{\mathrm{MB}}(e)$ to the explicit properties of the PEL. Here, one has to take into account the average over all MBs of energy e. If MB i is visited with probability φ_i (which in the harmonic approximation is temperature independent) one has for the average waiting time

$$\langle\tau(e)\rangle = \sum_i \varphi_i \langle\tau_i\rangle \tag{65}$$

$\langle\tau_i\rangle$ is the average waiting time of MB i. Then one can write

$$-\frac{\mathrm{d}\ln\langle\tau(e)\rangle}{\mathrm{d}\beta} = -\frac{\sum_i \varphi_i\langle\tau_i\rangle}{\langle\tau(e)\rangle}\frac{\mathrm{d}\ln\langle\tau_i\rangle}{\mathrm{d}\beta}$$
$$= \frac{1}{\langle\tau(e)\rangle}\sum_i \varphi_i\langle\tau_i\rangle\sum_a p_{a,i}E_{0.5,a,i} \tag{66}$$

where in the last step we have used equation (50). Applying this to the finite trajectory, sampled during the MD simulations, one can thus estimate

$$V_{\mathrm{MB}}(e) \approx \frac{\sum_j \tau_j E_{0.5,j}}{\sum_j \tau_j}. \tag{67}$$

Again, the correct weighting factors are implicit here. Note that in equation (67) the average over individual MBs no longer enters. Equation (67) establishes a relation between $V_{\mathrm{MB}}(e)$, obtained from analyzing the average waiting time, and $E_{0.5,j}$, extracted from an explicit saddle analysis; see section 4.

It turns out for BMLJ that the right side of equation (67) is indeed an excellent estimate of $V_{\mathrm{MB}}(e)$ for $e < e_{\mathrm{cross}}$ [53]. Thus, the function $V_{\mathrm{MB}}(e)$ can be directly related to the specific PEL properties.

Interestingly, the constant value $V_{\mathrm{MB}}(e) = V_0$ in the high-energy limit is close to the additional contribution of the last saddle before $p_{\mathrm{back}} < 0.5$. Thus, there are two distinct contributions to $V_{\mathrm{MB}}(e)$: (i) $V_{\mathrm{MB}}(e) - V_0$ reflects the topology of the PEL, related to differences between IS energies; (ii) V_0 is the additional contribution due to saddles. In the low-energy limit, accessible by computer simulations, the first contribution is dominant.

Recently, de Souza and Wales analyzed the temperature dependence of the mean square displacement, evaluated for a fixed time τ [236]. Of course, for very large τ this analysis recovers the standard diffusion coefficient. For ambient τ, which for the lowest temperatures is significantly shorter than τ_α, the authors observe a simple Arrhenius behavior with the high-temperature activation energy V_0. For lower temperatures this approach is sensitive to the local forward–backward motion within an MB. The barriers in this regime are of the order of V_0 so that the local processes remain activated with the high-temperature activation energy. This strengthens the observation that it is roughly the same value V_0 which governs the additional barrier height at low and high energies.

Interestingly, the function $V_{\mathrm{MB}}(e)$ somewhat resembles the energy-dependent barrier height in figure 10 with a value of $\lambda \approx 0.5$. Note, however, that in one case the MB description and in the other the IS description is used.

(2) $\Gamma_0(e)$. $\Gamma_0(e)$ is constant for $e > e_{\mathrm{cross}}$. Its value $\Gamma_0 \approx 1/20\ \mathrm{fs}^{-1}$ for BKS-SiO_2 is of the order of typical molecular timescales. For $e < e_{\mathrm{cross}}$ one observes to a good approximation $\ln(\Gamma_0(e)/\Gamma_{\mathrm{micro}}) \propto (e_{\mathrm{cross}} - e)$. For BKS-$SiO_2$ the increase of $\Gamma_0(e)$ is nearly four orders of magnitude. In contrast, for BMLJ a variation by only one order of magnitude is observed. In both cases the behavior can be described by using equation (55).

In summary, the data for both systems can be to a good approximation described by equation (61) (for $e < e_{\mathrm{cross}}$ and $\tilde{\beta} > 0$) and $\Gamma(e) = \Gamma_0 \exp(-\beta V_0)$ otherwise. In particular, for $e < e_{\mathrm{cross}}$ $\Gamma_0(e)$ indeed displays an exponential dependence on energy. The arguments, put forward to derive equation (61) from model considerations, strongly suggest the relevance of percolation-like effects. This means that only for $e \geqslant e_{\mathrm{cross}}$ there is a significant probability to find adjacent MB with similar energy.

For BMLJ and BKS-SiO_2 the PEL parameters are listed in table 1. Note that if not mentioned otherwise from now on all energies are expressed relative to $e_{0,\mathrm{eff}}$, i.e. the maximum of $G_{\mathrm{eff}}(e)$. For the analytical calculations, to be presented below, it is convenient to exclusively use equation (61), i.e. using $e < e_{\mathrm{cross}}$ and $\tilde{\beta} > 0$. The first relation starts to be very well fulfilled if $e_{\mathrm{cross}} - \langle e(T)\rangle > \sigma$, which roughly implies $T < 0.6$

in the case of BMLJ and $T < 3600$ K in the case of BKS-SiO_2. In this temperature range one also has $\tilde{\beta} > 0$.

How do these results compare with the model suggestions for $\Gamma(e)$? First, it turns out that $e_{\rm cross}$ is significantly smaller than $e_{0,\rm eff}$. As will become clear below, this difference is crucial for properties like the fragility. Second, the additional barrier height V_0 is present both for BKS-SiO_2 and BMLJ (and has similar height after normalization by σ). Therefore, V_0 cannot be of any relevance for the question of fragility. It can be directly extracted from the high-temperature behavior.

The observation $\lambda < 1$ suggests than even these small systems are not elementary. This is equivalent to the result reported in [229] that a consistent mapping on an elementary trap model is not possible.

In table 2 the related temperature scales are listed for both systems. $T_{\rm cross}$ and $T_{\rm cut}$ are determined from the condition that $\langle e(T)\rangle$, evaluated via equation (35), correspond to the respective energies $e_{\rm cross}$ and $e_{\rm cut}$, respectively. $T_{\rm K}$ is determined via equation (37). Furthermore, the normalized temperatures are also listed in table 2. The additional factor λ is rationalized by the fact that σ^2 as well as $1/\lambda$ are proportional to the system size (see also section 8). Thus, the normalized temperatures are system properties and do not depend on the chosen system size.

Two major differences are evident when comparing BKS-SiO_2 and BMLJ. First, the low-energy cutoff for BKS-SiO_2 is significantly larger than the cutoff dictated by entropy. Thus, the amorphous ground state is a finite-entropy state. Second, $T_{\rm cross}/\sqrt{\lambda\sigma^2}$ (or, equivalently, $(-e_{\rm cross})/\sqrt{\lambda\sigma^2}$) is much lower for BKS-$SiO_2$. This means that activated processes become relevant only for states much lower in the PEL. As a consequence, a characteristic temperature like $T_{\rm MCT}$ should be lower for silica than for BMLJ because of its significantly smaller value of $(-e_{\rm cross})/\sigma$. Indeed, $\Delta(\sigma/T_{\rm MCT}) \equiv (\sigma/T_{\rm MCT})_{\rm silica} - (\sigma/T_{\rm MCT})_{\rm BMLJ} \approx 12.2 - 6.7 = 5.5$ [53, 68] and $\Delta((-e_{\rm cross})/\sigma) = 6.4$ are similar. Furthermore, the energy dependence of $\Gamma_0(e)$ for BKS-SiO_2 is much more prominent.

For small systems the mobility of the total system is strongly correlated with energy. Do these correlations also hold on the single-particle level? In previous work little correlation has been observed between single-particle mobility and single-particle energy [30, 55]. Of specific interest in this context is the very recent work of Poole and co-workers on water. They determined the mobility of the single particles and correlated it with its potential energy [237]. Interestingly, when choosing the potential energy of the initial configuration (denoted u_i^0 in their work) for which the isoconfigurational runs are performed, only very little correlation is observed, in agreement with what was reported above; see figure 35(a). If, however, the energy is defined as the average single-particle energy after the isoconfigurational runs (denoted $\langle u_i\rangle_{ic}$) the immobile particles clearly possess the lowest potential energies, whereas there is still no distinction between mobile and very mobile particles in terms of energy; see figure 35(b). The authors relate this effect to the fact that in the isoconfigurational ensemble there is an explicit average over the neighbor configurations which reduces the noise. In general, the difficulty to relate energy and mobility

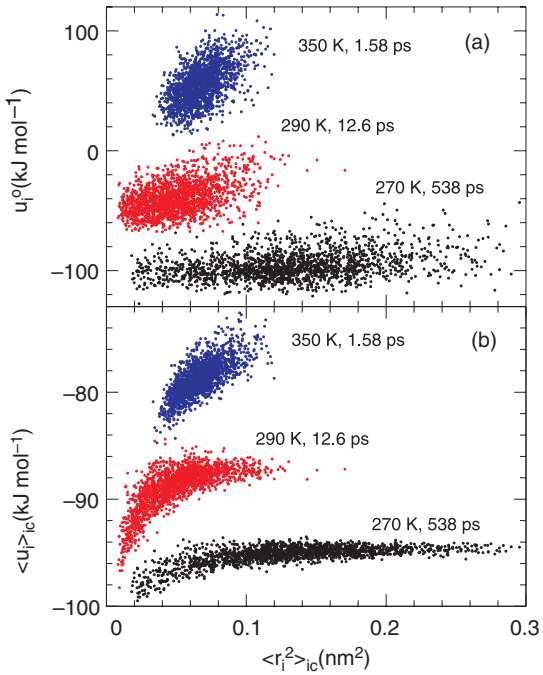

Figure 35. The (a) instantaneous potential energy and (b) potential energy in the isoconfigurational ensemble versus the displacement of the different particles in the isoconfigurational ensemble for water. Reprinted with permission from [237]. Copyright 2006 by the American Physical Society.

on a single-particle scale probably reflects the omnipresence of cooperative effects for the dynamics of supercooled liquids.

Recently, Wang and Stratt have analyzed the topology of the PEL by restricting the dynamics to configurations with a maximum energy $E_{\rm L}$ [238, 239]. Interestingly, it turned out that upon decreasing the value of $E_{\rm L}$ there exists a critical energy from which point on the system is no longer able to explore the whole configuration space but is rather constrained to some region. This observation has been related to the geometric features of the PEL by stating that *there is a timescale-independent percolation transition*. This is exactly the interpretation following from the results shown in figures 33 and 34. Interestingly, the temperature thermodynamically related to their critical value of $E_{\rm L}$ is very close to $T_{\rm MCT}$.

6. The average dynamic behavior as determined by the thermodynamics

Via the rates $\Gamma(e) = 1/\langle\tau(e)\rangle$, gained from general considerations and simulations, we have made a first step towards the connection between thermodynamics and dynamics. In this section we will go one step further by estimating the different moments $\langle\tau^n\rangle$ of the waiting time distribution. Naturally, the Boltzmann weights enter to bring in the dependence on temperature. We start by showing that the diffusion constant D is proportional to $1/\langle\tau\rangle$ and the structural relaxation time τ_α to $\langle\tau^2\rangle/\langle\tau\rangle$. Therefore, the moments $\langle\tau^n\rangle$ are indeed of central relevance.

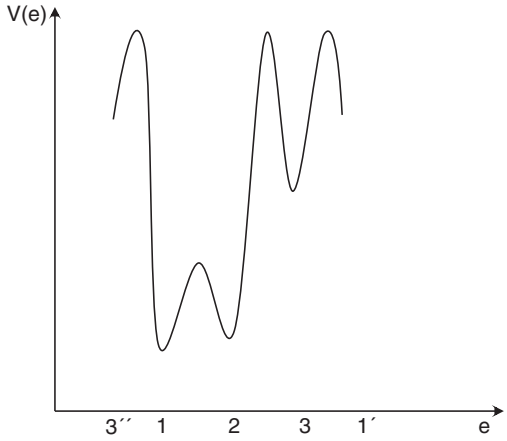

Figure 36. A simple periodic PEL to rationalize the difference between $\varphi(e)$ and $G_{\rm eff}(e)$.

6.1. MB probability densities and the waiting time distribution

The average waiting time $\langle\tau\rangle$ can be estimated as $(\sum_k \tau_k)/K$ where the summation is over the different MBs visited by the system. In section 5 we have seen that there is a distinct relation between energy and mobility. Thus, one may try to express $\langle\tau\rangle$ and, more generally, $\langle\tau^n\rangle$ in terms of the energy distribution.

For this purpose we first introduce $\varphi(e)$ as the probability density that in a series of different MBs visited by the system a randomly chosen MB has energy e. Then the average waiting time is given by averaging $\langle\tau(e)\rangle$ over all MBs, i.e.

$$\langle\tau\rangle = \int \mathrm{d}e\, \varphi(e)\langle\tau(e)\rangle = \int \mathrm{d}e\, \varphi(e)/\Gamma(e). \qquad (68)$$

$\varphi(e)$ is distinctly different from the Boltzmann distribution $p_{\rm eq}(e)$ which denotes that at a randomly given time the present MB has energy e, i.e. $p_{\rm eq}(e) \propto \varphi(e)\langle\tau(e)\rangle$. Including a normalization factor this can be rewritten as

$$p_{\rm eq}(e) = \frac{\varphi(e)}{\Gamma(e)\langle\tau\rangle}. \qquad (69)$$

Qualitatively, this relation expresses that low-energy states (small $\Gamma(e)$) are often observed (at randomly chosen times), although their actual number $\propto \varphi(e)$ may be very small.

From equations (26) and (69) it follows that $\varphi(e) \propto G_{\rm eff}(e)$ if $\Gamma(e) \propto \exp(\beta e)$. However, in general, this is not the case (e.g. for $\lambda < 1$). Due to the utmost importance of the φ-distribution in the theoretical description (see, in particular, section 7) this is rationalized for a simple example. In figure 36 a PEL with three states is shown. Thus, $G_{\rm eff}(e)$ has three equal contributions at three energies. However, the sequence of minima as obtained from a standard kinetic simulation will mostly display jumps between minima 1 and 2. Thus for state 3 $\varphi(e)$ is somewhat smaller. This difference would disappear (and, thus, $\varphi(e) \propto G_{\rm eff}(e)$) if the barrier between states 2 and 3 had the same height as the barrier between states 1 and 2. In general, $\varphi(e)$ is expected to have a weaker temperature dependence than $G_{\rm eff}(e)$.

Multiplication of equation (69) by $\Gamma(e)$ and subsequent integration yields

$$\langle\tau\rangle^{-1} = \int \mathrm{d}e\, p_{\rm eq}(e)\Gamma(e) \equiv \langle\Gamma\rangle_p. \qquad (70)$$

Thus, the average waiting time is also related to the rate average over the equilibrium probability distribution. Note the different notations ($\langle\cdot\rangle$ as the φ-average versus $\langle\cdot\rangle_p$ as the p-average).

So far no information about the nature of the relaxation process has entered the analysis. In the simplest case the escape from a state with energy e is governed by a single barrier height. Then the waiting time distribution, related to this energy, is just $\Gamma(e)\exp(-\Gamma(e)t)$. For the BMLJ($N = 65$) system one has $1/\lambda \approx 2$ subsystems. In the simplest picture the total energy is then the sum of two independent subsystems, each with energy e_i ($e_1 + e_2 = e$), and for a given energy decomposition the total rate $\Gamma(e)$ is given by $\Gamma(e_1) + \Gamma(e_2)$. Actually, as outlined in section 8.2, the normalized second moment $\langle\tau(e)^2\rangle/\langle\tau(e)\rangle^2$ is expected to be around 16 for $T = 0.5$ for two subsystems as compared to 2 for an elementary system. The broadening of the waiting time distribution at fixed energy is due to the fact that for a given total energy e several decompositions $e = e_1 + e_2$ are possible, each giving rise to different escape rates. The numerically observed value is approximately 8 [212]. This means that the BMLJ($N = 65$) system behaves, to first approximation, like two independent subsystems (each described by $\lambda = 1$ and variance $\sigma^2/2$ if σ^2 is the variance of the original system). A possible reason for the decrease from 16 to 8 will be given below. In what follows we neglect this effect and postulate that the elementary system behaves like an ideal Gaussian glass-former with $\lambda = 1$ and an exponential waiting time distribution at given energy. Note that the waiting time distribution at fixed energy is a well defined observable in the MB approach and can be easily obtained numerically. This is different to previous approaches, where on a phenomenological level quantities like a local viscosity have been introduced for which a strict definition does not exist [132, 240]. In any event, the subsequent calculations can be easily generalized to take into account possible deviations from a purely exponential behavior of the waiting time distribution of the elementary system.

As a result, the total waiting time distribution $\varphi(\tau)$ of the MB residences can be written as a superposition of exponential functions, i.e.

$$\varphi(\tau) \propto \int \mathrm{d}e \int \mathrm{d}t\, \varphi(e)\exp(-\Gamma(e)t)\delta(t-\tau) \qquad (71)$$

where the energy-weighting is via $\varphi(e)$.

This aspect of exponential versus non-exponential local relaxation is strongly related with the old discussion of homogeneous versus heterogeneous relaxation [16, 17]. Heterogeneous relaxation would simply mean that one has a superposition of exponentially relaxing entities. Experimentally it has been shown that the dynamics at the glass transition is basically heterogeneous [18]. This also indicates that the choice of an exponential waiting time distribution is indeed not too bad.

6.2. Temperature-dependent moments of the waiting time distribution

For an ideal Gaussian glass-former we know its energy distribution as well as the relation between energy and dynamics. Based on this one can now characterize the temporal properties of the hopping events. $\Gamma(e)$ is dictated by the two energies $e_{\rm cross}$ and $e_{\rm cut}$. We always assume that $\tilde{\beta}$ is sufficiently low that $e > e_{\rm cross}$ is not relevant. With respect to $e_{\rm cut}$ two temperature regimes can be distinguished. Whereas for $\sigma^2\tilde{\beta} < |e_{\rm cut}|$ the low-energy cutoff does not play any role, for even lower temperatures $\sigma^2\tilde{\beta} > |e_{\rm cut}|$ it starts to dominate the thermodynamics and thus also the dynamics. These two cases are now discussed.

Note that within the present formalism the dynamics can even be predicted for temperature regimes below those accessible nowadays by computer simulations [224]. Here one may exploit that the temperature dependence of $p_{\rm eq}(e)$ and $\Gamma(e)$ is known from knowledge of the parameters listed in table 1.

6.2.1. No influence of cutoff energy. Using the explicit form of $G_{\rm eff}(e)$ one obtains after a straightforward integration of equation (70)

$$\langle\tau\rangle^{-1} = \Gamma_0 \exp((\lambda^2/2-\lambda)\mu^2/2)\exp(-\beta V_0). \tag{72}$$

This relation holds without any assumption about the nature of the waiting time distribution. To calculate the moments of $\varphi(\tau)$ beyond the first moment one needs to specify the waiting time distribution as discussed above. Here we present results for an exponential waiting time distribution for the elementary subsystem, i.e. equation (71). Therefore we always choose $\lambda = 1$.

Its different moments $\langle\tau^n\rangle$ can be directly calculated by multiplication of equation (71) with τ^n and subsequent integration, i.e.

$$\langle\tau^n\rangle = n!\int {\rm d}e\, \varphi(e)\Gamma(e)^{-n} = n!\langle\tau\rangle\langle\Gamma^{1-n}\rangle_p \exp(n\beta V_0). \tag{73}$$

For the second equality equation (69) has been employed. Straightforward evaluation of Gaussian integrals yields

$$\langle(\Gamma/\Gamma_0)^m\rangle_p = \exp[(m^2/2-m)\mu^2 - m\beta V_0]. \tag{74}$$

The case $m = 1$ recovers equation (72). Furthermore, the case $m = -1$ yields

$$\langle\tau^2\rangle = \exp(\mu^2)\langle\tau\rangle^2. \tag{75}$$

In most models no distinction between $e_{\rm cross}$ and $e_{0,\rm eff}$ is made; i.e., $e_{\rm cross} = 0$ in the present notation. Then μ can be identified with β. The relations for this special case can already be found in the literature [220]. Note that in this limit equation (72) corresponds to the well known $1/T^2$ temperature dependence, discussed, e.g., in [223].

From the theoretical perspective the case of an exponential distribution of energies $p_{\rm eq}(e) \propto \exp(-e/e_0)$ is of special interest [220]. Then for the temperature $T = e_0$ the first moment of the waiting time distribution diverges. Qualitatively, this can be interpreted as a glass transition in terms of a real phase transition. Below this temperature the system displays specific aging properties.

6.2.2. Influence of cutoff energy. In general, every system will have a lowest energy (see equation (38) for a Gaussian distribution), which might suggest a transition to an Arrhenius temperature dependence at low temperatures. In what follows we use the notation $e_{\rm cut}$ for the lowest energy—independent of whether this energy is characterized by a finite or vanishing entropy. We restrict ourselves to the discussion of $\langle\tau\rangle$ and thus consider the case of general λ.

Qualitatively, one expects that at sufficiently low T the Boltzmann distribution reads $p_{\rm eq}(e) \approx \delta(e - e_{\rm cut})$. Then equation (70) predicts that $\langle\tau(T)\rangle$ is activated with an activation energy of $V_{\rm MB}(e_{\rm cut})$. Indeed, for BKS-SiO_2 the macroscopic activation energy of diffusion and $V_{\rm MB}(e_{\rm cut})$ agree within statistical uncertainty [215].

For a quantitative analysis we assume for reasons of simplicity that $G_{\rm eff}(e)$ is Gaussian for $e > e_{\rm cut}$ and $G_{\rm eff}(e) = 0$ for $e < e_{\rm cut}$. For $\lambda = 1$ the transition to an Arrhenius behavior happens around $\tilde{\beta}\sigma^2 \approx -e_{\rm cut}$. The average waiting time is calculated in appendix B. The result reads

$$\Gamma_0\langle\tau\rangle \approx \exp(\beta V_{\rm MB}(e_{\rm cut}))\exp((e_{\rm cross}^2 - e_{\rm cut}^2)/2\sigma^2). \tag{76}$$

Note that the microscopic prefactor $(1/\Gamma_0)$ is supplemented by the additional term $\exp((e_{\rm cross}^2 - e_{\rm cut}^2)/2\sigma^2)$.

The situation is somewhat more subtle for $\lambda < 1$. In this case the Arrhenius temperature dependence only sets in for an even lower temperature regime $\tilde{\beta}\sigma^2(1-\lambda) > [e_{\rm cross} - e_{\rm cut}]$. One obtains (see, again, appendix B)

$$\Gamma_0\langle\tau\rangle \approx \exp(\beta V_{\rm MB}(e_{\rm cut}))\exp((\lambda e_{\rm cross}^2 - \lambda e_{\rm cross}e_{\rm cut})/\sigma^2). \tag{77}$$

Because of the additional temperature regime emerging for $\lambda < 1$, there is no continuous transition between both expressions. The latter expression is of relevance for the actual simulations. Note that here the microscopic prefactor $(1/\Gamma_0)$ has another factor $\exp(\lambda(e_{\rm cross}^2 - \lambda e_{\rm cross}e_{\rm cut})/\sigma^2)$. For example, for BKS-$SiO_2$ this prefactor is of the order of 10^5, in very good agreement with the actual simulation data [175].

In the next step one can calculate the timescale from which point on Arrhenius behavior is observed by evaluating equations (76) and (77) for the respective transition temperature. One obtains $\Gamma_0\langle\tau\rangle = \exp((e_{\rm cross} - e_{\rm cut})^2/2\sigma^2)$ for $\lambda = 1$ and

$$\Gamma_0\langle\tau\rangle = \exp((\lambda/(1-\lambda))(e_{\rm cross} - e_{\rm cut})^2/\sigma^2) \tag{78}$$

for $\lambda < 1$. From equation (78) it turns out for BKS-SiO_2 that for $\Gamma_0\langle\tau\rangle \approx 10^2$ one has the crossover to the Arrhenius regime (neglecting the additional minor influence of $\kappa < 1$) [68, 116, 118, 174, 241].

More generally, the low-temperature Arrhenius dependence can be clearly related to the cutoff in the PEL, which itself reflects the network structure of silica. On a qualitative level the possible relation to the tetrahedral ordering has been already described in [242]. Interestingly, the Arrhenius behavior of BKS-SiO_2 disappears upon application of pressure when the tetrahedral network structure starts to be destroyed. Also for metallic glasses a correlation has been reported that systems with larger icosahedral ordering are more Arrhenius-like [243].

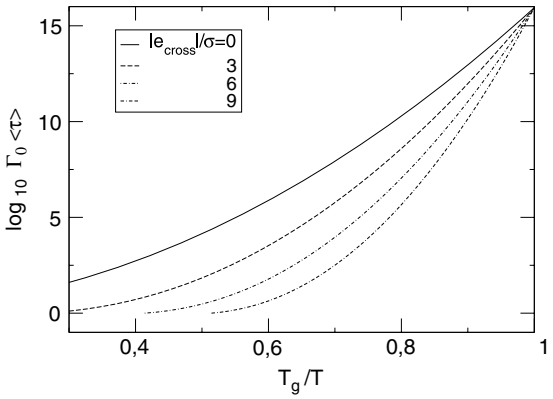

Figure 37. The temperature dependence of $\Gamma_0\langle\tau\rangle(\propto D(T))$ for different values of the crossover energy with $\lambda = 1$ (the values are given with respect to $e_{0,\mathrm{eff}}$, following the present convention). Reproduced with permission from [226]. Copyright 2008 by the American Physical Society.

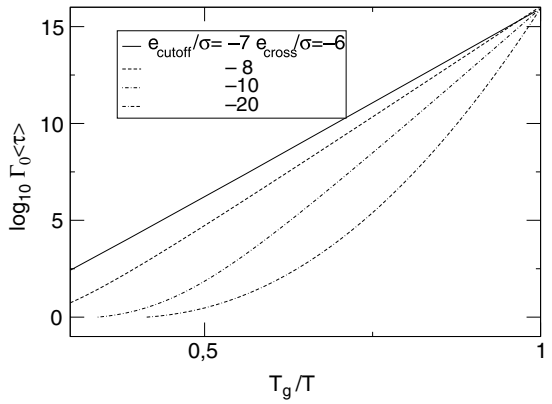

Figure 38. The temperature dependence of $\Gamma_0\langle\tau\rangle$ for different values of the cutoff energy for intermediate crossover energy.

Estimating e_{cut} for BMLJ65 via equation (38) one obtains $\Gamma_0\langle\tau\rangle \approx 10^{10}$. This is beyond current computer facilities. This shows, however, that for experimental systems it is well conceivable that in the range of experimentally accessible temperatures a transition to Arrhenius-type behavior might occur (note that $1/\Gamma_0 \approx 20$ fs for BKS-SiO_2; see table 1).

6.3. Fragility

6.3.1. Kinetic fragility. Here we discuss the temperature dependence of $\langle\tau\rangle$ (and thus of $D(T)$) and in particular the fragility for an ideal Gaussian glass-former (without or with a cutoff) for the limiting case $\lambda = 1$.

The glass transition temperature is defined by the condition

$$\Gamma_0\langle\tau(T_{\mathrm{g},K})\rangle = 10^K. \tag{79}$$

$T_{\mathrm{g},16} = 1/\beta_{\mathrm{g},16}$ corresponds to the calorimetric T_{g} because $\eta(T_{\mathrm{g}})/\eta(T \gg T_{\mathrm{g}}) \approx 10^{16}$. Here we assume that the viscosity, which is the typical basis for the fragility, displays the same temperature dependence as the diffusion constant. Since the Stokes–Einstein relation is not strictly fulfilled, the results for the diffusion constant in terms of the values of T_{g} and the resulting fragility are not exactly the same. Simple expressions emerge for the case $V_0 = 0$ (corrections can be simply calculated but only mildly influence the results). Using equation (74) for the case without cutoff a straightforward calculation yields [226]

$$\sigma\beta_{\mathrm{g},K} = k_{\mathrm{entro}}\sigma + \sqrt{2K\ln(10)}. \tag{80}$$

Moreover, the fragility

$$m_{\mathrm{kin},K} \equiv -\mathrm{d}\log\langle\tau(T)\rangle/\mathrm{d}(T_{\mathrm{g},K}/T)|_{T=T_{\mathrm{g},K}}, \tag{81}$$

here expressed via $\langle\tau(T)\rangle$, turns out to be

$$m_{\mathrm{kin},K} = 2K + \sqrt{2K/\ln(10)}k_{\mathrm{entro}}\sigma. \tag{82}$$

In this regime the fragility depends on the dimensionless parameter $k_{\mathrm{entro}}\sigma = -e_{\mathrm{cross}}/\sigma$. Thus, with the dynamic crossover energy we have identified a central PEL parameter determining the fragility. These results are visualized in figure 37. One can clearly see how the fragility increases with increasing $-e_{\mathrm{cross}}/\sigma$.

Note that equation (82) implies that BMLJ would be stronger than BKS-SiO_2 if the cutoff were artificially removed so that the PEL were purely Gaussian. The non-fragile behavior of BMLJ has already been mentioned in [244].

If the cutoff energy enters before the glass transition temperature is reached the evaluation for the low-temperature Arrhenius-regime yields

$$m_{\mathrm{kin},K} = K + [e_{\mathrm{cut}}^2 - e_{\mathrm{cross}}^2]/(2\ln 10\sigma^2). \tag{83}$$

In figure 38 we explicitly show the dependence on the cutoff energy. In agreement with our theoretical discussion one observes that for increasing cutoff energy the system becomes stronger.

Of course, since the temperature dependence of τ_α is in general not identical to that of $\langle\tau\rangle$, the results would slightly differ if $m_{\mathrm{kin},K}$ were calculated for τ_α or η rather than for the diffusivity.

Empirical relations to correlate the fragility with, e.g., the Poisson ratio have been suggested [245], but are questioned in [246]. It would be interesting to check whether there exists a physical connection between the observables suggested in that work and the value of e_{cross}, determining the crossover from liquid-like behavior to solid-like behavior.

The present analysis has shown that at least two more or less independent energy scales e_{cut} and e_{cross} have a strong influence on the fragility. As a consequence, ordering the glass-forming systems by fragility does not fully reflect their underlying differences.

6.3.2. Relation to the AG approach. Alternatively, one can calculate the value of β_{g} under the assumption of the AG relation equation (8) and a Gaussian PEL (using $\beta_{\mathrm{harm}} = 0$). Then one has to solve the equation

$$10^K = \exp(\beta_{\mathrm{g}}B_{\mathrm{AG}}/(\alpha - \beta_{\mathrm{g}}^2\sigma^2/2N)). \tag{84}$$

For large K one obtains

$$\beta_g = \frac{\sqrt{2\alpha N}}{\sigma} - \frac{B_{AG}\sqrt{N}}{\sigma K \ln(10)}. \tag{85}$$

Then a straightforward calculation yields for the fragility (again in the limit of large K)

$$m_{\mathrm{kin},K} = \frac{\sqrt{2\alpha}K^2(\ln 10)^2\sigma}{B_{AG}\sqrt{N}}; \tag{86}$$

within the AG approach the fragility depends on the density of states, i.e. α, as well as the empirical constant B_{AG}. A large number of states implies larger fragility (at least for fixed B_{AG} which, of course, could also depend on α [24]).

It may be interesting to compare this relation with the fragility equation (82), obtained for an ideal Gaussian glass-forming system. Qualitatively, both relations would show a somewhat similar behavior if systems with large α are related to systems with a low crossover energy e_{cross}, i.e. large k_{entro}. This is not unreasonable because in the spirit of percolation-like arguments for a larger number of ISs the system would be able to find a path with a lower barrier to move between two low-energy ISs. However, in a strict way it will not be possible to map equation (86) onto (82) because of the different K dependence. Formally, this problem could be solved if α decreases with increasing K, i.e. going to longer timescales and thus lower glass transition temperatures. Qualitatively this statement is equivalent to the requirement that $G(e)$ decays faster than a Gaussian. As discussed in section 3.5 this would be the case if the distribution were influenced by the presence of a broadened cutoff energy.

6.3.3. Thermodynamic fragility. In the spirit of the thermodynamic fragility as discussed in [20, 127] one can define the thermodynamic fragility index via [24]

$$m_{\mathrm{thermo},K} = -\beta_g \frac{S_c'(\beta_g)}{S_c(\beta_g)}. \tag{87}$$

Without cutoff we obtain, using equation (36),

$$m_{\mathrm{thermo},K} = \frac{\sigma^2(\beta_g - \beta_{\mathrm{harm}})\beta_g}{N\alpha - \sigma^2(\beta_g - \beta_{\mathrm{harm}})^2/2}. \tag{88}$$

Note that the denominator must be positive, because otherwise the entropy of the system would be negative. Under this condition, an increase of $\sigma k_{\mathrm{entro}}$ (which is the only relevant dimensionless parameter, characterizing ideal Gaussian glass-formers) and thus of $\sigma\beta_g$ (via equation (80)) gives rise to an increase of $m_{\mathrm{thermo},K}$ and $m_{\mathrm{kin},K}$, independent of the values of β_g or α. This strong correlation of $m_{\mathrm{kin},K}$ and $m_{\mathrm{thermo},K}$ is in agreement with the experimental observation for most systems [20].

Interestingly, increasing the value of β_{harm} yields a decrease in $m_{\mathrm{thermo},K}$. However, a different behavior emerges if one includes the vibronic contribution in the entropy, i.e. by using $S_{\mathrm{ex}}(T) = S_c(T) + S_{\mathrm{harm}}(T)$ rather than $S_c(T)$. $S_c(T)$ is given in equation (36). $S_{\mathrm{harm}}(T)$ can be determined from equations (23) and (35). Apart from a constant and a term depending logarithmically on β, one finds $S_{\mathrm{ex}}(T, \beta_{\mathrm{harm}}) = S_c(T, -\beta_{\mathrm{harm}})$. Accordingly, when defining $m_{\mathrm{thermo},K}$ on the basis of $S_{\mathrm{ex}}(T)$ one obtains an increasing thermodynamic fragility for increasing β_{harm} in agreement with the qualitative discussion in [20].

If the cutoff starts to influence the system a detailed calculation is no longer possible because the behavior of the configurational entropy at low temperatures depends on the details of $G(e)$ at low energies. Thus, it is not surprising that for SiO_2 the thermodynamic fragility does not follow the general trend [20].

The present discussion complements the work in [84] where the kinetic and the thermodynamic fragility have been discussed with reference to the AG relation. Simulations have also revealed a significant correlation between both fragilities.

6.4. Relaxation properties and violation of the Stokes–Einstein relation

Here we ask for the probability $S_0(t)$ that a system in equilibrium has not performed a hopping process until time t. It is given by

$$S_0(t) = \int \mathrm{d}e\, p_{\mathrm{eq}}(e) \exp(-\Gamma(e)t). \tag{89}$$

In what follows the trivial factor $\exp(\beta V_0)$ will be omitted. Furthermore, only the case $\lambda = 1$ is discussed. Naturally, one has

$$S_0(t) = \lim_{q\to\infty} S(q,t), \tag{90}$$

if $S(q,t)$ (defined in equation (1)) is evaluated for the MB trajectory. Equation (90) follows from the observation that for large q a single MB transition is sufficient for full decorrelation of the incoherent scattering function. The q-dependence of $S(q,t)$ will be discussed in more detail in section 7.3.

For a given temperature we define $\Gamma^\star = \Gamma(\langle e(T)\rangle)$ as the typical rate for this temperature. One obtains (neglecting the possible effect of $\beta_{\mathrm{harm}} \neq 0$)

$$\Gamma^\star = \exp(-\mu^2). \tag{91}$$

Introducing the normalized variables $u = \ln(t\Gamma^\star)$ and $v = \ln(\Gamma(e)/\Gamma^\star)$ equation (89) reads after substitution [247] (note that u contains the time dependence)

$$S_0(u) = 1/\sqrt{2\pi\mu^2}\int \mathrm{d}v\, \exp(-v^2/2\mu^2)\exp(-\exp(u-v)). \tag{92}$$

The last factor represents the $\exp(-\Gamma t)$ term. Thus, the distribution of relaxation rates corresponds to a log-normal distribution.

As discussed in the appendix C, an interesting relation to stretched exponential relaxation functions can be drawn, yielding $S_0(t) \approx \exp(-(t/\tau_{\mathrm{KWW}})^{\beta_{\mathrm{KWW}}})$ with (see also [247])

$$\beta_{\mathrm{KWW}} = 1/\sqrt{1+\mu^2} \tag{93}$$

and $\tau_{\mathrm{KWW}} = 1/\Gamma^\star$, holding for times around τ_{KWW}. This may justify the use of the stretched exponential as a fitting function

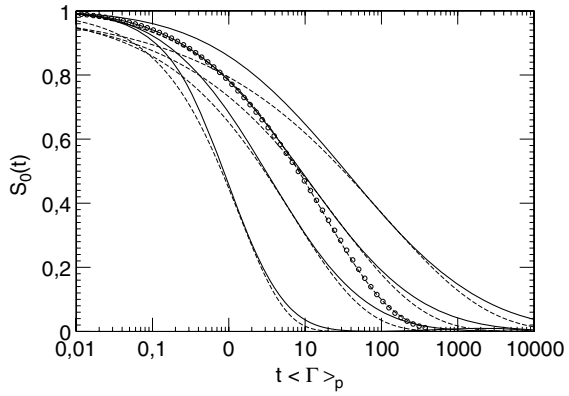

Figure 39. The function $S_0(t)$ for $\sqrt{\mu^2} = 1, 2, 2.5, 3$ (solid lines from left to right). The approximation by stretched exponentials with $\beta_{\mathrm{KWW}} = 1/\sqrt{1+\mu^2}$ is indicated by broken lines. Furthermore, for $\sqrt{\mu^2} = 2.5$ the case of finite k_{ex} is included (circles) together with its fit by a stretched exponential (see section 9).

at least for intermediate times. Note that the specific form of $\Gamma(e)$ only enters via $\Gamma^\star$.

In figure 39 we have numerically calculated $S_0(t)$ for different values of μ^2 and compared with the corresponding stretched exponential functions. Deviations are present at short and long times. Actually, from equation (92) one can directly extract the long-time limit. Due to the double-exponential term the contribution to the integral is restricted to $v \approx u$. For large u the first factor can thus be substituted by $\exp(-u^2/2\mu^2)$ so that

$$S_0(t) \propto \exp(-u^2/2\mu^2) \propto t^{-u/2\mu^2}, \tag{94}$$

i.e. a nearly algebraic behavior (note that u depends logarithmically on t).

One can define the α-relaxation time τ_α via

$$\tau_\alpha = \int \mathrm{d}t\, S_0(t) \tag{95}$$

which corresponds to the typical time until a particle jumps for the first time. This definition may sound surprising because typically τ_α is related to the decay of $S(q_{\max}, t)$, see equation (2). However, as shown in section 7.2, in the limit of low temperatures the $q \to \infty$ limit is already reached for relatively small values of q, if evaluated for the MB trajectory.

From equation (89) one immediately obtains (also using equation (74))

$$\tau_\alpha = \langle \Gamma^{-1} \rangle_p = (1/\Gamma_0) \exp(3\mu^2/2). \tag{96}$$

This has to be compared with the average hopping time $\langle \tau \rangle$ (equation (72)). One obtains

$$\tau_\alpha / \langle \tau \rangle = \exp(\mu^2). \tag{97}$$

Since the left side is proportional to $D\tau_\alpha$, equation (97) expresses the invalidation of the Stokes–Einstein relation for ideal Gaussian glass-forming systems. Using the definition of the exponent α in equation (4), i.e. $\langle \Gamma \rangle \langle \Gamma^{-1} \rangle \propto \langle \Gamma^{-1} \rangle^\alpha$, one obtains $\alpha = 2/3$. Experimental values are smaller (e.g. 0.25 for orthoterphenyl [21] and 0.23 for TNB [248]). Thus, the decoupling seems to be too strong. Qualitatively, the strong increase of τ_α with decreasing temperature is due to the very long-time tail of $S_0(t)$, contributing to the present definition of τ_α in equation (95).

These arguments can be generalized to a Gaussian distribution of barriers, with average barrier height $\bar{V}$ and variance $(\delta V)^2$. Then a straightforward calculation yields [112] $\langle \Gamma \rangle_p = \exp(\beta^2(\delta V)^2/2) \exp(-\beta \bar{V})$ and $\langle \Gamma^{-1} \rangle_p = \exp(\beta^2(\delta V)^2/2) \exp(\beta \bar{V})$. Thus, one obtains

$$\alpha = \frac{2}{1 + 2\bar{V}/(\beta(\delta V)^2)}. \tag{98}$$

Formally, the ideal Gaussian glass-former (with $V_0 = 0$) can be mapped on this general case by choosing $\bar{V} = \beta\sigma^2$ and $\delta V = \sigma$ as the average barrier height and the standard deviation, respectively. Of course, these barriers are only effective barriers since they just represent the difference of the average energy and the value of e_{cross} (of course, β has to be substituted by $\tilde{\beta}$ if $e_{\mathrm{cross}} \neq 0$). Consistently, one obtains $\alpha = 2/3$ for this case. Wolynes *et al* (for the dynamics of a probe molecule) [249] as well as Schweizer *et al* [112] have estimated the static as well as the fluctuating part of the barriers. The latter work reports values for α around 0.1–0.3 when choosing reasonable model parameters.

For the KCM it possible to estimate the waiting time distribution at a given spin and thus to obtain information about the average as well as the inverse average waiting time (conveniently expressed via the persistence time; see section 7.3) [148]. It turns out that for the Fredrickson–Andersen model (Arrhenius behavior) the value of α depends on the dimension ($\alpha(d = 1) = 1/3, \alpha(d = 3) = 0.05$) whereas for the East model (non-Arrhenius behavior) $\alpha \approx 0.27$ for all dimensions.

Since the relations derived above are fully compatible with the local dynamics (via $\Gamma(e)$) and the thermodynamics, these general results hold in particular for BMLJ and BKS-SiO_2 for the small system sizes discussed above. A generalization to larger systems is sketched in section 9.

If the cutoff energy does not interfere and V_0 can be neglected, the temperature dependence of the dynamics is fully captured by the value of μ. This means in particular that at T_{g} an ideal Gaussian glass-former is characterized by a fixed value of μ, independent of $\sigma k_{\mathrm{entro}}$ and thus independent of its fragility. This implies via equation (93) that the stretching parameter β_{KWW} does not depend on the fragility if determined exactly at T_{g}. Of course, residual fluctuations are expected when systems with different values of λ, κ and V_0 are taken into account. This argument will not change when the effects discussed in section 9 are additionally taken into account.

6.5. Exploration of MBs in different temperature regimes

We have seen that the escape rate from a MB strongly depends on energy. Therefore, the typical hopping characteristics will strongly depend on temperature and thus may reflect the different temperature regimes for a supercooled liquid. This temperature dependence can be explicitly analyzed for

the temperature dependence of the waiting time distribution $\varphi(t)$. It is shown in figure 40 for different temperatures [224]. It turns out that there is one crossover timescale $\tau^\star$ where the distribution changes its slope. To elucidate its physical interpretation the angle α between the entry point, the lowest minimum of the MB and the exit point of the trajectory have been determined for every MB. The average value of $\langle \cos \alpha(t) \rangle$ versus the lifetime t of the respective MB is also shown in figure 40. Visiting a MB with waiting time larger than $\tau^\star$ implies that the entry and exit points of this MB are largely uncorrelated. This happens after a long residence inside an MB with many possible exits. In some sense, the system has equilibrated within the MB. In contrast, for $t < \tau^\star$ the dynamics of the system is not strongly attracted by the underlying minima so that it can immediately escape. In some sense, these transitions can be regarded as *bookkeeping events* [250]. More generally, one can say that the system in a MB with $t > \tau^\star$ is *solid-like* and in the other MBs the system behaves as *liquid-like*. These terms just reflect the intuition that for liquid-like behavior barriers are not relevant. To a good approximation $\tau^\star$ is temperature independent; see figure 40. This is not surprising because the timescale to explore a minimum does not strongly depend on temperature.

At lower temperatures the system, first, stays longer in MBs of a given energy and, second, explores lower energy states with even longer waiting times. For both reasons the contribution of solid-like MBs should strongly increase with decreasing temperature. To capture this effect we introduce the probability $p(\tau)$ that at a randomly given time the waiting time has a value τ. The distribution $p(\tau)$ will be shifted to larger times than $\varphi(\tau)$ because it is more likely to randomly choose MB with a large waiting time than vice versa. The relation between $p(\tau)$ and $\varphi(\tau)$ is given by

$$p(\tau) = \frac{\varphi(\tau)\tau}{\langle \tau \rangle} \tag{99}$$

which, conceptually is equivalent to equation (69).

This effect can be captured in two different ways. (i) The fraction of solid-like configurations encountered by the system during its walk through configuration space is given by

$$\varphi_{\rm sol} \equiv \int_{\tau^\star}^{\infty} {\rm d}\tau\, \varphi(\tau). \tag{100}$$

(ii) The fraction of time spent in solid-like configurations can be expressed as

$$p_{\rm sol} \equiv \int_{\tau^\star}^{\infty} {\rm d}\tau\, p(\tau). \tag{101}$$

In figure 41 we show the temperature dependence of both quantities for BMLJ. Three different temperature regimes can be identified. First, for $T > 2T_{\rm c}$ one has $\varphi_{\rm sol}, p_{\rm sol} < 0.5$. Thus, the system can be described as a simple liquid. This temperature regime, as defined by the *dynamics*, is exactly the regime for which anharmonic effects become dominant. For $T_{\rm c} < T < 2T_{\rm c}$ one has $p_{\rm sol} > 0.5$ and $\varphi_{\rm sol} < 0.5$. Although the system still mainly visits liquid-like MBs, at a randomly given time it is most likely in a solid-like MB (landscape-influenced regime). Around $T_{\rm c}$ there is a slow crossover to

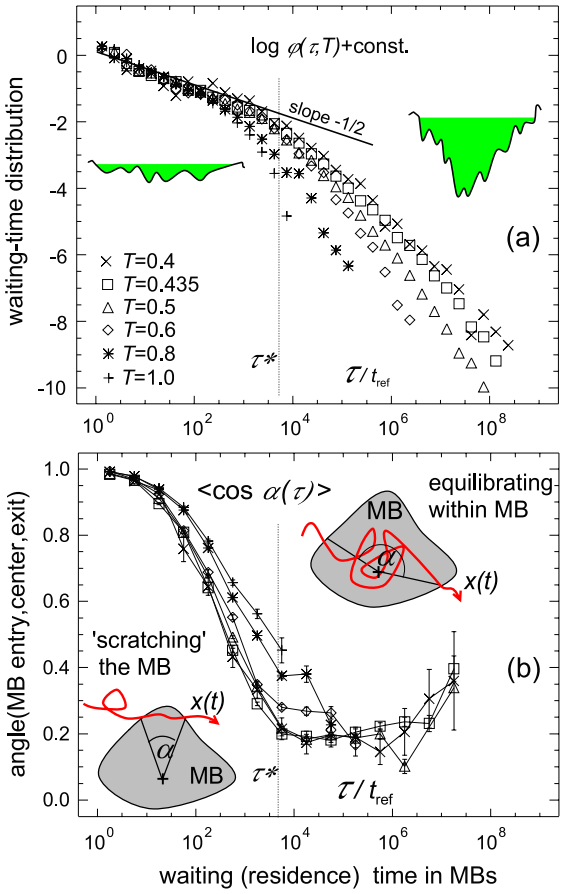

Figure 40. Rationalizing the presence of solid-like and liquid-like MBs for BMLJ for a range of different temperatures. (a) The distribution $\varphi(t, T)$ of MB waiting times for different temperatures. (b) The average value of $\langle \cos \alpha(t) \rangle$ versus the lifetime t (see text for definition). Reprinted with permission from [224]. Copyright 2003 by the American Physical Society.

the regime where liquid-like MBs are hardly visited any more (landscape-dominated regime). This analysis may therefore help to uniquely define the different dynamic regimes observed for a supercooled liquid.

In the spirit of the AG relation Odagaki has rationalized that the waiting time distribution for the escape from trapped configurations should display an algebraic behavior [251, 252]. The essential parameter is $\rho(T) + 1 \propto T s_{\rm c}(T)$. He has shown that the mth moment of $\varphi(\tau)$ is finite if $\rho(T) + 1 > m - 1$. On this basis he identifies the temperature for which $\rho(T) = -1$ as the Vogel–Fulcher temperature, the temperature for which $\rho(T) = 0$ as $T_{\rm g}$ where a transition from Gaussian (finite second moment) to non-Gaussian dynamics occurs. Finally, at the temperature for which $\rho(T) = 1$ a kinetic transition takes place.

As discussed in section 2 it has been numerically observed that the number of diffusive directions $f_{\rm dw}$ is proportional to D even in the low-temperature regime, where according to the above results activated processes should be dominant [67]. One might be tempted to conclude that the long-range transport is not restricted by high barriers but rather by the number of free directions. This would disagree with the previous

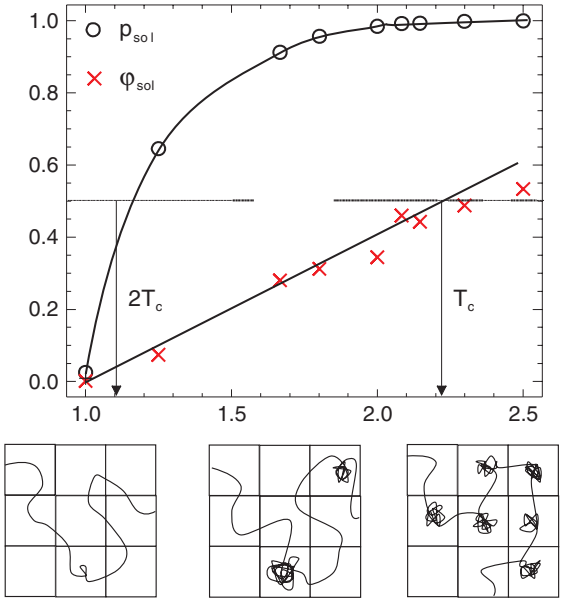

Figure 41. Temperature dependence of $p_{\rm sol}$ and $\varphi_{\rm sol}$. In the lower panel the resulting scenario of the exploration of the PEL is sketched for the three temperature regimes. Reprinted with permission from [224]. Copyright 2003 by the American Physical Society.

interpretation. However, this apparent discrepancy can be (at least qualitatively) removed for the regime $\varphi_{\rm sol} < 0.5$. The number of diffusive directions will be proportional to the probability to be in a liquid-like configuration, because in solid-like configurations the system will mainly reside close to the minimum. Thus one has to a good approximation

$$f_{\rm dw} \propto 1 - p_{\rm sol} \equiv p_{\rm liq}. \tag{102}$$

To proceed further we define $\langle\tau_x\rangle$ ($x \in$ liq, sol) as the average waiting time of the liquid-like and solid-like configurations. Note that $\langle\tau_{\rm liq}\rangle$ is basically temperature independent and that $\langle\tau_{\rm liq}\rangle \ll \langle\tau_{\rm sol}\rangle$. Then one can write

$$D \propto \frac{1}{\langle\tau\rangle} = \frac{p_{\rm liq}}{\langle\tau_{\rm liq}\rangle} + \frac{p_{\rm sol}}{\langle\tau_{\rm sol}\rangle} \approx \frac{p_{\rm liq}}{\langle\tau_{\rm liq}\rangle}. \tag{103}$$

For the last approximation we have used that the first term is proportional to $\varphi_{\rm liq}$ and the second proportional to $\varphi_{\rm sol}$. Because $\langle\tau_{\rm liq}\rangle$ is basically temperature independent we have the desired relation $D \propto p_{\rm liq} \propto f_{\rm dw}$. This does *not* imply that in this temperature regime the slow processes are irrelevant to understand the temperature dependence of $p_{\rm liq}$. Rather one has $p_{\rm liq} = \varphi_{\rm liq}\langle\tau_{\rm liq}\rangle/(\varphi_{\rm liq}\langle\tau_{\rm liq}\rangle + \varphi_{\rm sol}\langle\tau_{\rm sol}\rangle)$. Since this is much smaller than unity and since the main temperature dependence comes from $\langle\tau_{\rm sol}\rangle$, it is the escape from the slow configurations which determines the temperature dependence of $p_{\rm liq}$.

In [240] it has been proposed that there exist fluidized domains with a very small volume fraction around $T_{\rm g}$ in order to rationalize the invalidation of the Stokes–Einstein relation. Actually, this fraction can be identified with $p_{\rm liq}$ and this is indeed a very small number at low temperatures. Furthermore it has been postulated that the diffusion mainly occurs when a particle belongs to a fluidized domain. From equation (103) one may conclude that the contribution to the diffusion constant in the fluidized domain is indeed governed by $\varphi_{\rm liq}$.

7. Sequences of MBs and their real space realization

So far we have discussed the emergence of waiting times for the description of the escape characteristics from a *single* IS or MB with strong emphasis on the energy of that corresponding state. In this section the properties of *sequences* of MB are discussed. Of special interest is the real space realization. In particular, it turns out that the dynamics can be quantitatively described in the framework of the continuous-time random walk (CTRW).

7.1. Properties of MB transitions

First, the properties of individual transitions as well as sequences of transitions are discussed. The real space realization of the transitions is emphasized.

7.1.1. Single MB transitions. A convenient measure for the localization of single transition events is the participation ratio

$$z_1 = \sum_i \frac{\delta r^i}{\delta R^{\max}} \tag{104}$$

where δr^i is the shift of the ith particle and $\delta R^{\max}$ the shift of the most mobile particle. $z_1 = 1$ corresponds to a strict single-particle dynamics. For BMLJ the results are shown in figure 42 for two temperatures $T_h = 0.5$ and $T_l = 0.435$ [37]. Two important observations can be made. First, there is basically no temperature dependence for the participation ratio. Thus, the degree of localization of MB transitions is to a large extent temperature independent in the range of simulation temperatures. This does not mean that there are no temperature-dependent length scales in the PEL approach (see below). Second, the participation ratio only slightly increases when comparing IS with MB transitions. This implies that basically the same atoms are active during subsequent IS transitions within an MB. The individual IS transitions as well as the MB transitions have a string-like pattern where the string size of the MB transitions is more extended (containing on average seven particles) [37]. A more extended string-like structure was also seen in [253] for CS_2.

A different measure to quantify the dynamics is the van Hove self-correlation function in one dimension, denoted $\pi_n(x)$. It denotes the probability $\pi_n(x)$ that along a given axis a randomly chosen particle moves by x after n transitions. For isotropic systems $\pi_n(x)$ is symmetric around $x = 0$.

For BMLJ($N = 65$), $\pi_1(x)$ is to a very good approximation an exponentially decaying function [254]. Interestingly, it has been reported that for a large system the van Hove self-correlation function of a single IS transition is exponential for large and algebraic for small distances [62]. This is fully compatible with the present situation because the atoms with very small displacements correspond to those far

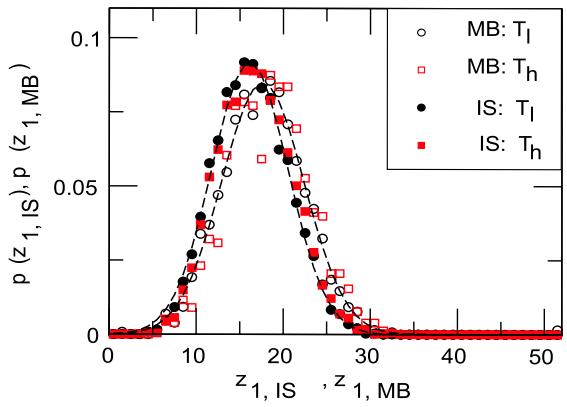

Figure 42. The participation ratio for MB and IS transitions for BMLJ($N = 65$) at two different temperatures. Reprinted with permission from [37]. Copyright 2004, American Institute of Physics.

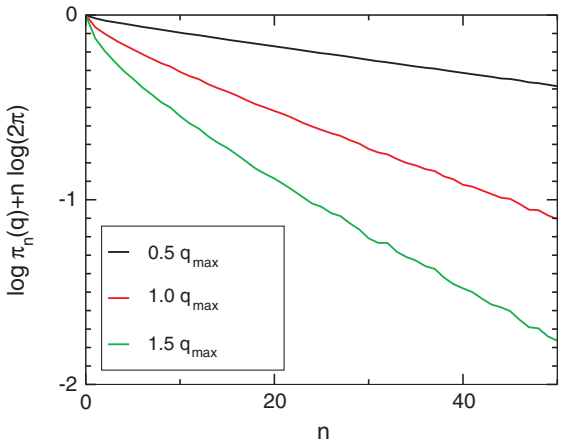

Figure 43. The dependence of $\pi_n(q)$ on n for different values of q for BMLJ. Reprinted with permission from [254]. Copyright 2008 by the American Physical Society.

away from the region of major mobility. Exactly these atoms are not taken into account when considering small systems.

Further below, the Fourier transform of $\pi_1(x)$, i.e. $\pi_1(q)$, is of major interest. For small q one can approximate (independent of the actual form of $\pi_1(x)$)

$$\pi_1(q) \approx 1 - q^2a^2/6 \tag{105}$$

where $a^2/3$ is the second moment of the distribution $\pi_1(x)$ whereas for $q \to \infty$ one obtains $\pi_1(q) = 0$. Both limits are captured by the choice

$$\pi_1(q) \approx \frac{1}{1 + a^2q^2/6}. \tag{106}$$

This relation is exact for an exponential distribution $\pi_1(x)$.

7.1.2. Correlations of successive MBs: waiting times and energies. As shown in [212] to a good approximation successive waiting times are statistically uncorrelated for BMLJ($N = 65$). Thus, the time evolution can be regarded as a sequence of randomly chosen waiting times. For the same data, the energies display some residual correlations with a decay time of approximately ten MB transitions. This behavior is to be expected if even the small BMLJ system is not elementary; because after a MB transition only one of the subsystems changes its energy, see section 5.3. Apparently, these correlations do not imply the presence of correlated waiting times. This can be explained by the fact that the waiting time is to a large extent determined by the faster component.

7.1.3. Correlations of successive MBs: real space properties. In the simplest description subsequent MB transitions are uncorrelated in real space, i.e. correspond to a Markovian random walk process. This hypothesis would be invalidated, e.g., by the presence of correlated forward–backward dynamics or the simultaneous presence of slow and fast particles. In the latter case a particle moving a large distance would most likely also move a large distance in the subsequent MB transition.

The Markov hypothesis can be formally written as

$$\pi_n(x) = \int \mathrm{d}x' \pi_{n-1}(x')\pi_1(x - x'). \tag{107}$$

In Fourier space this convolution implies

$$\pi_n(q) = \pi_1(q)^n. \tag{108}$$

The n-dependence of $\pi_n(q)$ is studied in [254] for BMLJ($N = 65$). As shown in figure 43 for $q \approx q_{\max}$ the limiting behavior $\log(\pi_n(q)) \propto n$ is already reached for $n \geqslant 5$. For smaller q-values this holds for even smaller values of n.

The same feature can be also observed by analyzing the total average MSD of the system after n transitions $\langle R^2(n)\rangle$ ($\langle R^2(n)\rangle/3$ is the second moment of $\pi_n(x)$). The above Markov hypothesis would show up as $\langle R^2(n)\rangle = a^2n$. Indeed, apart from very small n this relation is very well fulfilled for the MB transitions; see figure 44. Most importantly, the value of a^2 does not depend on temperature in the range of analyzed temperatures. As a consequence (see below) the temperature dependence of the diffusion constant $D(T)$ is fully determined by the temperature-dependent waiting time. Note that for the BMLJ system $(a^2/3)q_{\max}^2 \approx 0.3$, where $q_{\max}$ is the maximum of the static structure factor.

Interestingly, when repeating this analysis for the IS transitions dramatic deviations can be seen in figure 44: the deviations from linear behavior strongly increase and the behavior for large n strongly depends on temperature, indicating a temperature dependence of forward–backward processes. These results just reflect the fact that direct forward–backward correlations have been eliminated when going from ISs to MBs. Thus, the theoretical description of the macroscopic transport is much simpler in terms of MBs than of ISs; see also [255] for a quantification of this effect.

In the same spirit also the long-time dynamics for BKS-SiO_2 has been analyzed [215]. The oxygen dynamics shows a very similar behavior as described above for BMLJ. In contrast, the value of a^2 for the silicon atoms displays a weak temperature dependence. As shown in [256] this can

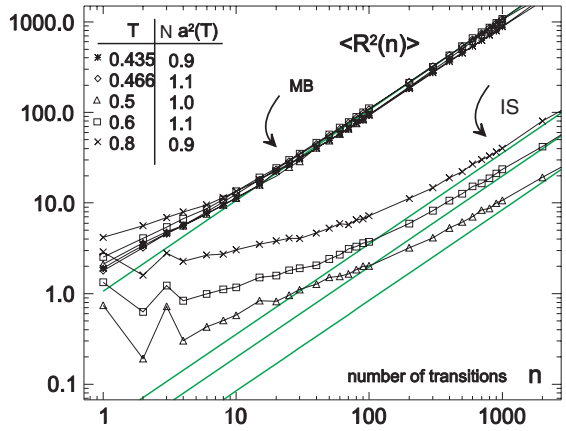

Figure 44. The mean square displacement $R^2(n)$ for MBs as well as for ISs, evaluated for the majority fraction of large particles. Reprinted with permission from [230]. Copyright 2003 by the American Physical Society.

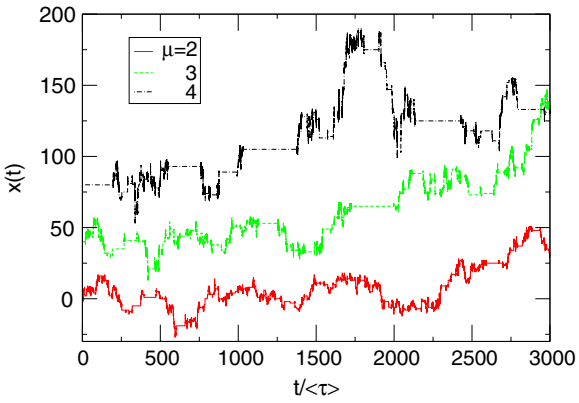

Figure 45. Visualization of the real space dynamics. Shown is a random walk with the waiting time distribution of an ideal Gaussian glass-former. The spatial dynamics is a simple random walk with an average step size of unity.

be related to the presence of oxygen permutations like simple C_3-rotations which become more relevant at low temperatures and which force the silicon atoms to return to the original positions. If one excludes the time intervals during which permutations happen the temperature dependence of a^2 (Si) disappears. Thus, the temperature dependence of $D(T)$ for BKS-SiO_2 is again fully characterized by the average waiting time. Interestingly, the probability for an oxygen permutation starts to increase as soon as the MB energy is below e_{cross} [256]. Thus, e_{cross} is indeed a crucial PEL parameter, characterizing many aspects of the dynamics and in particular the availability of adjacent configurations with similar activation energies.

7.2. Time-resolved dynamics

New features emerge if the MB scenario is interpreted in dependence on time rather than the number of MB transitions.

7.2.1. Dynamic heterogeneities. The broad distribution of waiting times in glass-forming systems gives rise to specific properties for the time evolution. This is exemplified in figure 45. Shown is the trajectory of a simple random walker with step size unity, performing a jump after every waiting time. The new waiting times are drawn randomly. The emergence of short time intervals with many dynamical processes is a simple consequence of the broad distribution of waiting times and is thus particularly pronounced at low temperatures. One can thus interpret the dynamics as a sequence of residences in a single long-living MB interrupted by mobile periods, typically involving many successive transitions between short-lived MBs. A similar observation has been made for CS_2, where long-range jumps could be interpreted as a correlated sequence of many IS transitions [253].

The time dependence of the mobility can be captured by the observable

$$\mu(t,\theta) = (1/N)\sum_i [r_i(t+\theta/2) - r_i(t-\theta/2)]^2. \quad (109)$$

Qualitatively, it describes the mobility determined during the time interval θ at time t. Using this quantity for $\theta = \tau_\alpha$ [231] or for a significantly smaller value of θ for the BMLJ system [52] and water [257], one can see that the mobility strongly varies with time t. Another convenient way is to use the distance matrix, which allows one to judge whether or not the system was mobile between two times t' and t'' as introduced by Ohmine [96] and used in recent numerical [52, 213, 257] as well as experimental work [258] to characterize the dynamic heterogeneities. The low-mobility time periods can be identified with the residence in an MB with a long waiting time. In any event, the observed patterns are a direct consequence of the mechanism reflected in figure 45. The resulting displacement field after a mobile time period is quite compact [96] and involves 30–60 particles [52] (denoted *democratic* particle motion by these authors), in contrast to the string-like pattern after a single MB transition.

Several possibilities exist to explain the observation of these compact clusters. (1) They result from collective rearrangements happening in a short time interval. Using the term *cooperative relaxing units* this scenario seems to be favored, e.g., in [257]. (2) They consist of individual processes, which, however, are triggered one after the other. (3) They result from fully uncorrelated processes.

For the further discussion it is helpful to consider the simple model in figure 45. Here, scenario (3) is realized. One clearly sees the presence of bursts of mobility at low temperatures. They are just a consequence of the broad waiting time distribution. If, by chance, the neighbor region is stuck in some immobile region the numerically observed mobility patterns may result from scenario (3). Within the KCM these patterns can be produced, too, by a sequence of localized and facilitated events [259]. By definition this corresponds to scenario (2). Some type of correlation in the spirit of the KCM is suggested by the results in [149, 150]. In any event, the question of possible couplings of dynamic processes is discussed in more detail in section 9. An argument against (1) is that the bursts of mobility can be traced back to individual MB transitions, basically performing a random

walk in configuration space (see above). This seems to be incompatible with a collective rearrangement.

A different way to characterize the dynamics of a single particle is to record the time t_1 when a particle has for the first time moved a specific distance d. At this moment one starts again and waits for the next time (t_2 later) when again the same distance d is moved etc. In this way one can obtain a series $t_1, t_2, \ldots$ [259]. Two observations are made: first, at low temperatures the times t_i are broadly distributed. This just reflects the presence of dynamic heterogeneities. Second, the time t_1 is longer than the average of the later times. This is rationalized below (see section 7.3.2).

In this context it is interesting to note that the simulations in the isoconfigurational ensemble have clearly revealed that the particles which are mobile on the α-timescale already belong to the most mobile particles on a much shorter timescale (fast β-regime) [55]. Although a precise connection to the MB picture has not been established so far, a simple connection might indeed exist. Also recent NMR experiments point in this direction [260].

7.2.2. Diffusion process. The observations, reported above, have immediate consequences for the estimation of the MSD, which is one of the central dynamic observables. In the limit of large $t \gg \langle\tau\rangle$ the number of MB transitions can be taken as $n = t/\langle\tau\rangle$ with negligible relative fluctuations around this value. Therefore one can write

$$D = \frac{\langle r^2(t)\rangle}{6t} = \frac{R^2(n = t/\langle\tau\rangle)/N}{6t}. \tag{110}$$

As discussed, for large n one can write $R^2(n) = Na^2n$ with a temperature-independent distance a. This yields [230]

$$D = \frac{a^2}{6\langle\tau\rangle}. \tag{111}$$

This means that the complexity of the glass transition can be to a large extent related to the temperature dependence of the waiting time distribution. In contrast the spatial aspects, expressed by a, are nearly temperature independent at least in the temperature regime analyzed so far via computer simulations. This property has been often used by many authors, e.g. when estimating the exponent α for the violation of the Stokes–Einstein relation. In this sense it is fortunate that this property indeed seems to hold for a variety for glass-forming systems.

7.2.3. Connection to the AG relation. In recent work La Nave and Sciortino have analyzed a large number of short trajectories for water and BMLJ [261, 262]. The time for every trajectory was adjusted such that for all temperatures the mean square displacement, averaged over all realizations, is unity. For a given trajectory they determined the average IS energy $\bar{e}$, obtained from regular quenching, and the diffusivity, obtained from calculating the Euclidean distance between the initial and the final configuration. After averaging over trajectories with similar $\bar{e}$ they could determine an energy-dependent diffusivity $D(\bar{e}, T)$. Using a slightly modified version of equation (70)

$$D(T) = \int \mathrm{d}\bar{e}\; p(\bar{e}, T) D(\bar{e}, T) \tag{112}$$

one can, of course, recover the macroscopic diffusion. In some sense in their approach the coarse-graining on the MB level has been replaced by a coarse-graining relative to a fixed timescale. As a drawback one loses the direct relation to the thermodynamics and to the specific saddles in the PEL. A possible advantage of this type of coarse-graining is the fact that $D(\bar{e}, T)$ can be compared with the AG expression $D_\infty \exp(B_{\mathrm{AG}}/T s_{\mathrm{c}}(\bar{e}))$. Using the input for s_{c}, known from the thermodynamic analysis (see section 3), one can extract the value of α from an appropriate fitting procedure. Thus, within the AG framework the absolute value of the configurational entropy can be estimated from the dynamics.

7.3. Continuous-time random walk (CTRW) formalism

The simple spatial aspects of the dynamics suggests that not only the diffusion constant but also more complex dynamic observables can be related to properties of the waiting time distribution $\varphi(t)$. The results, reported below, will hold for *arbitrary* $\varphi(t)$ as long as finite moments exist and thus equilibrium properties can be calculated.

It will be shown that the framework of the CTRW formalism can be used to describe the dynamics. The background of this approach can be found, e.g., in [220, 263–265].

7.3.1. Conditions for a CTRW. Three conditions can be formulated. If they are fulfilled the van Hove correlation function $G_s(x, t)$ can be fully expressed in terms of $\pi_n(x)$ and $\varphi(\tau)$.

(C1) The transition pattern during a hop does not depend on the waiting time since the previous hop. As a consequence, the spatial and temporal contributions separate and one can strictly write

$$G_s(x, t) = \sum_n S_n(t)\pi_n(x). \tag{113}$$

Here $S_n(t)$ denotes the probability to have exactly n transitions during time t and generalizes the definition of $S_0(t)$ in equation (90). This is the central equation of the CTRW because it expresses the total dynamics during time t in terms of discrete processes with well defined probabilities. Of course, one may also analyze rotational correlation functions with an analogous formalism. This independence has been shown to be true for BMLJ with good accuracy [254].

(C2) Successive waiting times are statistically uncorrelated so that the time evolution can be regarded as a sequence of randomly chosen waiting times. Also (C2) has been confirmed (see above).

(C3) Subsequent jumps are uncorrelated. (C3) has been discussed above and shown to be true with minor deviations which hardly matter for $q \leqslant q_{\max}$.

Figure 46. Sketch of a random sequence of broadly distributed waiting times. It is most likely that at a randomly chosen time one starts in a time interval with a long waiting time.

Thus, the general physical picture is that of a random walk in configuration space where all steps are uncorrelated and the waiting times may be (in generalization to the standard random walk) broadly distributed.

7.3.2. Prediction of $S(q,\lambda)$. Of crucial importance is the (*persistence time distribution*) $\xi(t)$ that for a randomly chosen starting point exactly a time t later the system hops for the first time [266]. The average persistence time is defined as

$$\langle\tau\rangle_\xi = \int \mathrm{d}t\, t\, \xi(t). \tag{114}$$

In appendix D it is shown that for the Laplace transforms one has

$$\xi(\lambda) = \frac{1-\varphi(\lambda)}{\lambda\langle\tau\rangle} \tag{115}$$

and

$$S_0(\lambda) = \frac{1-\xi(\lambda)}{\lambda}. \tag{116}$$

Furthermore, one can show (see also appendix 4) that $\langle\tau\rangle_\xi$ can be expressed as

$$\langle\tau\rangle_\xi = \langle\tau^2\rangle/(2\langle\tau\rangle). \tag{117}$$

For broad waiting time distributions one thus obtains $\langle\tau\rangle_\xi \gg \langle\tau\rangle$. To understand this relation one has to realize that the initial time zero will on average lie in a time interval with a long waiting time, i.e. a long time is required for the next hop to occur; see figure 46 for a sketch of this effect.

Based on conditions (C1)–(C3) the temporal Laplace transform of the incoherent scattering function $S(q,\lambda)$ can be calculated analytically. Note that for a strict comparison one has to use the function evaluated for the MB trajectory. Of course, as shown in section 1.2, the α-relaxation part of $S(q,\lambda)$, evaluated for continuous trajectories, can be taken as well for sufficiently low temperatures.

As derived in appendix D one obtains [266]

$$S(q,\lambda) = S_0(\lambda) + \pi_1(q)\xi(\lambda)S_{\mathrm{MW}}(q,\lambda) \tag{118}$$

with

$$S_{\mathrm{MW}}(q,\lambda) = \frac{\langle\tau\rangle\xi(\lambda)}{1-\varphi(\lambda)\pi_1(q)}. \tag{119}$$

$S_{\mathrm{MW}}(q,t)$ can be interpreted as the incoherent scattering function under the condition that the initial time is directly after a hop. In summary, $S(q,t)$ is fully determined by the waiting time distribution $\varphi(t)$ (determining also $\xi(t)$) and the function $\pi_1(x)$, characterizing the real space properties of the MB transitions. Equation (118) has been used to characterize the dynamics of so-called probe molecules within the KCM [51].

Table 3. Relation between β_{KWW}, τ_0, and β_{m}.

β_{KWW}	$\tau_0/\langle\tau\rangle$	β_{m}
1	1	1
1/2	2	1/3
1/3	6	1/10
1/4	24	1/35

7.3.3. Calculating moments. The inverse Laplace transformation of $S(q,\lambda)$ in general cannot be performed analytically. However, the general form equation (118) already allows one to draw some important conclusions about the properties of $S(q,t)$. For this purpose, we define the two timescales

$$\tau_0(q) \equiv \int \mathrm{d}t\, S(q,t) \tag{120}$$

and

$$\tau_1(q) = \int \mathrm{d}t\, t\, S(q,t) \Big/ \int \mathrm{d}t S(q,t). \tag{121}$$

From this we define

$$\beta_{\mathrm{m}}(q) = \frac{\tau_0(q)}{\tau_1(q)}. \tag{122}$$

For general non-exponential relaxation $S(q,t) = \exp[-(t/\tau)^{\beta_{\mathrm{KWW}}}]$ one obtains

$$\tau_0 = \langle\tau\rangle/\beta_{\mathrm{KWW}}\Gamma(1/\beta_{\mathrm{KWW}}) \tag{123}$$

and

$$\tau_1 = \langle\tau\rangle\Gamma(2/\beta_{\mathrm{KWW}})/\,\Gamma(1/\beta_{\mathrm{KWW}}). \tag{124}$$

Whereas $\tau_0(q)$ expresses the average decay time of $S(q,t)$, the ratio β_{m} is a measure for the non-exponentiality. Correspondingly, for $\beta_{\mathrm{KWW}} = 1$ one has $\beta_{\mathrm{m}} = 1$. In table 3 some special values are listed.

For later purposes we rewrite β_{m} as

$$\beta_{\mathrm{m}}^{-1}(q) - 1 = \frac{\int \mathrm{d}t\, t\, S(q,t) - \tau_0(q)}{\tau_0(q)^2} \equiv \frac{T_\beta(q)}{\tau_0(q)^2}. \tag{125}$$

Importantly, both quantities can be calculated in the framework of the CTRW [254]; see appendix E. The results read

$$\tau_0(q) = \langle\tau\rangle\left(V + \frac{1}{1-\pi_1(q)}\right) \approx \langle\tau\rangle\left(V + 1 + \frac{6}{q^2a^2}\right) \tag{126}$$

and

$$\beta_{\mathrm{m}}^{-1}(q) - 1 = \frac{T_\beta}{\tau_0(q)^2}, \tag{127}$$

where we have defined

$$V = \frac{\langle\tau^2\rangle}{2\langle\tau\rangle^2} - 1 = \frac{\langle\tau\rangle_\xi}{\langle\tau\rangle} - 1 \tag{128}$$

and

$$T_\beta = \frac{\langle\tau^3\rangle}{6\langle\tau\rangle} - \frac{\langle\tau^2\rangle^2}{4\langle\tau\rangle^2} = \frac{\langle\tau^2\rangle_\xi}{2} - \langle\tau\rangle_\xi^2. \tag{129}$$

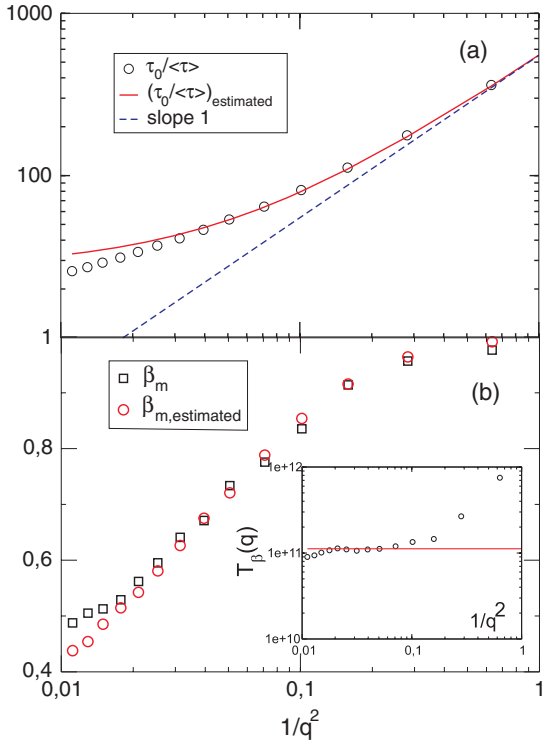

Figure 47. The q-dependence of (a) $\tau_0(q)$ together with its estimation via equation (126) and (b) of $\beta_m(q)$ together with its estimation. In the inset the validity of the theoretical expectation $(d/dq)T_\beta(q) = 0$ is tested. Reprinted with permission from [254]. Copyright 2008 by the American Physical Society.

The last equation follows from the general relation

$$\langle t^n \rangle_\xi = \frac{\langle t^{n+1} \rangle}{n+1}. \tag{130}$$

Note that equation (127) implies $(d/dq)T_\beta(q) = 0$. V characterizes the width of the waiting time distribution and T that of the persistence time distribution. In particular, both disappear for purely exponential relaxation. Note that equations (126) and (127) imply that the whole q-dependence of the relaxation time and the non-exponentiality parameter β_{KWW} can be expressed in terms of one or two parameters, respectively, characterizing the waiting time distribution.

The validity of the CTRW assumptions for BMLJ allows one to perform a self-consistency check of equations (126) and (127); see figure 47. The expected dependences are directly observed. This shows that the q-dependence of the relaxation time as well as the degree of non-exponentiality can be very well understood in the framework of the CTRW and can be related to the values of V and T. The deviations at large q are clearly related to the slight presence of correlated forward–backward dynamics, as already seen in figure 43. Actually, due to the extreme dependence of the third moment on the fine details of $\varphi(t)$ at long times, the value of T_β has been taken as a fitting parameter. Note that the q-dependence of $\tau_{KWW}(q)$ is similar to the data reported in [22] and [267].

7.3.4. Large- and small-q limits. Of special interest are the large- and small-q limits of $\tau_0(q)$. For large q one expects a full decorrelation of $S(q,t)$ after one MB transition, i.e. $S(q,t)$ has the same meaning as $S_0(t)$. Thus, $\tau_0(q \to \infty)$ can be identified with τ_α. From equation (126) follows [51]

$$\tau_\alpha = \langle \tau \rangle (1+V) = \langle \tau \rangle_\xi. \tag{131}$$

Around $1/q^2 \approx Va^2/6 (\equiv (\xi_{single})^2)$ there is a crossover of $\tau_0(q)$ from the q-independent large-q limit to the small-q limit $\tau_0(q) = 6\langle\tau\rangle/(q^2a^2)$. This result can be easily rationalized; see also [51]. During a time of $\langle\tau\rangle_\xi$ roughly $\langle\tau\rangle_\xi/\langle\tau\rangle$ MB transitions are performed. This results in an MSD of $(a^2/3)\langle\tau\rangle_\xi/\langle\tau\rangle \approx Va^2/3 = 2(\xi_{single})^2$ along one coordinate. Therefore, ξ_{single} corresponds to the distance a particle moves on the timescale of the persistence time. Why does the crossover happen for $q \approx 1/\xi_{single}$? After a randomly chosen time origin the subsequent dynamics of a particle can be divided into two parts. For a time of order $\langle\tau\rangle_\xi$ it remains immobile. Afterward it performs a random walk dynamics with average waiting time $\langle\tau\rangle$. The crossover to Fickian dynamics occurs when the time duration of the random walk dynamics exceeds the initial immobile time period, i.e. $\langle\tau\rangle_\xi$. Thus, according to the above, the crossover length scale should indeed be of the order of ξ_{single}. Naturally, for $q \approx 1/\xi_{single}$ also the non-exponentiality parameter β_m starts to approach its low-q limit $\beta_m(q) = 1$.

For small q one expects for general reasons $\tau_0(q) = 1/(q^2D)$. Comparison with equation (126) naturally yields equation (111) as already derived in section 7.1. Together with equation (131) this results in

$$D\tau_\alpha = (a^2/6)(1+V) \approx \xi^2_{single}. \tag{132}$$

Thus, as stated in several models, the temperature dependence of $D\tau_\alpha$ is directly related to the increase of dynamic heterogeneity via the value of V. For the special case of an ideal Gaussian glass-former the temperature dependence of $D\tau_\alpha$ is given in equation (97). The resulting increase of ξ_{single} shows that also within the PEL approach increasing length scales naturally emerge.

If the waiting time distribution results from an elementary system with well defined hopping rates one can express the averages over the φ-distribution in equation (132) via the corresponding Boltzmann averages, as outlined in section 6. Using $1 + V = \langle\Gamma^{-1}\rangle_p\langle\Gamma\rangle_p$, equation (132) can be strictly rewritten as

$$D\tau_\alpha = \langle\tau\rangle_\xi/\langle\tau\rangle = \langle\Gamma\rangle_p\langle 1/\Gamma\rangle_p. \tag{133}$$

This has already been used in section 6.4 for the discussion of the violation of the Stokes–Einstein relation.

By fitting $G_s(r,t)$ with a bimodal distribution of waiting times for different systems, the typical timescales $\langle\tau\rangle_\xi$ and $\langle\tau\rangle$ have recently been obtained numerically [268]. On this basis equation (133) has been successfully tested. Furthermore, $G_s(r,t)$ has been compared with the hypothetical function one would obtain for ideal Gaussian diffusion [269]. For sufficiently long times $G_s(r,t)$ approaches the ideal Gaussian. On this timescale τ_F the dynamics can be considered to be Fickian. Naively, one might expect that τ_F should be directly related to $\langle\tau\rangle_\xi$ and thus to τ_α. It turns out, however, that τ_F has a stronger temperature dependence.

7.3.5. The van Hove self-correlation function. It has been reported that $G_s(r, t)$ displays an exponential tail for a variety of systems [267, 268]. Interestingly, as soon as the process is discrete with respect to time, i.e. can be described by the presence of waiting times, such behavior seems to be generic [268]. This can already be seen in the simplest version of the CTRW approach, involving only a single relaxation time Γ. Choosing $\lambda = \Gamma t$ and following the arguments in [268], one can use a Poisson process in equation (113), yielding

$$G_s(x, t) = \sum_n \frac{\lambda^n}{n!} \exp(-\lambda)\pi_n(x). \tag{134}$$

According to the central limit theorem $\pi_n(x)$ can be approximated by a Gaussian $\propto \exp(-x^2/2na^2)$. Using Stirling's formula and transforming the sum into an integral, one can perform a saddle point approximation to get the dominant value of n, denoted $n_{\max}$. One obtains for large x that apart from logarithmic corrections $n_{\max} \propto x/a$. Physically this means that particles with large x have performed a large number of jumps, proportional to their value of x. As a consequence, $G_s(x, t) \propto \exp(-x^2/2n_{\max}a^2) \propto \exp(-\text{const} \cdot x/a)$. In summary, the exponential tail in $G_s(x, t)$ (or $G_s(r, t)$) is just a signature that the dynamics is governed by waiting times which result, e.g., as a consequence of activated behavior and is thus very general.

8. Comparison of different system sizes

Finally, one is interested in understanding the properties of supercooled liquids of macroscopic size. In most hopping models presented in the literature and reviewed in section 5 one concentrates on the local dynamics. This reflects the well accepted fact that the dynamic processes in supercooled liquids are localized so that these models aim to grasp the relevant dynamic processes on this length scale. Implicitly it is assumed that the dynamics of the total system can be described as an *independent* superposition of these local processes. This is naturally true when adding up very large systems. Here we analyze whether the superposition hypothesis is already valid for smaller systems.

8.1. Superposition of elementary systems: theory

8.1.1. Definition of independent systems. Simpler relations can be formulated if the subsystems are characterized by equation (61), i.e. obey the direct correlation between energy and hopping rate. Here we consider a large system which contains M elementary subsystems. Each subsystem of the large system is characterized by its energy e_i and the corresponding hopping rate $\Gamma(e_i)$. The total energy reads $e = e_1 + \ldots + e_M$. A single hopping process on a subsystem level is, of course, equivalent to a hopping process of the total system because the total configuration changes.

What are the properties of the waiting time distribution of the large system? This question is analyzed under two assumptions.

(I1) The equilibrium probability distribution reads $p_{\text{eq},M}(e_1, \ldots, e_M) = p_{\text{eq}}(e_1) \cdots p_{\text{eq}}(e_M)$.

(I2) The overall hopping rate $\Gamma_M(e_1, \ldots, e_M)$ is given by $\sum_i \Gamma(e_i)$.

The first assumption reflects the lack of finite-size effects for the distribution of states, the second the locality of the individual particle displacements during one MB transition.

8.1.2. Waiting time distribution of the total system. In a first step we start with a single system with N particles, characterized by some waiting time distribution $\varphi_N(\tau)$. What is the waiting time distribution $\varphi_{2N}(\tau)$ of a system with $2N$ particles, using (I1) and (I2)? Starting from some equilibrium configuration both subsystems have independent persistence times (characterized by $\xi_N(t)$). Then it is possible to predict the next hopping event of either subsystem 1 or 2. This has to be identified with a hopping event of the total system. One can immediately write

$$\xi_{2N}(t) = 2\xi_N(t)(S_0)_N(t), \tag{135}$$

i.e. one system performs its first hop at time time t (with probability $\xi_N(t)$) whereas the second system is still immobile (with probability $(S_0)_N(t)$). Using the notation $p(\tau) = \varphi(\tau)\tau/\langle\tau\rangle$ it is shown in appendix F that one can rewrite equation (135) as [170]

$$p_{2N}(\tau) = -\frac{\mathrm{d}}{\mathrm{d}\tau} \int_\tau^\infty \mathrm{d}\tau'\, p_N(\tau') \int_\tau^\infty \mathrm{d}\tau''\, p_N(\tau'') \times \left(1 - \frac{\tau^2}{\tau'\tau''}\right). \tag{136}$$

This has been successfully used in [170] and [270] to check the possibility to predict the waiting time distribution of a system from that of smaller systems for BMLJ and BKS-SiO_2, respectively (see below).

8.1.3. Calculation of moments. The calculation of the different moments of the waiting time distribution for the case of the system, composed of M independent subsystems (each characterized by $\lambda = 1$), can be found in appendix G. For the first moment one obtains

$$\langle\tau(e)\rangle_M^{-1} = M\Gamma(e/M)\exp[\mu^2(1 - 1/M)/2]. \tag{137}$$

and

$$\langle\tau\rangle_M^{-1} = M\exp[-\mu^2/2] \tag{138}$$

which, as expected, is just M times the rate of the elementary system.

Without the exponential term equation (137) corresponds to the case where all e_i are identical and equal to e/M; see the discussion before equation (61). Thus, the exponential term reflects the energy fluctuations among the subsystems.

It is instructive to consider the limit of large M in equation (137). The distribution of normalized energies e/M in thermal equilibrium approaches a delta-function centered around $e = -M\tilde{\beta}\sigma^2$. Substituting this energy into equation (137) one obtains $\langle\tau(e)\rangle_M^{-1} \approx \langle\tau\rangle_M^{-1}$. Thus, the energy dependence of the average waiting time disappears and naturally approaches the average value. This explicitly

shows that important information contained in small systems disappears when approaching the thermodynamic limit.

Higher moments can also be calculated. It follows that

$$\langle \tau(e)^2 \rangle_M / \langle \tau(e) \rangle_M^2 = 2 f_M(\mu) \exp[\mu^2(1 - 1/M)/2] \quad (139)$$

and

$$\langle \tau^2 \rangle_M / \langle \tau \rangle_M^2 = 2 f_M(\mu) \exp[\mu^2(1 + 1/M)/2] \quad (140)$$

with a function $f_M(\mu)$ defined in appendix G. From equation (139) follows that the energy dependence disappears when considering this ratio. Again, for large M it does not matter whether or not the observables are resolved with respect to energy. Naturally, for $M = 1$ the results agree with the previous ones for elementary systems.

8.1.4. Problems of large system sizes. For the MSD the validity of (I1) and (I2) guarantees that the diffusion constant remains the same when increasing the system size. This is explicitly reflected by equation (138). In general, however, it is no longer possible to use the CTRW approach for the macroscopic system. Let us assume that for a subsystem one has $\pi_2(x) = \int \mathrm{d}y\, \pi_1(y)\pi_1(x - y)$, i.e. (C3) is fulfilled. Does (C3) also hold for a large system? In physical terms, validity of the convolution implies that the probability for a particle to move is independent of its translation during the previous hopping process. This will be definitely invalidated for large systems. Even in the case of independent processes it is likely (see section 7) that one group of atoms performs several hopping transitions before other groups of atoms can start. This means that the probability to move is strongly correlated during successive events so that (C3) will no longer hold. As a consequence, for the calculation of $S(q, t)$ one has to resort to the local dynamics. Therefore, for the application of the CTRW approach one has to define the waiting time distribution on a local spatial scale as automatically done for small systems, in the KCM approach [266] or particle-based definitions [259].

As will be discussed in section 9, even for systems fulfilling the independence criteria (I1) and (I2), the local dynamics may change when going from an elementary system to a collection of subsystems. As a consequence, finite-size effects for $S(q, t)$ turn out to be stronger than for the diffusion constant.

8.2. Simulation of different system sizes

8.2.1. Complete characterization of very small systems. For very small systems (e.g. $N = 32$ monatomic Lennard-Jones) a nearly complete characterization of *all* relevant low-energy ISs and their connectivity is possible [158, 271]. It turns out that apart from the fcc crystal there are few low-energy configurations which dominate the properties already at ambient temperatures. As a consequence the low-temperature dynamics is always Arrhenius-like because it is governed by the escape from a single or a few states [164]. Thus, it is difficult to extract the relevant physics of glass formation from such a small system. In general, the qualitative behavior seems to be simpler. For example, no forward–backward processes are observed between ISs [271]. One can, however, obtain information which for larger systems cannot be obtained. In [271], e.g., the complete distribution of barriers in dependence on the starting IS energy is reported. Of course, for the real dynamics only the lowest barriers are of actual interest.

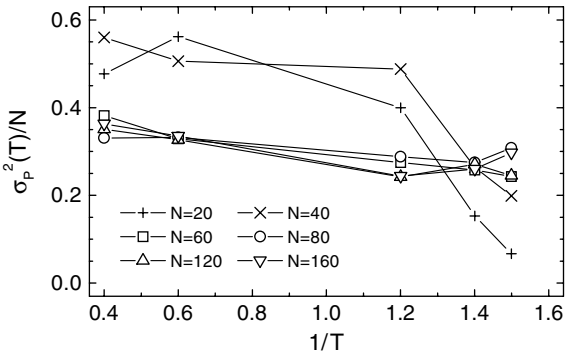

Figure 48. The normalized variance σ^2/N, calculated for different temperatures for the BMLJ system. Reprinted with permission from [164]. Copyright 1999 by the American Physical Society.

8.2.2. Minimum representative system size and finite-size effects. As discussed above the analysis of small systems has many conceptual advantages. Thus, in the meantime several groups use relatively small glass-forming systems in order to extract as much information as possible; see, e.g., [213, 262] for some recent work along this line. However, one has to deal with the possible problem of finite-size effects. The optimum system size for the PEL analysis fulfills two requirements: (i) extension of the system size does not change the system properties; (ii) reduction of the system size starts to generate significant finite-size effects. Of course, in general one expects a crossover phenomenon. Furthermore, *a priori* it is not evident to what degree the optimum system size depends on temperature.

To analyze finite-size effects of thermodynamic quantities one may analyze how $\langle \sigma^2(T)/N \rangle$ varies with system size; see figure 48. Interestingly, around a relatively small region of system sizes (N between 40 and 60) the system starts to show significant finite-size effects. Also for BKS-SiO_2 $N \approx 60$ is a critical system size below which the thermodynamic properties start to deviate. Given the strong relation between thermodynamics and dynamics, it is not surprising that for BMLJ the diffusion constant also starts to deviate for $N \leqslant 40$ [164] whereas for $N = 60$ for all temperatures no significant finite-size effect (variation of the diffusion constant by less than 15%) has been observed [170]. This may come as a surprise because in the analyzed temperature regime the value of ξ_{coll} changes significantly [47, 48].

For the dynamics of BKS-SiO_2 it is known that the diffusion constant displays a significant finite-size effect up to $N \approx \mathrm{O}(10^3)$ [241, 272, 273]. This effect is related to the presence of significant vibrational contributions for short times in silica. The activation energy, however, does not change

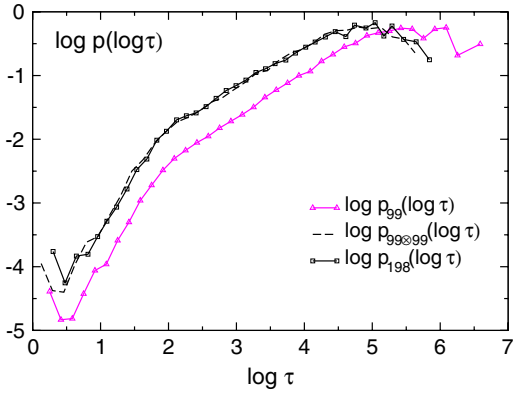

Figure 49. Estimation of $p_{198}(\tau)$ for BKS-SiO_2 based on $p_{99}(\tau)$ under the assumption of independent subsystems. This estimation is compared with the actual waiting time distribution $p_{198}(\tau)$. The data have been scaled with respect to each other by a factor of 1.3 to account for the shift in the diffusion constant. Reprinted with permission from [270]. Copyright 2007 IOP Publishing.

significantly when N is varied for $N \geqslant 99$. Interestingly, the degree of non-exponentially of the incoherent scattering function for $q = q_{\max}$ is somewhat decreasing (from $\beta_{\mathrm{KWW}} = 0.86$ to 0.80) when going from $N = 1002$ to 60 and even more dramatic upon further size reduction ($\beta_{\mathrm{KWW}} = 0.65$) for $N = 30$ [270].

Furthermore, analyzing the q-dependence of the incoherent scattering function $S(q, t)$, i.e. $\tau_{\mathrm{KWW}}(q)$, for the BMLJ system it turns out that the finite-size effects are barely visible for small q (equivalent to the statement of a missing finite-size effect for the diffusion constant) but strongly increase for large q. For $q = 2q_{\max}$ one has an increase of a factor 2.5 [267]. Obviously, finite-size effects become relevant when leaving the small-q limit of the incoherent scattering function and measuring quantities such as τ_α and β_{KWW}. This at first sight counterintuitive behavior (finite-size effects for small length scales, corresponding to large q) will be rationalized in section 9.

Interestingly, Kim and Yamamoto [274] have observed massive finite-size effects for a soft-sphere system. They have simulated a monoatomic soft-sphere system. In the range of temperatures studied in that work, for a binary mixture soft-sphere system, system sizes of $N = 130$ were sufficiently large to avoid finite-size effects (unpublished work). Thus, one may speculate that the tendency of crystallization for a monatomic system strongly depends on system size and thus induces strong finite-size effects for transport quantities. This has been explicitly checked for the Dzugutov liquid [275].

8.2.3. Doubling the system size. A very sensitive way to check (I1) and (I2) is the comparison of the waiting time distribution for a system with N and $2N$ particles via equation (136). The result obtained for BKS-SiO_2 is shown in figure 49. Apart from a simple scaling factor (see above), there is perfect agreement between the actual waiting time distribution and the predicted one for $N = 198$. Thus, in terms of MB transitions the system with $N = 198$ behaves like a superposition of two independent $N = 99$ systems (in the sense of (I1) and (I2)) and the waiting time distribution of the larger system does not contain any new information as compared to the smaller system.

A similar agreement can be found for BMLJ when going from $N = 65$ to 130 [170]. Using some appropriately defined time correlation function between ISs it has been verified for BMLJ that the transition from 130 to 250 particles also follows the rule expected from the assumption of independent subsystems [255].

8.2.4. On BMLJ($N = 65$). We have seen that BMLJ($N = 65$) is large enough that in the considered range of temperatures the extension of the system size obeys (I1) and (I2). The remaining question is how to interpret the observed value of $\lambda = 0.55 < 1$. A simple interpretation would be that BMLJ($N = 65$) can be regarded as an independent superposition of $M = 1/0.55 \approx 2$ independent subsystems. Then the elementary system would approximately contain 30–40 particles. The simulations have shown (see figure 48) that finite-size effects are already very pronounced for this system size (30–40). *A priori* this observation does not invalidate the superposition hypothesis. An elementary subsystem is unlikely to have the shape of a cube. Thus, simulating a system of the size of an elementary subsystem with periodic boundary conditions will most likely change the nature of the excitations.

There is a second argument which questions the superposition hypothesis. The simulations have shown that $\Gamma(e)$ does not display any significant deviations from an Arrhenius behavior; see figure 34. If BMLJ($N = 65$) were a superposition of two independent systems $\Gamma(e)$ should have the additional temperature-dependent factor $\exp[\mu^2(1 - 1/M))/2]$ (here $M = 2$) appearing in equation (137). This factor does not seem to be present for the simulation data because otherwise Arrhenius behaviour would not be expected. Another deviation can be seen for the quantity $\langle\tau(e)^2\rangle/\langle\tau(e)\rangle^2$. In agreement with equation (139) this ratio is energy independent [212] but its absolute value is a factor of two smaller than predicted by equation (139). Whereas for $T = 0.5$ the simulated ratio is 8, equation (139) yields (using $\tilde{\beta} = 1.6$ and $\sigma = 3/\sqrt{2}$) a ratio of 16.

For a pure superposition the additional temperature-dependent factor $\exp[\mu^2(1 - 1/M)/2]$ as well as the large values of $\langle\tau(e)^2\rangle/\langle\tau(e)\rangle^2$ reflect the fluctuations of local energy (e_1 and e_2 for $M = 2$) for fixed total energy. Obviously, these fluctuations are reduced for BMLJ($N = 65$) (albeit not absolutely suppressed). In other words, a system of 65 particles cannot be characterized via two independent relaxation modes. Conceptually, this is no problem at all. It simply means that it is not possible to strictly define a hypothetical small system with $\lambda = 1$ (and appropriately reduced values such as σ etc). For a comparison of the theoretical formulas with the actual systems one therefore has to take into account $\lambda < 1$.

In section 9 we suggest a mechanism for how the fluctuations of the waiting time can be suppressed via some specific interaction between the subsystems.

9. Length scales and dynamic coupling effects

So far we have analyzed the total system for different system sizes. In particular, we have confirmed the superposition

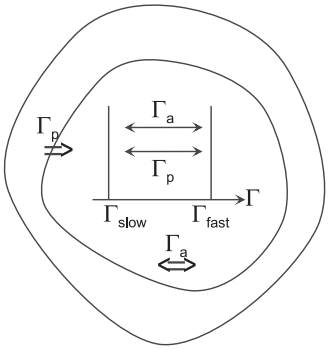

Figure 50. Sketch of active and passive exchange processes for a bimodal system.

hypothesis expressed by (I1) and (I2) for BMLJ as well as BKS-SiO_2 (with some specific features; see above) as long as a system is larger than some small system size (e.g. 65 particles for BMLJ are sufficient). The waiting time distribution of the larger system thus does not contain new information as compared to the smaller one. The superposition hypothesis also holds for thermodynamic observables such as σ or α [170]. Finite-size effects, however, show up for τ_α [267] and the non-exponentiality parameter β_{KWW} [270]. Furthermore, the model of an ideal Gaussian glass-former predicts a violation of the Stokes–Einstein relation which is significantly stronger than observed experimentally. Do these observations imply deviations from the superposition hypothesis?

As discussed in section 8 the α-relaxation time depends on a locally defined waiting time distribution which only for small systems can be identified with the total waiting time distribution. As will be shown, this local waiting time distribution can depend on whether or not the small system is embedded in a larger system. The ideas used in this context have been, e.g., discussed in the context of the rate memory in the 1990s [221, 276–278]. The key step is expressed in figure 50. A tagged subsystem can have two relaxation rates (Γ_{slow} and Γ_{fast}). For reasons of simplicity we assume that the Boltzmann probability of both states is the same. Now variation of the relaxation rate for this subsystem, also denoted the *exchange process*, is possible in two ways. First, via a relaxation process the system acquires a random new rate. The related exchange process is called *active*, with an exchange rate $\Gamma_a \approx \Gamma_{\mathrm{slow}}$. However, due to relaxation processes in adjacent regions of the subsystem the local mobility can also change (without performing a relaxation process). Formally, this can be denoted a *passive* exchange process, occurring with some rate Γ_{p}.

Naturally, the presence of passive exchange processes will remove the very long waiting times because finally a very immobile situation will be relieved. As shown below this removes the long-time tails, appearing for an ideal Gaussian glass-former. To quantify these ideas one has to formulate the dynamic interaction between different subensembles such that the distribution of states (I1) as well as the average waiting time (I2) of a tagged subsystem do not change. Thus, this interaction enters in a somewhat subtle way; see also [223]. Note that these passive exchange processes reflect the interaction between the relatively small elementary subsystems.

9.1. Energy master equation

9.1.1. Mean-field approach. To proceed we introduce the probability $p(e_i, t)$ that a state in a tagged subsystem with energy e_i at $t = 0$ has not performed a relaxation process until time t. As before, we explicitly restrict ourselves to the description of the equilibrium situation. If no passive exchange processes are present, the time evolution of $p(e_i, t)$ is simply given by

$$\frac{\mathrm{d}p(e_i,t)}{\mathrm{d}t} = -p(e_i,t)\Gamma(e_i). \tag{141}$$

To take into account fixed passive exchange processes one may introduce the rate $k_{i,\pm}$ that a state with energy i changes to a state with energy $i \pm 1$. Demanding detailed balance, i.e. $k_{i,+}/k_{i+1,-} = p_{\mathrm{eq}}(e_{i+1})/p_{\mathrm{eq}}(e_i)$, guarantees (I1). A simple choice is $k_{i,+} = k_0 p_{\mathrm{eq}}(e_{i+1})$ and $k_{i+1,-} = k_0 p_{\mathrm{eq}}(e_i)$. Then equation (141) is generalized to

$$\begin{aligned}\frac{\mathrm{d}p(e_i,t)}{\mathrm{d}t} &= -p(e_i,t)\Gamma(e_i) - (k_{i,+} + k_{i,-})p(e_i,t) \\ &\quad + k_{i-1,+}p(e_{i-1},t) + k_{i+1,-}p(e_{i+1},t).\end{aligned} \tag{142}$$

This approach may be relevant in the limit of high dimensions and corresponds to the mean-field case. Basically, it is a generalization of the simple system with just two rates, described above.

In the continuous description equation (142) can be rewritten as

$$\begin{aligned}\frac{\mathrm{d}p(e,t)}{\mathrm{d}t} &= -p(e,t)\Gamma(e) + K(\mathrm{d}/\mathrm{d}e)[(p_{\mathrm{eq}}(e)(\mathrm{d}/\mathrm{d}e)p(e,t) \\ &\quad - p(e,t)(\mathrm{d}/\mathrm{d}e)p_{\mathrm{eq}}(e))].\end{aligned} \tag{143}$$

As required by (I2) the average waiting time of the system does not change by additional passive exchange processes.

A similar set of equations also appears in the description of the energy diffusion in [220, 279]. In that work, however, the stationary distribution depends on K, thereby invalidating (I1) and (I2).

For the ideal Gaussian glass-former we have numerically checked the effect of passive exchange processes via equation (143). In figure 39 we show the numerical solution for $S_0(t)$. As expected, the long-time decay is much faster and the total curve can now be very well described by a stretched exponential.

Simple model systems can be also treated analytically. To elucidate the main features we discuss the simplest case of only two rates, i.e.

$$\begin{aligned}\dot{p}_1(t) &= -\Gamma_1 p_1(t) - k_0 p_{\mathrm{eq},2} p_1(t) + k_0 p_{\mathrm{eq},1} p_2(t) \\ \dot{p}_2(t) &= -\Gamma_2 p_2(t) - k_0 p_{\mathrm{eq},1} p_2(t) + k_0 p_{\mathrm{eq},2} p_1(t).\end{aligned} \tag{144}$$

Here we set $k_0 = q/\langle\tau\rangle$, i.e. q is a measure of how efficiently relaxation processes in adjacent regions influence the local mobility.

We are particularly interested in $\tau_\alpha = \int \mathrm{d}t\, S_0(t) = p_1(t) + p_2(t)$. Numerical simulations can be found in figure 51. To understand its behavior we also derive an

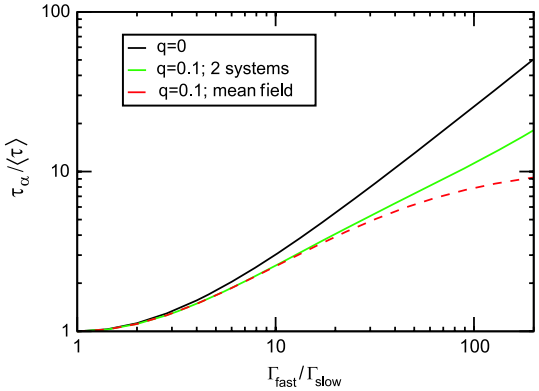

Figure 51. Checking the invalidation of the Stokes–Einstein relation $\tau_\alpha/\langle\tau\rangle = 1$ for a two-state system. For $q = 0$ no passive exchange processes are taken into account. For $q = 0.1$ the mean-field case is compared with the explicit case of two subsystems.

analytical expression for τ_α (see appendix 8). For the special case $p_{i,eq} = 1/2$ one obtains

$$\tau_\alpha/\langle\tau\rangle = \frac{1+q}{q + 4\Gamma_1\Gamma_2/(\Gamma_1+\Gamma_2)^2}. \tag{145}$$

Since $D \propto 1/\langle\tau\rangle$, equation (145) is a measure for the deviation from the Stokes–Einstein relation. For $\Gamma_2/\Gamma_1 = 1$ (qualitatively corresponding to high temperatures) this expression is unity, independent of the strength q of the passive exchange. For larger (or smaller) values of $\Gamma_2/\Gamma_1 = 1$ the decoupling increases. However, the deviations from the Stokes–Einstein relation become smaller with increasing q. In general, for $\Gamma_2 \neq \Gamma_1$ the passive exchange process decreases the timescale of relaxation τ_α by allowing the very slow molecules to relax faster and thus decreasing the deviations from the Stokes–Einstein relation (equation (4)). Furthermore, the degree of non-exponentiality decreases. All features agree with the simulation results. This indicates that consideration of the passive exchange is a key feature to understand the relaxation processes in glass-forming systems. However, $\tau_\alpha/\langle\tau\rangle$ cannot increase beyond $(1+q)/q$. This is a direct consequence of the mean-field approach. In the limit $\Gamma_{slow} \to 0$ a state with rate Γ_{slow} will effectively relax with a rate $q/\langle\tau\rangle$ because of passive exchange processes. This is the limiting value of the inverse structural relaxation time. Thus $\tau_\alpha/\langle\tau\rangle \approx 1/q$, which is in qualitative agreement with the exact result $1 + 1/q$. As will be discussed below this limiting behavior is an artifact of the mean-field approximation.

9.1.2. Non-mean-field case. Here we go beyond the mean-field approximation. For reasons of simplicity we discuss a system with two subsystems. Again we assume that (I1) and (I2) are obeyed. What happens after a relaxation process of subsystem 2? First, subsystem 2 chooses a random new energy according to its energy density $\varphi(e_2)$. This corresponds to the active exchange process. Furthermore, it may change the state of subsystem 1. In contrast to subsystem 2 its probability distribution is given by $p_{eq}(e_1)$. Thus, a passive exchange process can be realized by choosing a new energy of subsystem 1 such that its equilibrium distribution is kept. This can be implemented such that after MB transition of subsystem 2 two alternatives are possible. With probability q subsystem 1 selects a new energy according to the Boltzmann distribution $p_{eq}(e_1)$ whereas with probability $1-q$ the energy e_1 remains the same.

For a quantitative analysis we introduce $p_{ij}(t)$ as the probability that subsystem 1 is in state i, subsystem 2 in state j, and subsystem 1 has not performed a relaxation process between time 0 and time t. $p_{ij}(0)$ corresponds to the standard Boltzmann distribution $p_{eq}(e_i)\,p_{eq}(e_j)$. To formulate a master equation for $p_{ij}(t)$ one first considers the loss term $-[\Gamma_i + \Gamma_j]p_{ij}(t)$. However, the actual decay of $p_{ij}(t)$ is much weaker because relaxation processes of subsystem 2 need not change the state (i, j) of the total system. If only active exchange processes are present ($q = 0$), the gain term for $p_{ij}(t)$ is given by $\varphi(e_j)\Gamma_{i,tot}$ with

$$\Gamma_{i,tot}(t) \equiv \sum_j \Gamma_j\, p_{ij}(t). \tag{146}$$

This just expresses the fact that after an MB transition of subsystem 2 the system ends in state j with probability $\varphi(e_j)$. If $q > 0$ this scenario only happens with probability $1-q$. With probability q the state of subsystem 1 may also change. In this case the gain term is given by $p_{eq}(e_i)\varphi(e_j)\Gamma_{tot}$ with

$$\Gamma_{tot}(t) = \sum_i \Gamma_{i,tot}. \tag{147}$$

In total one thus obtains

$$(\mathrm{d}/\mathrm{d}t)\,p_{ij}(t) = -[\Gamma_i + \Gamma_j]p_{ij}(t) + \varphi(e_j)[(1-q)\Gamma_{i,tot}(t) + q p_{eq}(e_i)\Gamma_{tot}(t)]. \tag{148}$$

For a numerical analysis we first consider a system with just two relaxation rates and equal Boltzmann probabilities $p_{eq}(e_i) = 1/2$. The probability $S_{0,sub}(t)$ that subsystem 1 has not performed an MB transition until time t is given by

$$S_{0,sub}(t) = \sum_{ij} p_{ij}(t). \tag{149}$$

As discussed in the context of the CTRW it is necessary to define the structural relaxation time on a local basis, i.e.

$$\tau_\alpha = \int \mathrm{d}t\, S_{0,sub}(t). \tag{150}$$

The numerical results are also displayed in figure 51. One can see that for $\Gamma_1 \approx \Gamma_2$, i.e. weak dynamic heterogeneities, the behavior is very close to the mean-field case, whereas for larger dynamic heterogeneities the deviation from Stokes–Einstein is stronger than the mean-field case but weaker than the case without passive exchange. The latter inequality is trivial because naturally passive exchange processes suppress very long relaxation times. The comparison with the mean-field case is the main result of this analysis. Let us consider the case where subsystem 1 is in a slow state, which, for reasons of simplicity, we consider as immobile. In the mean-field case there is a passive exchange process with a fixed rate $(q\Gamma_{fast}/2)$ which renders the immobile subsystem 1 mobile,

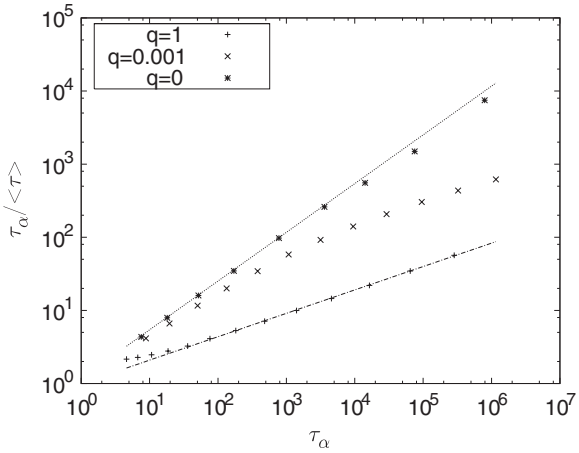

Figure 52. The dependence of $\tau_\alpha/\langle\tau\rangle$ on τ_α for an ideal Gaussian glass-former with coupling parameters $q = 0, 0.001$ and 1, respectively. The data are obtained via Monte Carlo simulations. For $q = 0$ the theoretical slope 2/3 is observed. For finite q the low-temperature behavior is described by a slope of approximately 0.32.

giving rise to a finite τ_α. In contrast, in the non-mean-field case one has to take into account that with a probability of 0.25 both subsystems are in an immobile state. Thus the average relaxation time τ_α is infinity. This exemplifies that the mean-field approximation reduces the deviation from the Stokes–Einstein relation too strongly.

Finally, we present a numerical solution for the ideal Gaussian glass-former in three dimensions where nearest neighbors experience the possibility of a passive exchange process. The results are shown in figure 52 [280]. One can see that in qualitative agreement with expectation the exponent α, characterizing the violation of the Stokes–Einstein relation, decreases from 2/3 to approximately 1/3, which is already quite close to the experimental value. This reduction does not depend on the chosen value of q. Thus, it seems that the ideal Gaussian glass-former, supplemented by the presence of passive exchange processes, can reproduce important features, observed in simulations and experiments.

9.1.3. Evidence from simulations. It would be interesting to identify the presence of passive exchange processes. In principle it can be obtained from analyzing the series of MB energies for systems composed of independent subsystems. Since mobile subsystems will remain mobile for many hopping processes the energetic contribution of slow subsystems does not change during that time. This gives rise to long-range correlations among successive MB energies (defined for the total system). The presence of passive exchange processes may strongly reduce these correlations as shown in [212]. A more detailed analysis of correlations between adjacent regions of supercooled liquids would be desirable for future work. The present formalism already reflects some key properties of interacting subsystems. However, a detailed description, reflecting all relevant observations, still has to be developed.

9.1.4. Alternative approach. To take into account the topology of the PEL the energy can be supplemented by a second variable, which characterizes the region of the corresponding state. In [281] the regions are characterized by dividing the energy axis into small energy intervals. The slow exploration of configuration space via transitions between these regions is taken into account by expressing the partition function in terms of the observation time. On a qualitative level this phenomenological model can reproduce thermodynamic properties in equilibrium and non-equilibrium situations.

9.2. Length scales in the PEL approach

In the context of identifying the temperature dependence of ξ_{single} it has been stated by Berthier that 'any theory in which timescales do not directly follow from the existence of spatial correlations growing when T is decreased ... is seriously challenged ...'. In particular, the relevance of the PEL approach is questioned [22, 282]. Indeed, due to the omnipresence of dynamic heterogeneities, this is an important question to be tackled.

First, we discuss the length scales appearing in the PEL approach. We start with an elementary system (or a nearly elementary system such as, e.g., BMLJ($N = 65$)). The basic length scale in the PEL approach characterizes the size of single-particle displacements during a single MB transition, characterized by the participation number [37]. In a temperature range where, e.g., the maximum of χ_4 displays a significant variation [42], this length scale is basically constant.

The next length scale ξ_{single} is a direct consequence of dynamic heterogeneities. As discussed above it is a measure for the number of successive hops of a fast subensemble until it becomes slow. Quantitatively, ξ_{single} is related to the second moment of the waiting time distribution as compared to its first moment. Most importantly, we get a non-trivial temperature dependence of ξ_{single} if only active exchange processes are taken into account. So far, the description of the dynamics in terms of the PEL is basically exact because for small systems the relevant parameters such as σ, e_{cross}, etc can be directly extracted from the simulations.

In a next step one has to take into account that the elementary system is embedded in a much larger system. As discussed above, the specific interaction of a tagged subsystem with its environment can be formulated in terms of passive exchange processes. In particular, this approach guarantees that the waiting time distribution of the total system as well its thermodynamics corresponds to the situation where the large system is a superposition of independent elementary systems. The waiting time distribution of an elementary subsystem, however, will in general change due to the passive exchange processes. Only its first moment remains the same. This has two consequences. First, it will give rise to a weaker temperature dependence of ξ_{single}. Second, successive subsystems will become correlated at low temperatures. A mobile subsystem will spread its mobility to adjacent subsystems via passive exchange processes. Thus, particles in adjacent volumes of the total system will become dynamically correlated, thereby contributing to ξ_{coll}. Furthermore, dynamic

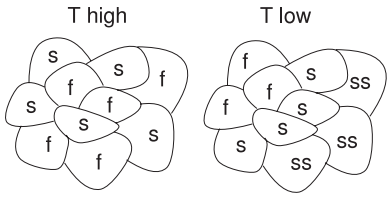

Figure 53. Sketch of the elementary systems of a glass-forming system at different temperatures (f, fast; s, slow; ss, very slow).

heterogeneities directly emerge from a non-trivial PEL. Thus, all observables which are related to dynamic heterogeneities (e.g., ξ_{single}, structural relaxation time, non-exponentiality parameter β_{KWW}) can be to a first approximation derived from the PEL of an elementary system. To obtain information about multi-particle correlations and to refine the properties of dynamic heterogeneities one has to take into account passive exchange processes and thus extend the elementary system to a superposition of elementary systems. This effect is sketched in figure 53.

Of course, we cannot exclude that at much lower temperatures, not accessible by present-day computer simulations, the elementary system size also changes. This would, e.g., show up as finite-size effects for the diffusion constant or a change of the thermodynamics. However, the analysis for the two systems analyzed so far suggests that this effect is less important than the increase of the length scales already contained in the present results.

9.3. Comparison with the KCM

In a qualitative way the KCM [145, 146] can be reformulated in the language we have used to characterize a supercooled liquid in terms of a PEL. The same holds for the Glarum defect dynamics [141]. We first consider the FA model [145]. Via the facilitation rules a single spin can be either immobile or fast, depending on the neighborhood. This spin can be regarded as an elementary system which is described by two states (immobile or fast). In the single-particle picture, developed in [148], the single-particle dynamics is related to a spin flip. In contrast to the PEL approach, active exchange processes are not present, i.e. the mobility of a spin does not change after a relaxation process of the related particle. A spin flip will have immediate consequences for the mobility of the adjacent spins (in particular at low temperatures where only a few spins are up). Thus, a relaxation process leads to a passive exchange process of the adjacent spins. In some sense the physical picture is similar to the PEL approach. In particular, the diffusion constant is not related to the interaction of adjacent spins since it is only related to the concentration of up-spins [148], whereas this interaction becomes important for observables such as the relaxation time. Furthermore, one may expect that the nature of the deviation from the Stokes–Einstein relation will be similar if calculated within the PEL approach.

From this perspective the major simplification in the KCM is the choice of the trivial elementary system. This is reflected by the fact that the FA model only displays Arrhenius behavior. To obtain non-Arrhenius behavior the kinetic rules become anisotropic or the rules for mobility have to be changed [148, 283]. In the PEL approach the non-Arrhenius temperature dependence naturally emerges from the complexity of the PEL of the elementary systems. Its physical origin is thus very different from the KCM.

In summary, to some extent the KCM has similarities with the PEL approach. As a consequence, it is, e.g., possible for both approaches to describe dynamic processes via a continuous-time random walk. The conceptual simplicity of the KCM allows one to obtain many interesting predictions, e.g. about the invalidation of the Stokes–Einstein relation. For a closer comparison with atomistic glass-forming systems, however, the PEL approach has several advantages. For example it is possible to describe the full range of different fragilities within the same physical model by just changing one relevant energy parameter (e_{cross}). Whereas the KCM is an interesting phenomenological model with relevant predictions, the PEL approach in its present version has been developed in full agreement with the results from computer simulations.

10. Summary

The dream of a theoretician is to start from a Hamiltonian and after some controllable approximations to end up with non-trivial predictions, which then hopefully agree with the experiment. Currently, no theory like this exists for the calorimetric glass transition. Either one has to resort to phenomenological models or to use computer simulations to characterize the thermodynamic and dynamic features of glass-forming systems. The goal of this review was, first, to give a short overview of relevant observations and models discussed in the literature and, second, to present a systematic approach in terms of the PEL.

The key idea, stressed in the literature for a long time, is the presence of localized activated events. Following the key ideas by Goldstein and Stillinger one first maps the real trajectory onto a discrete trajectory of transitions between inherent structures. In a second coarse-graining step one may combine inherent structures to metabasins. The dynamics between metabasins turns out to be close to a simple random walk in configuration space. This dramatic simplification in the description of the dynamics of supercooled liquids allows one to use the framework of the continuous-time random walk to characterize the dynamics of supercooled liquids. Using metabasins one can also relate the energy to the mobility, i.e. establishing a quantitative relation between thermodynamics and dynamics. In this context the ideal Gaussian glass-former has emerged as a suitable model system because it characterizes the properties of systems as different as BMLJ and BKS-SiO_2 to a very good approximation. In this framework one can identify three relevant energy scales: the width of the Gaussian distribution σ, the crossover energy e_{cross}, which describes the energy from which point on activated processes become relevant, and the cutoff energy e_{cut} at the low-energy end of the PEL. Both energies reflect distinctive geometric properties of the PEL. The emergence of e_{cross} can be related to a percolation-like process when the

system moves between different regions of the configuration space.

If $e_{\rm cut}$ is not accessible in the considered temperature range, the ideal Gaussian glass-former describes systems of moderate to very pronounced fragility. To first approximation, it is governed by only a single dimensionless parameter $e_{\rm cross}/\sigma$, and any temperature-dependent observable depends (to a good approximation) on the dimensionless parameter $\mu = \beta - |e_{\rm cross}/\sqrt{\lambda}\sigma|$. Many of the experimentally observed properties of supercooled liquids are recovered: (i) increase of dynamic heterogeneities with decreasing temperature, (ii) violation of the Stokes–Einstein relation and (iii) a direct relation between dynamic and thermodynamic fragility. All predictions work without any additional model assumptions. Within this class of systems the non-exponentiality of relaxation does not depend on fragility, if evaluated at a fixed relaxation rate. If one restricts oneself to the group of organic molecules, the experimental situation of the possible relation of non-exponentiality and fragility is not clear-cut [26]. More generally, all properties (such as non-exponentiality and dynamic length scales) turn out to be mainly a function of τ_α. This is consistent with the observed independence of the dynamic length scales from the fragility [49]. Of course, taking into account the remaining dimensionless parameters λ, and V_0/σ of the ideal Gaussian glass-formers and κ for some additional minor deviations, residual fluctuations among different glass-formers can be expected.

If the cutoff is relevant, one has a transition from non-Arrhenius to Arrhenius behavior. This naturally renders the relaxation only weakly non-exponential and furthermore displays a strong behavior in the fragility classification scheme. This effect may be particularly pronounced for network-forming supercooled liquids, being related to the disappearance of local defects at low temperatures. Comparing systems with and without relevant cutoff-effects, some overall correlation between non-exponentiality and fragility is recovered.

If the energy is interpreted as stemming from strongly interacting two-level systems, one may well envisage a distribution for which the width of $p_{\rm eq}(e)$, i.e. σ^2, decreases with decreasing temperature; see [185]. In some sense this might interpolate between the description of strong systems (using a well defined cutoff energy) and that of Gaussian systems without cutoff, and would introduce a weak coupling between fragility and non-exponentiality. Whether or not this scenario is relevant is still an open question.

More generally, the PEL approach has a strong relation to models postulating the presence of free energy barriers (e.g. RFOT), as well as the KCM. In the first type of model the important ingredients are the barriers as well as their fluctuations. This can be directly mapped on the PEL description. The fluctuations can be related to the effect of the dynamics of adjacent subsystems on the local configuration. What is missing in the PEL approach is the direct relation between dynamics and configurational entropy. Nevertheless, thermodynamics is very important since it determines the typical height of the PEL where the system resides at a given temperature. The concept of passive exchange processes as well as the possibility to use the framework of the continuous-time random walk gives the PEL approach a direct link to the KCM, but avoids the oversimplification of the elementary system.

Naturally, the present analysis can be directly extended to take into account non-equilibrium effects. Furthermore, transitions between inherent structures may account for the properties of the slow β-process. In general, the PEL approach is very versatile to elucidate basic mechanisms of the thermodynamics and dynamics of supercooled liquids. Hopefully, the present review will stimulate further activities along this line of research.

Acknowledgments

First of all I would like to acknowledge my direct co-workers S Büchner, B Doliwa, C Rehwald, O Rubner, A Saksaengwijit, and M Vogel for sharing the excitement to elucidate the properties as well as the relevance of the potential energy landscape of glass-forming systems and for comments on this paper. Furthermore I acknowledge very constructive comments from R D Banhatti, L Berthier, J C Dyre, D R Reichmann and F Sciortino about this review. I would like to thank my previous mentors in Mainz (K Binder, R Schilling, H W Spiess) for the initial encouragement to work in the field of the glass transition. Finally, I would like to thank many of my colleagues in this field for stimulating discussions. Financial support is acknowledged from the DFG (SFB 458 and SFB 262).

Appendix A

An IS can be uniquely mapped on a sequence of N numbers x_i which are either 0 or 1 and denote the distance between particles i and $i+1$. By definition $N/2$ values have to be 0 and $N/2$ values to be 1. Thus, G_N^∞ is the number of ways in which $N/2$ sites out of N sites can be selected, i.e. $G_N^\infty = N!/(N/2)!(N/2)!$. Using Stirling's approximation, valid for large N, one has $\ln G_N^\infty \approx N\ln 2 - (1/2)\ln N$. Writing $G_N^\infty = \exp(\alpha(N)N)$ one can identify $\alpha = \ln 2 - \ln N/(2N)$. Thus for large $N\alpha$ becomes N independent.

To determine the number of adjacent ISs one has to realize that during a transition between two ISs a pair (0, 1) changes to (1, 0) or vice versa. Therefore the number of adjacent ISs is equivalent to the number of pairs (0, 1) or (1, 0) in the sequence of N numbers introduced above. Naturally, the number of adjacent ISs depends on the initial IS. It is possible, however, to determine an average number of adjacent ISs. Starting from some number (0 or 1) the probability that the next number (e.g. on the right) is different is $p_r = N/(2N-2)$. For a given sequence of N numbers there exist on average $Np_r = N^2/(2N-2)$ adjacent ISs which for large N is approximated by $N/2$. Thus the number of adjacent ISs scales with the system size for large N.

Appendix B

The inverse average waiting time can be written (for not too high temperatures for which the population of states with

$e > e_{\rm cross}$ is not relevant) as

$$\langle\tau\rangle^{-1}\Gamma_0^{-1} = \int_{e_{\rm cut}}^{\infty} {\rm d}e\; p_{\rm eq}(e)\exp(-\lambda\tilde{\beta}(e-e_{\rm cross}))$$
$$= \frac{\int_{e_{\rm cut}}^{\infty} {\rm d}e\;\exp(-(e-e_{\rm cross}+\tilde{\beta}\sigma^2)^2/2\sigma^2)\exp(-\lambda\tilde{\beta}(e-e_{\rm cross}))}{\int_{e_{\rm cut}}^{\infty} {\rm d}e\;\exp(-(e-e_{\rm cross}+\tilde{\beta}\sigma^2)^2/2\sigma^2)}$$
$$= \frac{\int_{e_{\rm cut}-e_{\rm cross}+\tilde{\beta}\sigma^2(1-\lambda)}^{\infty} {\rm d}e\exp(-e^2/2\sigma^2)\exp(-(2\lambda-\lambda^2)\tilde{\beta}^2\sigma^2/2)}{\int_{e_{\rm cut}-e_{\rm cross}+\tilde{\beta}\sigma^2}^{\infty} {\rm d}e\exp(-e^2/2\sigma^2)}. \tag{B.1}$$

For the explicit calculation of $\langle\tau\rangle$ one has to take into account the limits of the Gaussian integrals. Neglecting factors of order unity one can approximate $\int_a^{\infty} {\rm d}x\;\exp(-x^2) \propto \exp(-a^2/2)$ for $a \gg 1$. For $\lambda = 1$ Arrhenius behavior starts for $\sigma^2\tilde{\beta} > -e_{\rm cut}$. In the low-temperature limit one can approximate

$$\langle\tau\rangle^{-1}\Gamma_0^{-1} \approx \frac{\exp(-\tilde{\beta}^2\sigma^2/2)}{\exp(-(e_{\rm cut}-e_{\rm cross}+\tilde{\beta}\sigma^2)^2/2\sigma^2)}$$
$$= \exp(-\beta(e_{\rm cross}-e_{\rm cut}))\exp((e_{\rm cut}^2-e_{\rm cross}^2)/2\sigma^2). \tag{B.2}$$

This result directly translates into equation (76). The situation is somewhat different for $\lambda < 1$. Here, a true activated behavior is obtained if $\tilde{\beta}\sigma^2(1-\lambda) \gg e_{\rm cross} - e_{\rm cut}$. Using again the approximations for the Gaussian integrals one ends up with equation (77).

Appendix C

First, one may calculate

$${\rm d}S_0(u)/{\rm d}u = -1/\sqrt{2\pi\mu^2}\int {\rm d}v\;\exp(-v^2/2\mu^2)\exp(u-v)$$
$$\times\;\exp(-\exp(u-v)). \tag{C.1}$$

This term can be approximated for small u, i.e. $t \approx 1/\Gamma^{\star}$. The function $\exp(x)\exp(-\exp(x))$ has a relevant contribution only for small x and can to a good approximation be written as $\exp(-1-x^2/2)$. Using this approximation in equation (C.1) one gets after evaluation of the Gaussian integral

$$\ln(-{\rm d}S_0(u)/{\rm d}u) = -1-(1/2)\ln(1+\mu^2)-u^2/[2(1+\mu^2)]. \tag{C.2}$$

One can compare this expression with a stretched exponential $S_{\rm KWW}(u) = \exp(-(t/\tau_{\rm KWW})^{\beta_{\rm KWW}}) = \exp(-\exp(\beta(u-w)))$ with $w = -\ln(\tau_{\rm KWW}\Gamma^{\star})$. One obtains (for small $|u-w|$)

$$\ln(-{\rm d}S_{\rm KWW}(u)/{\rm d}u) \approx -1-\ln\beta_{\rm KWW}-\beta(u-w)^2/2. \tag{C.3}$$

Interestingly, equation (C.3) can be mapped onto equation (C.2) when choosing $\beta_{\rm KWW} = 1/\sqrt{1+\mu^2}$ and $\tau_{\rm KWW} = 1/\Gamma^{\star}$. Actually, a more detailed analysis shows that for the above parameters $S_0(u) - S_{\rm KWW}(u)$ is a small but finite constant for $u \approx 0$. This can be accounted for by choosing $\tau_{\rm KWW} > 1/\Gamma^{\star}$ in the fitting procedure.

Appendix D

For a discussion of the CTRW a few probability functions become relevant [265, 266].

(1) The key quantity is the probability $S_0(t)$ that during a time interval of length t the system does not hop. In analogy we define the probability $S_n(t)$ to display exactly n hops during this time interval.

(2) $(S_0(t)-S_0(t+\Delta t))$ $(=-S_0'(t)\Delta t$ for small $\Delta t)$ denotes the probability that the system hops during a time interval of length Δt *and* does not hop in the previous (alternatively subsequent) time interval of length t. From this quantity, two different probabilities can be derived. First, the probability density $\xi(t)$ (*persistence time distribution*) that for a randomly chosen starting point exactly a time t later the system hops for the first time is directly given by $-S_0'(t)$. Second, the probability $\chi(t)$ that after a hop there is no further hop during the subsequent time interval of length t can be interpreted as a conditional probability. Note that the probability that a transition happens during a randomly chosen infinitesimally small time interval Δt is given by $\Delta t/\langle\tau\rangle$, where $\langle\tau\rangle$ is the average waiting time. Then $\chi(t)$ can be simply written as

$$\chi(t) = -S_0'(t)\Delta t/(\Delta t/\langle\tau\rangle) = -S_0'(t)\langle\tau\rangle = \xi(t)\langle\tau\rangle. \tag{D.1}$$

(3) Analogously,

$$\varphi(t) \equiv (\chi(t)-\chi(t+\Delta t))/\Delta t = \langle\tau\rangle S_0''(t) = -\langle\tau\rangle\xi'(t) \tag{D.2}$$

denotes the probability density that after a hop the next hop happens exactly a time t later. This is exactly the waiting time distribution (sometimes also denoted the exchange time distribution [51]). From equation (D.2) one can express the average persistence time via partial integration in terms of the waiting time distribution:

$$\langle\tau\rangle_{\xi} = \langle\tau^2\rangle/(2\langle\tau\rangle). \tag{D.3}$$

Using the rules of Laplace transformations these relations can be rewritten as

$$\chi(\lambda) = \frac{1-\varphi(\lambda)}{\lambda} \tag{D.4}$$

$$\xi(\lambda) = \frac{\chi(\lambda)}{\langle\tau\rangle} \tag{D.5}$$

and

$$S_0(\lambda) = \frac{1-\xi(\lambda)}{\lambda}. \tag{D.6}$$

This means that all probabilities can be finally expressed in terms of the waiting time distribution $\varphi(t)$.

Following condition (C3) the observable $S_n(t)$ can be expressed as a convolution of $n+1$ terms $\xi\star\varphi\cdots\star\varphi\star\chi$. This convolution just expresses that for a randomly chosen time there are exactly n transitions during the subsequent time interval of length t. Using the Laplace transformation one can then write $(n \geqslant 1)$

$$S_n(\lambda) = \xi(\lambda)\varphi(\lambda)^{n-1}\chi(\lambda). \tag{D.7}$$

Switching to q-space from equation (113) one directly obtains (keeping the $n = 0$ term separate)

$$S(q,\lambda) = S_0(\lambda) + \sum_{n=1}^{\infty} \xi(\lambda)\varphi(\lambda)^{n-1}\chi(\lambda)\pi_1(q)^n$$
$$= S_0(\lambda) + \pi_1(q)\xi(\lambda)S_{\mathrm{MW}}(q,\lambda) \tag{D.8}$$

with

$$S_{\mathrm{MW}}(q,\lambda) = \frac{\chi(\lambda)}{1-\varphi(\lambda)\pi_1(q)}. \tag{D.9}$$

Appendix E

First, one can rewrite

$$\tau_0(q) = S(q,\lambda=0) \tag{E.1}$$

and

$$\tau_1(q) = -[(\mathrm{d}/\mathrm{d}\lambda)S(q,\lambda=0)]/S(q,\lambda=0). \tag{E.2}$$

Now the goal is to evaluate the different ingredients of equation (118) up to linear order in λ. From the Taylor expansion of $\varphi(t)$ and successive partial integration one obtains

$$\varphi(\lambda) = \sum_n (-\lambda)^n\langle\tau^n\rangle/n!. \tag{E.3}$$

For the calculation of $\tau_0(q)$ and $\tau_1(q)$ one needs the linear expansions (using the abbreviation $z \equiv \pi_1(q)$)

$$S_0(\lambda) = \frac{1}{\lambda} - \frac{1-\varphi(\lambda)}{\lambda^2\langle\tau\rangle} \approx \frac{\langle\tau^2\rangle}{2\langle\tau\rangle} - \lambda\frac{\langle\tau^3\rangle}{6\langle\tau\rangle}$$
$$\xi(\lambda) \approx 1 - \lambda\frac{\langle\tau^2\rangle}{2\langle\tau\rangle}$$
$$S_{\mathrm{MW}}(q,\lambda) \approx \frac{\langle\tau\rangle - (\lambda/2)\langle\tau^2\rangle}{1-z+\lambda z\langle\tau\rangle}$$
$$\approx \frac{\langle\tau\rangle}{1-z} - \lambda\left[\frac{\langle\tau^2\rangle}{2(1-z)} + \frac{z\langle\tau\rangle^2}{(1-z)^2}\right]. \tag{E.4}$$

This yields for small λ

$$S(q,\lambda) \approx \frac{\langle\tau^2\rangle}{2\langle\tau\rangle} + \frac{z\langle\tau\rangle}{1-z}$$
$$+ \lambda\frac{\left[\frac{(1-z)^2\langle\tau^3\rangle}{6\langle\tau\rangle} + z(1-z)\langle\tau^2\rangle + z^2\langle\tau\rangle^2\right]}{(1-z)^2}. \tag{E.5}$$

From the λ-independent term of $S(q,\lambda)$ equation (126) can be directly reproduced. Furthermore, one can easily check that the λ^1-term of $S(q,\lambda)$ can be rewritten as $\tau_0(q)^2 + T_\beta\langle\tau\rangle^2$. This immediately gives rise to equation (127).

Appendix F

From the derivative of equation (135) one directly obtains (setting $\langle\tau\rangle = 1$ for reasons of simplicity and using equations (D.1))

$$p_{2N}(t) = 2t(\varphi_N(t)(S_0(t))_N + \xi_N(t)^2). \tag{F.1}$$

The right side of equation (F.1) can be further manipulated as (omitting the index N)

$$-(\mathrm{d}/\mathrm{d}t)[2\xi(t)tS_0(t) + S_0(t)^2]$$
$$= -(\mathrm{d}/\mathrm{d}t)\left[\xi(t)t + \int_t^\infty \mathrm{d}\tau\xi(\tau)\right]^2 + (\mathrm{d}/\mathrm{d}t)[t^2\xi(t)^2]^2$$
$$= -(\mathrm{d}/\mathrm{d}t)\left[\int_t^\infty \mathrm{d}\tau\varphi(\tau)\tau\right]^2 + (\mathrm{d}/\mathrm{d}t)[t^2\xi(t)^2]^2$$
$$= -\frac{\mathrm{d}}{\mathrm{d}t}\int_t^\infty \mathrm{d}t'\,p(t')\int_t^\infty \mathrm{d}t''\,p(t'')\left(1-\frac{t^2}{t't''}\right). \tag{F.2}$$

This proves equation (136).

Appendix G

To calculate the different moments (here we restrict ourselves to $\lambda = 1$) we first recognize that the energy e of the total system is distributed according to

$$p_{\mathrm{eq},M}(e) = \frac{1}{\sqrt{2\pi M\sigma^2}}\exp[-(e - Me_{\mathrm{cross}} + M\sigma^2\tilde{\beta})^2/(2M\sigma^2)]. \tag{G.1}$$

This is a generalization of equation (60) by multiplying the energies as well as the variance by M as implied by (I1). For the further analysis we introduce $\epsilon_i = e_i - e/M$ as the deviation from the average energy. Now the partitioning of the system is characterized by the ϵ_i. With these new variables $p_{\mathrm{eq},M}(e_1,\ldots,e_M)$ is directly translated into $p_{\mathrm{eq},M}(\epsilon_1,\ldots,\epsilon_M)$.

In what follows we will use the notation $\langle\cdots\rangle_{p,M}$ as the average over $p_{\mathrm{eq},M}(e_1,\ldots,e_M)$ and $\langle\cdots\rangle_{p,M}(e)$ as the same average but for fixed total energy $e = e_1 + \cdots + e_M$.

In the next step we introduce the conditional probabilities $p_{\mathrm{eq},M}(\epsilon_1,\ldots,\epsilon_M|e)$ for a fixed energy e of the total system. According to the definition of the ϵ_i this requires $\sum_i \epsilon_i = 0$. Using equation (G.1) one obtains

$$p_{\mathrm{eq},M}(\epsilon_1,\ldots,\epsilon_M|e) = p_{\mathrm{eq},M}(\epsilon_1,\ldots,\epsilon_M)/p_{\mathrm{eq},M}(e)$$
$$= \prod_j \exp(-\epsilon_j^2/2\sigma^2)(2\pi M\sigma^2)^{1/2}(2\pi\sigma^2)^{-M/2}\delta\left(\sum_i \epsilon_i\right). \tag{G.2}$$

Furthermore, one can write

$$\Gamma_M(\epsilon_1,\ldots,\epsilon_M|e) = \exp[(\tilde{\beta}/M)(e - Me_{\mathrm{cross}})]\sum_i \exp(\tilde{\beta}\epsilon_i). \tag{G.3}$$

One can proceed with the help of

$$\int \mathrm{d}\epsilon_1\ldots\mathrm{d}\epsilon_M \prod_{j=1}^M \exp(-x_j^2/2)\exp(\mu x_1)\delta\left(\sum_{j=1}^M x_j\right)$$
$$= \int \mathrm{d}\epsilon_1\ldots\mathrm{d}\epsilon_M\,\mathrm{d}q\prod_j \exp(-x_j^2/2)$$
$$\times \exp(\mu x_1)\exp\left(\mathrm{i}q\sum_j x_j\right)$$
$$\propto \int \mathrm{d}q\exp[(\mu+\mathrm{i}q)^2/2]\exp[(M-1)(\mathrm{i}q)^2/2]$$
$$\propto \exp[\mu^2(1-1/M)/2]. \tag{G.4}$$

To obtain the last two lines appropriate quadratic substitutions have been performed. This directly yields

$$\langle\Gamma_M\rangle_{p,M}(e) = 1/\langle\tau\rangle_M(e) = M\Gamma(e/M)\exp[\mu^2(1-1/M)/2]. \tag{G.5}$$

Energy integration yields

$$1/\langle\tau\rangle_M = M\exp[-\mu^2/2]. \tag{G.6}$$

Of further interest is the product $\langle\Gamma_M\rangle_{p,M}(e)\langle\Gamma_M^{-1}\rangle_{p,M}(e)$. Note that the e-dependence of Γ_M cancels out. The first factor involves the integral

$$f_M(\mu) \equiv M\int \mathrm{d}\epsilon_1 \cdots \int \mathrm{d}\epsilon_M\, p(\epsilon_1,\ldots,\epsilon_M|e) \times \left[\sum_i \exp(\tilde{\beta}\epsilon_i)\right]^{-1} \tag{G.7}$$

which cannot be solved analytically. For the case $M = 2$ it can be approximated by

$$f_2(\mu) \approx \frac{2+\frac{2}{1+4\mu}}{\frac{2\mu}{\sqrt{\pi}}+1} \tag{G.8}$$

which correctly reproduces the limits of small and large μ. With the definition of $f_M(\mu)$ one can finally write

$$\langle\Gamma_M\rangle_{p,M}(e)\langle\Gamma_M^{-1}\rangle_{p,M}(e) = f_M(\mu)\exp[\mu^2(1-1/M)/2]. \tag{G.9}$$

Thus, one obtains in particular

$$\frac{\langle\tau^2\rangle_M(e)}{[\langle\tau\rangle_M(e)]^2} = 2f_M(\mu)\exp[\mu^2(1-1/M)/2]. \tag{G.10}$$

Appendix H

Starting from a set of linear differential equations $(\mathrm{d}/\mathrm{d}t)\vec{p}(t) = A\vec{p}(t)$ ($\vec{p}$, vector with n components; A, nxn-matrix with a constant coefficient) the solution can be formally written as $\vec{p}(t) = \exp(At)\vec{p}(0)$. As a consequence one has

$$\int \mathrm{d}t\,\vec{p}(t) = -A^{-1}\vec{p}(0). \tag{H.1}$$

In the present case one has

$$A = \begin{pmatrix} -\Gamma_1 - k_0/2 & k_0/2 \\ k_0/2 & -\Gamma_2 - k_0/2 \end{pmatrix} \tag{H.2}$$

and thus

$$A^{-1} = \frac{1}{\Gamma_1\Gamma_2 + k_0}\begin{pmatrix} -\Gamma_2 - k_0/2 & -k_0/2 \\ -k_0/2 & -\Gamma_1 - k_0/2 \end{pmatrix} \tag{H.3}$$

and $\vec{p}(0) = (0.5, 0.5)$.

Summing over the different components of equation (H.1) yields

$$\tau_\alpha = \frac{(\Gamma_1+\Gamma_2)/2 + k_0}{k_0(\Gamma_1+\Gamma_2)/2 + \Gamma_1\Gamma_2}; \tag{H.4}$$

with $\langle\tau\rangle^{-1} = (\Gamma_1+\Gamma_2)/2$ and $k_0 = q/\langle\tau\rangle$ one immediately ends up with equation (145).

References

[1] Debenedetti P G and Stillinger F H 2001 *Nature* **410** 259
[2] Debenedetti P G 1997 *Metastable Liquids* (Princeton, NJ: Princeton University Press)
[3] Sillescu H 1999 *J. Non-Cryst. Solids* **243** 81
[4] Ediger M D 1996 *J. Phys. Chem.* **100** 13200
[5] Ngai K L 2000 *J. Non-Cryst. Solids* **275** 7
[6] Angell C A 1995 *Science* **267** 1924
[7] Angell C A, Ngai K L, McKenna G B, McMillan P F and Martin S W 2000 *J. Appl. Phys.* **88** 3113
[8] Debenedetti P G, Truskett T M and Lewis C P 2001 *Adv. Chem. Eng.* **28** 21
[9] Richert R 2002 *J. Phys.: Condens. Matter* **14** R703
[10] Wales D J 2003 *Energy Landscapes* (Cambridge: Cambridge University Press)
[11] Sciortino F 2005 *J. Stat. Mech.* P05015
[12] Andersen H C 2005 *Proc. Natl Acad. Sci.* **102** 6686
[13] Binder K and Kob W 2005 *Glassy Materials and Disordered Solids* (Singapore: World Scientific)
[14] Dyre J C 2006 *Rev. Mod. Phys.* **78** 953
[15] Lubchenko V and Wolynes P G 2006 *Annu. Rev. Phys. Chem.* **58** 235
[16] Schmidt-Rohr K and Spiess H W 1991 *Phys. Rev. Lett.* **66** 3020
[17] Richert R 1993 *Chem. Phys. Lett.* **216** 223
[18] Bohmer R *et al* 1998 *J. Non-Cryst. Solids* **235** 1
[19] Weiss M, Moske M and Samwer K 1998 *Phys. Rev.* B **58** 9062
[20] Martinez L M and Angell C A 2001 *Nature* **410** 663
[21] Fujara F, Geil B, Sillescu H and Fleischer G 1992 *Z. Phys.* B **88** 195
[22] Berthier L 2004 *Phys. Rev.* E **69** 020201
[23] Reichman D R 2008 private communication
[24] Ruocco G, Sciortino F, Zamponi F, De Michele C and Scopigno T 2004 *J. Chem. Phys.* **120** 10666
[25] Bohmer R, Ngai K L, Angell C A and Plazek D J 1993 *J. Chem. Phys.* **99** 4201
[26] Dyre J C 2007 *J. Phys.: Condens. Matter* **19** 205105
[27] Hurley M M and Harrowell P 1995 *Phys. Rev.* E **52** 1694
[28] Kob W, Donati C, Plimpton S J, Poole P H and Glotzer S C 1997 *Phys. Rev. Lett.* **79** 2827
[29] Donati C, Douglas J F, Kob W, Plimpton S J, Poole P H and Glotzer S C 1998 *Phys. Rev. Lett.* **80** 2338
[30] Donati C, Glotzer S C, Poole P H, Kob W and Plimpton S J 1999 *Phys. Rev.* E **60** 3107
[31] Donati C, Glotzer S C and Poole P H 1999 *Phys. Rev. Lett.* **82** 5064
[32] Heuer A and Okun K 1997 *J. Chem. Phys.* **106** 6176
[33] Qian J, Hentschke R and Heuer A 1999 *J. Chem. Phys.* **110** 4514
[34] Moynihan C T and Schroeder J 1993 *J. Non-Cryst. Solids* **16** 52
[35] Richert R 1988 *Macromolecules* **21** 923
[36] Cicerone M T, Blackburn F R and Ediger M 1995 *J. Chem. Phys.* **102** 471
[37] Vogel M, Doliwa B, Heuer A and Glotzer S C 2004 *J. Chem. Phys.* **120** 4404
[38] Tracht U, Wilhelm M, Heuer A, Feng H, Schmidt-Rohr K and Spiess H W 1998 *Phys. Rev. Lett.* **81** 2727
[39] Reinsberg S A, Qiu X H, Wilhelm M, Spiess H W and Ediger M D 2001 *J. Chem. Phys.* **114** 7299
[40] Reinsberg S A, Heuer A, Doliwa B, Zimmermann H and Spiess H W 2002 *J. Non-Cryst. Solids* **307** 208
[41] Franz S, Donati C, Parisi G and Glotzer S C 1999 *Phil. Mag.* B **79** 1827
[42] Glotzer S C, Novikov V N and Schroder T B 2000 *J. Chem. Phys.* **112** 509
[43] Doliwa B and Heuer A 2000 *Phys. Rev.* E **61** 6898

[44] Toninelli C, Wyart M, Berthier L, Biroli G and Bouchaud J P 2005 *Phys. Rev.* E **71** 041505
[45] Szamel G and Flenner E 2006 *Phys. Rev.* E **74** 021507
[46] Berthier L, Biroli G, Bouchaud J P, Kob W, Miyazaki K and Reichman D R 2007 *J. Chem. Phys.* **126** 184503
[47] Berthier L and Jack R L 2007 *Phys. Rev.* E **78** 041509
[48] Whitelam S P, Berthier L and Garrahan J P 2004 *Phys. Rev. Lett.* **92** 185705
[49] Berthier L *et al* 2005 *Science* **310** 1797
[50] Swallen S F, Mapes M K, Kim Y S, McMahon R J, Ediger M D and Satija S 2006 *J. Chem. Phys.* **124** 184501
[51] Berthier L, Chandler D and Garrahan J P 2005 *Europhys. Lett.* **69** 320
[52] Appignanesi G A, Fris J A R, Montani R A and Kob W 2006 *Phys. Rev. Lett.* **96** 057801
[53] Doliwa B and Heuer A 2003 *Phys. Rev.* E **67** 031506
[54] Widmer-Cooper A and Harrowell P 2004 *Phys. Rev. Lett.* **93** 135701
[55] Widmer-Cooper A and Harrowell P 2006 *Phys. Rev. Lett.* **96** 185701
[56] Ladadwa I and Teichler H 2006 *Phys. Rev.* E **73** 031501
[57] Widmer-Cooper A and Harrowell P 2005 *J. Phys.: Condens. Matter* **17** S4025
[58] Goldstein M 1969 *J. Chem. Phys.* **51** 3728
[59] Stillinger F H and Weber T A 1982 *Phys. Rev.* A **25** 978
[60] Stillinger F H and Weber T A 1984 *Science* **225** 983
[61] Stillinger F H 1995 *Science* **267** 1935
[62] Schrøder T B, Sastry S, Dyre J C and Glotzer S C 2000 *J. Chem. Phys.* **112** 9834
[63] Sastry S, Debenedetti P G and Stillinger F H 1998 *Nature* **393** 554
[64] Jonsson H and Andersen H C 1988 *Phys. Rev. Lett.* **60** 2295
[65] Doye J P K 2002 *Phys. Rev. Lett.* **88** 8701
[66] Donati C, Sciortino F and Tartaglia P 2000 *Phys. Rev. Lett.* **85** 1464
[67] La Nave E, Scala A, Starr F W, Stanley H E and Sciortino F 2001 *Phys. Rev.* E **64** 036102
[68] La Nave E, Stanley H E and Sciortino F 2002 *Phys. Rev. Lett.* **88** 035501
[69] Gezelter J D, Rabani E and Berne B J 1997 *J. Chem. Phys.* **107** 4618
[70] Coslovich D and Pastore G 2006 *Europhys. Lett.* **75** 784
[71] Doye J P K and Wales D J 2002 *J. Chem. Phys.* **116** 3777
[72] Angelani L, Leonardo R D, Ruocco G, Scala A and Sciortino F 2000 *Phys. Rev. Lett.* **85** 5356
[73] Angelani L, Ruocco G, Sampoli M and Sciortino F 2003 *J. Chem. Phys.* **119** 2120
[74] Grigera T S, Cavagna A, Giardina I and Parisi G 2002 *Phys. Rev. Lett.* **88** 055502
[75] Broderix K, Bhattacharya K K, Cavagna A, Zippelius A and Giardina I 2000 *Phys. Rev. Lett.* **85** 5360
[76] Fabricius G and Stariolo D A 2002 *Phys. Rev.* E **66** 1501
[77] Mossa S and Sciortino F 2004 *Phys. Rev. Lett.* **92** 045504
[78] Anderson P W, Halperin B I and Varma C M 1972 *Phil. Mag.* **25** 1
[79] Phillips W A 1972 *J. Low Temp. Phys.* **7** 351
[80] Phillips W A 1987 *Rep. Prog. Phys.* **50** 1657
[81] Speedy R J 2003 *J. Phys.: Condens. Matter* **15** S1243
[82] Tarjus G, Kivelson D, Mossa S and Alba-Simionesco C 2004 *J. Chem. Phys.* **120** 6135
[83] Reiser A and Kasper G 2006 *Europhys. Lett.* **76** 1137
[84] Sastry S 2001 *Nature* **409** 164
[85] Middleton T F and Wales D J 2003 *J. Chem. Phys.* **118** 4583
[86] Shell M S, Debenedetti P G, Lave E and Sciortino F 2003 *J. Chem. Phys.* **118** 8821
[87] Mauro J C and Loucks R J 2007 *Phys. Rev.* B **76** 174202
[88] Binder K, Horbach J, Kob W, Paul W and Varnik F 2004 *J. Phys.: Condens. Matter* **16** S429
[89] Van Beest B W H, Kramer G J and Van Santen R A 1990 *Phys. Rev. Lett.* **64** 1955
[90] Stillinger F H and Weber T A 1985 *Phys. Rev.* B **31** 5262
[91] Kob W and Andersen H C 1995 *Phys. Rev.* E **52** 4134
[92] Kob W and Andersen H C 1995 *Phys. Rev.* E **51** 4626
[93] Lewis L J and Wahnström G 1994 *Phys. Rev.* E **50** 3865
[94] Dzugutov M, Simdyankin S I and Zetterling F H M 2001 *Preprint* cond-mat/0109057
[95] Berendsen H J, Postma J P M, van Gunsteren W F, Dinola A and Haak J R 1984 *J. Chem. Phys.* **81** 3684
[96] Ohmine I 1995 *J. Phys. Chem.* **99** 6767
[97] Gleim T, Kob W and Binder K 1998 *Phys. Rev. Lett.* **81** 4404
[98] Szamel G and Flenner E 2004 *Europhys. Lett.* **76** 779
[99] Berthier L and Kob W 2007 *J. Phys.: Condens. Matter* **19** 205130
[100] Götze W and Sjogren L 1992 *Rep. Prog. Phys.* **55** 241
[101] Goetze W 1999 *J. Phys.: Condens. Matter* **11** 1
[102] Das S P and Mazenko G F 1968 *Phys. Rev.* A **34** 2265
[103] Goetze W and Sjoegren L 1987 *Z. Phys.* B **65** 415
[104] Flenner E and Szamel G 2005 *Phys. Rev.* E **72** 011205
[105] Cates M E and Ramaswamy S 2006 *Phys. Rev. Lett.* **96** 135701
[106] Biroli G and Bouchaud J P 2004 *Europhys. Lett.* **67** 21
[107] Fuchs M, Goetze W and Mayr M R 1998 *Phys. Rev.* E **58** 3384
[108] Mayer P, Miyazaki K and Reichman D R 2006 *Phys. Rev. Lett.* **97** 095702
[109] Biroli G, Bouchaud J P, Miyazaki K and Reichman D R 2006 *Phys. Rev. Lett.* **97** 195701
[110] Götze W and Sjögren L 1989 *J. Phys.: Condens. Matter* **1** 4183
[111] Schweizer K and Saltzman E 2003 *J. Chem. Phys.* **119** 1181
[112] Schweizer K and Saltzman E 2004 *J. Phys. Chem.* B **108** 19729
[113] Schweizer K 2005 *J. Chem. Phys.* **123** 244501
[114] Adam G and Gibbs J H 1965 *J. Chem. Phys.* **43** 139
[115] Mossa S, La Nave E, Stanley H E, Donati C, Sciortino F and Tartaglia P 2002 *Phys. Rev.* E **65** 041205
[116] Saika-Voivod I, Poole P H and Sciortino F 2001 *Nature* **412** 514
[117] Giovambattista N, Buldyrev S V, Starr F W and Stanley H E 2003 *Phys. Rev. Lett.* **90** 085506
[118] Saika-Voivod I, Sciortino F and Poole P H 2004 *Phys. Rev.* E **69** 041503
[119] Gebremichael Y, Vogel M, Bergroth M, Starr F W and Glotzer S C 2005 *J. Phys. Chem.* B **109** 15068
[120] Richert R and Angell C A 1998 *J. Chem. Phys.* **108** 9016
[121] Bouchaud J P and Biroli G 2004 *J. Chem. Phys.* **121** 7347
[122] Yamamuro O, Tsukushi I, Lindqvist A, Takahara S, Ishikawa M and Matsuo T 1998 *J. Phys. Chem.* B **102** 1605
[123] Stillinger F H and Debenedetti P G 2002 *J. Chem. Phys.* **116** 3353
[124] Kirkpatrick T R, Thirumalai D and Wolynes P G 1989 *Phys. Rev.* A **40** 1045
[125] Xia X and Wolynes P G 2001 *Phys. Rev. Lett.* **86** 5526
[126] Ediger M D 1998 *J. Non-Cryst. Solids* **235** 10
[127] Wang L M, Angell C A and Richert R 2006 *J. Chem. Phys.* **125** 074505
[128] Lubchenko V and Wolynes P G 2003 *J. Chem. Phys.* **119** 9088
[129] Bhattacharya K K, Broderix K, Kree R and Zippelius A 1999 *Europhys. Lett.* **47** 449
[130] Kirkpatrick T R and Thirumalai D 1987 *Phys. Rev. Lett.* **58** 2091
[131] Cavagna A, Grigera T and Verrocchio P 2007 *Phys. Rev. Lett.* **98** 187801
[132] Tarjus G and Kivelson D 1995 *J. Chem. Phys.* **103** 3071
[133] Ngai K L 2005 *J. Non-Cryst. Solids* **351** 2635
[134] Capaccioli S and Ngai K L 2005 *J. Phys. Chem.* B **109** 9727
[135] Dyre J C 2006 *Phys. Rev.* E **74** 021502

[136] Dasgupta C and Valls O T 1999 *Phys. Rev.* E **59** 3123
[137] Kaur C and Das S P 2001 *Phys. Rev. Lett.* **86** 2062
[138] Kim K and Munakata T 2003 *Phys. Rev.* E **68** 021502
[139] Odagaki T, Yoshidome T and Koyam A Y A 2006 *J. Non-Cryst. Solids* **352** 4843
[140] Singh Y, Stoessel J P and Wolynes P G 1985 *Phys. Rev. Lett.* **54** 1059
[141] Glarum S H 1960 *J. Chem. Phys.* **33** 639
[142] Bordewijk P 1975 *Chem. Phys. Lett.* **32** 592
[143] Shlesinger M F and Montroll E W 1984 *Proc. Natl Acad. Sci* **81** 1280
[144] Donth E 1999 *Acta Polym.* **50** 240
[145] Fredrickson G H and Andersen H C 1984 *Phys. Rev. Lett.* **53** 1244
[146] Garrahan J P and Chandler D 2002 *Phys. Rev. Lett.* **89** 035704
[147] Berthier L and Garrahan J P 2003 *Phys. Rev.* E **68** 041201
[148] Jung Y J, Garrahan J P and Chandler D 2004 *Phys. Rev.* E **69** 061205
[149] Vogel M and Glotzer S C 2004 *Phys. Rev. Lett.* **92** 255901
[150] Bergroth M N J, Vogel M and Glotzer S C 2005 *J. Phys. Chem.* B **109** 6748
[151] Kohen D and Stillinger F H 2000 *Phys. Rev.* E **1176** 61
[152] Bowles R K and Saika-Voivod I 2006 *Phys. Rev.* E **73** 011503
[153] Haener P and Schilling R 1989 *Europhys. Lett.* **8** 129
[154] Stillinger F H 1999 *Phys. Rev.* E **59** 48
[155] Keyes T and Chowdhary J 2002 *Phys. Rev.* E **65** 041106
[156] Schilling R 2006 *Physica* D **216** 157
[157] Wales D J and Doye J P K 2003 *J. Chem. Phys.* **119** 12409
[158] Heuer A 1997 *Phys. Rev. Lett.* **78** 4051
[159] Middleton T F and Wales D J 2001 *Phys. Rev.* B **64** 024205
[160] Palmer R G 1982 *Adv. Phys.* **31** 669
[161] La Nave E, Sciortino F, Tartaglia P, Michele C D and Mossa S 2003 *J. Phys.: Condens. Matter* **15** S1085
[162] Shell M S, Debenedetti P G and Panagiotopoulos A Z 2004 *Phys. Rev. Lett.* **92** 035506
[163] Sciortino F, Kob W and Tartaglia P 1999 *Phys. Rev. Lett.* **83** 3214
[164] Buechner S and Heuer A 1999 *Phys. Rev.* E **60** 6507
[165] Starr F W, Sastry S, La Nave E, Scala A, Stanley H E and Sciortino F 2001 *Phys. Rev.* E **63** 041201
[166] Giovambattista N, Stanley H E and Sciortino F 2003 *Phys. Rev. Lett.* **91** 115504
[167] Sciortino F, La Nave E and Tartaglia P 2003 *Phys. Rev. Lett.* **91** 155701
[168] Frenkel D and Smit B 1996 *Understanding Molecular Simulation* (New York: Academic)
[169] Coluzzi B, Parisi G and Verrocchio P 2000 *Phys. Rev. Lett.* **84** 306
[170] Doliwa B and Heuer A 2003 *J. Phys.: Condens. Matter* **15** S849
[171] Faller R and de Pablo J J 2003 *J. Chem. Phys.* **119** 4405
[172] Yan Q, Jain T S and de Pablo J J 2004 *Phys. Rev. Lett.* **92** 235701
[173] Ferrenberg A M and Swendsen R H 1988 *Phys. Rev. Lett.* **61** 2635
[174] Mezard M and Parisi G 2000 **12** 6655
[175] Saksaengwijit A, Reinisch J and Heuer A 2004 *Phys. Rev. Lett.* **93** 235701
[176] Derrida B 1981 *Phys. Rev.* B **24** 2613
[177] Angell C A 1988 *J. Phys. Chem. Solids* **49** 863
[178] Ito K, Moynihan C T and Angell C A 1999 *Nature* **398** 492
[179] La Nave E, Mossa S, Sciortino F and Tartaglia P 2000 *J. Chem. Phys.* **120** 6128
[180] Chakrabarti D and Bagchi B 2006 *Phys. Rev. Lett.* **96** 187801
[181] Stillinger F H 1998 *J. Phys. Chem.* B **102** 2807
[182] La Nave E, Mossa S and Sciortino F 2002 *Phys. Rev. Lett.* **88** 225701
[183] Buechner S and Heuer A 2000 *J. Phys.: Condens. Matter* **12** 6535
[184] Debenedetti P G, Stillinger F H and Shell M S 2003 *J. Phys. Chem.* B **107** 14434
[185] Matyushov D V and Angell C A 2005 *J. Chem. Phys.* **123** 034506
[186] Moreno A J *et al* 2005 *Phys. Rev. Lett.* **95** 157802
[187] Moreno A J *et al* 2006 *J. Chem. Phys.* **124** 204509
[188] Yuan X and Cormack A N 2002 *Comput. Mater. Sci.* **24** 343
[189] Stillinger F H 1988 *J. Chem. Phys.* **88** 7818
[190] Stillinger F H, Debenedetti P G and Truskett T M 2001 *J. Phys. Chem.* B **105** 11809
[191] Karpov V G, Klinger M I and Ignatiev F N 1983 *Sov. Phys.—JETP* **57** 439
[192] Buchenau U, Galperin Y M, Gurevich V L and Schober H R 1991 *Phys. Rev.* B **43** 5039
[193] Gil L, Ramos M A, Bringer A and Buchenau U 1993 *Phys. Rev. Lett.* **70** 182
[194] Parshin D A, Ramos M A, Bringer A and Buchenau U 1994 *Phys. Rev.* B **49** 9400
[195] Hunklinger S and Enss C 2000 *Series of Directions in Condensed Matter Physics* **17** 499
[196] Heuer A and Esquinazi P (ed) 1998 *Tunneling Systems in Amorphous and Crystalline Solids* (Berlin: Springer) chapter 8
[197] Reinisch J and Heuer A 2005 *Phys. Rev. Lett.* **95** 155502
[198] Reinisch J and Heuer A 2004 *Phys. Rev.* B **70** 064201
[199] Reinisch J and Heuer A 2006 *J. Phys. Chem.* B **110** 19044
[200] Trachenko K, Dove M T, Hammonds K D, Harris M J and Heine V 1998 *Phys. Rev. Lett.* **81** 3431
[201] Mousseau N, Barkema G T and de Leeuw S W 2000 *J. Chem. Phys.* **112** 960
[202] Heuer A and Silbey R J 1993 *Phys. Rev. Lett.* **70** 3911
[203] Reinisch J and Heuer A 2004 *J. Low Temp. Phys.* **137** 267
[204] Vollmayr K, Kob W and Binder K 1996 *Phys. Rev.* B **54** 15808
[205] Daldoss G, Pilla O, Viliani G, Brangian C and Ruocco G 1999 *Phys. Rev.* B **60** 3200
[206] Trygubenko S A and Wales D J 2004 *J. Chem. Phys.* **121** 6689
[207] Despa F and Berry R S 2001 *J. Chem. Phys.* **115** 8274
[208] Despa F, Wales D J and Berry R S 2005 *J. Chem. Phys.* **122** 024103
[209] Saksaengwijit A, Doliwa B and Heuer A 2003 *J. Phys.: Condens. Matter* **15** S1237
[210] Abkevich V I, Gutin A M and Shakhnovich E I 1994 *Biochemistry* **33** 10026
[211] Bolhuis P G, Chandler D, Dellago C and Geissler P L 2002 *Annu. Rev. Phys. Chem.* **53** 291
[212] Heuer A, Doliwa B and Saksaengwijit A 2005 *Phys. Rev.* E **72** 021503
[213] Appignanesi G A, Fris J A R and Frechero M A 2006 *Phys. Rev. Lett.* **96** 237803
[214] Vollmayr-Lee K 2004 *J. Chem. Phys.* **121** 4781
[215] Saksaengwijit A and Heuer A 2006 *Phys. Rev.* E **73** 061503
[216] Riggleman R A, Double J F and De Pablo J J 2007 *Phys. Rev.* E **76** 011504
[217] Brawer S A 1984 *J. Chem. Phys.* **81** 954
[218] Dyre J C 1987 *Phys. Rev. Lett.* **58** 792
[219] Arkhipov V I and Baessler H 1994 *J. Phys. Chem.* **98** 662
[220] Monthus C and Bouchaud J P 1996 *J. Phys. A: Math. Gen.* **29** 3847
[221] Diezemann G 1997 *J. Chem. Phys.* **107** 10112
[222] Diezemann G, Sillescu H, Hinze G and Bohmer R 1998 *Phys. Rev.* E **57** 4398
[223] Dyre J 1995 *Phys. Rev.* B **51** 12276
[224] Doliwa B and Heuer A 2003 *Phys. Rev. Lett.* **91** 235501
[225] Brawer S 1985 *Relaxation in Viscous Liquids and Glasses* (Columbus, OH: American Ceramic Society)
[226] Heuer A and Saksaengwijit A 2008 *Phys. Rev.* E **77** 061507
[227] Buchenau U 2003 *J. Phys.: Condens. Matter* **15** S955–66

[228] Kudlik A, Benkhof S, Blochowicz T, Tschirwitz C and Roessler E 1999 *J. Mol. Struct.* **479** 201
[229] Denny R A, Reichman D R and Bouchaud J P 2003 *Phys. Rev. Lett.* **90** 025503
[230] Doliwa B and Heuer A 2003 *Phys. Rev.* E **67** 030501
[231] Buechner S and Heuer A 2000 *Phys. Rev. Lett.* **84** 2168
[232] Mauro J C, Loucks R J and Gupta P K 2007 *J. Phys. Chem.* A **111** 7957
[233] Osborne M J and Lacks D J 2004 *J. Phys. Chem.* B **108** 19619
[234] Vallee R A L, Van der Auweraer M, Paul W and Binder K 2006 *Phys. Rev. Lett.* **97** 214801
[235] Wevers M A C, Schoen J C and Jansen M 2001 *J. Phys. A: Math. Gen.* **34** 4041
[236] de Souza V K and Wales D J 2006 *Phys. Rev. Lett.* **96** 057802
[237] Matharoo G S, Razul M S G and Poole P H 2006 *Phys. Rev.* E **74** 050502
[238] Wang C and Stratt R M 2007 *J. Chem. Phys.* **127** 224504
[239] Wang C and Stratt R M 2007 *J. Chem. Phys.* **127** 224504
[240] Stillinger F H and Hodgdon J A 1994 *Phys. Rev.* E **50** 2064
[241] Horbach J and Kob W 1999 *Phys. Rev.* B **60** 3169
[242] Jund P *et al* 2000 *J. Phys.: Condens. Matter* **12** 8777
[243] Busch R, Bakke E and Johnson W L 1998 *Acta Mater.* **46** 4725
[244] Tarjus G, Kivelson D and Viot P 2000 *J. Phys.: Condens. Matter* **12** 6497
[245] Novikov V H and Sokolov A P 2003 *Nature* **431** 961
[246] Yannopoulos S N and Johari G P 2006 *Nature* **442** E7
[247] Castaing B and Souletie J 1991 *J. Physique* I **1** 403
[248] Swallen S F, Bonvallet P A, McMahon R J and Ediger M 2003 *Phys. Rev. Lett.* **90** 015901
[249] Xia X and Wolynes P G 2001 *J. Phys. Chem.* B **105** 6570
[250] Keyes T and Chowdhary J 2001 *Phys. Rev.* E **64** 032201
[251] Odagaki T and Hiwatari Y 1990 *Phys. Rev.* A **41** 929
[252] Odagaki T 1995 *Phys. Rev. Lett.* **74** 2114
[253] Kim J and Keyes T 2004 *J. Chem. Phys.* **121** 4237
[254] Rubner O and Heuer A 2008 *Phys. Rev.* E **78** 011504
[255] Fabricius G and Stariolo D A 2004 *Physica* A **331** 90
[256] Saksaengwijit A and Heuer A 2006 *Phys. Rev.* E **74** 051502
[257] Rodriguez Fris J A, Appignanesi G A, La Nave E and Sciortino F 2007 *Phys. Rev.* E **75** 041501
[258] Vallee R A L, der Auweraer M V, Paul W and Binder K 2006 *Phys. Rev. Lett.* **97** 217801
[259] Hedges L O, Maibaum L, Chandler D and Garrahan J P 2007 *J. Chem. Phys.* **237** 211101
[260] Boehmer R, Diezemann G, Geil B, Hinze G, Nowaczyk A and Winterlich M 2006 *Phys. Rev. Lett.* **97** 135701
[261] La Nave E and Sciortino F 2004 *J. Phys. Chem.* B **108** 19663
[262] La Nave E, Sastry S and Sciortino F 2006 *Phys. Rev.* E **74** 050501
[263] Montroll E W and Weiss G H 1965 *J. Math. Phys.* **6** 167
[264] Odagaki T, Matsui J and Hiwatari Y 1994 *Physica* A **204** 464
[265] Barkai E and Cheng Y C 2003 *J. Chem. Phys.* **118** 6167
[266] Jung Y J, Garrahan J P and Chandler D 2005 *J. Chem. Phys.* **123** 084509
[267] Stariolo D A and Fabricius G 2006 *J. Chem. Phys.* **125** 064505
[268] Chaudhuri P, Berthier L and Kob W 2007 *Phys. Rev. Lett.* **99** 060604
[269] Szamel G and Flenner E 2006 *Phys. Rev.* E **73** 011504
[270] Saksaengwijit A and Heuer A 2007 *J. Phys.: Condens. Matter* **19** 205143
[271] Chowdhary J and Keyes T 2004 *J. Phys. Chem.* B **108** 19768
[272] Horbach J, Kob W, Binder K and Angell C A 1996 *Phys. Rev.* E **54** R5897
[273] Zhang Y, Guo G, Refson K and Zhao Y 2004 *J. Phys.: Condens. Matter* **16** 9127
[274] Kim K and Yamamoto R 2000 *Phys. Rev.* E **61** R44
[275] Roth J 2000 *Eur. Phys. J.* B **14** 449
[276] Heuer A, Wilhelm M, Zimmermann H and Spiess H W 1995 *Phys. Rev. Lett.* **75** 2851
[277] Sillescu H 1996 *J. Chem. Phys.* **104** 4877
[278] Heuer A 1997 *Phys. Rev.* E **56** 730
[279] Bouchaud J P, Comtet A and Monthus C 1995 *J. Physique* I **5** 1521
[280] Rehwald C and Heuer A 2008 in preparation
[281] Wales D J and Doye J P K 2001 *Phys. Rev.* B **63** 214204
[282] Berthier L and Garrahan J 2003 *J. Chem. Phys.* **119** 4367
[283] Jaeckle J and Eisinger S 1991 *Z. Phys.* B **84** 115